# Placental function estimated by T2*-weighted magnetic resonance imaging

Sinding, Marianne Munk

*DOI (link to publication from Publisher):*
10.5278/vbn.phd.med.00094

*Publication date:*
2017

*Document Version*
Publisher's PDF, also known as Version of record

# PLACENTAL FUNCTION ESTIMATED BY T2*-WEIGHTED MAGNETIC RESONANCE IMAGING

**BY**
**MARIANNE MUNK SINDING**

DISSERTATION SUBMITTED 2017

AALBORG UNIVERSITY
DENMARK

# PLACENTAL FUNCTION ESTIMATED BY T2*-WEIGHTED MAGNETIC RESONANCE IMAGING

PhD Thesis

Marianne Munk Sinding

AALBORG UNIVERSITY
DENMARK

March 2017

.

Dissertation submitted: March 17, 2017

PhD supervisor: Ole B. Christiansen, Professor, MD, DMSc
Department of Obstetrics and Gynecology
Aalborg University Hospital, Aalborg, Denmark

Assistant PhD supervisors: Anne N. W. Sørensen, Clinical associate Professor, MD, PhD
Department of Obstetrics and Gynecology
Aalborg University Hospital, Aalborg, Denmark

Niels Uldbjerg, Professor, MD, DMSc
Department of Obstetrics and Gynecology
Aarhus University Hospital, Skejby, Denmark

David A. Peters, MSc, PhD
Department of Clinical Engineering
Central Region, Denmark

PhD committee: Ulla Weinrich, Clinical Associate Professor (MD, PhD)
Aalborg University/Aalborg University Hospital, Denmark

Professor Ganesh Acharya (MD, PhD, FRCOG)
Karolinska Institutet, Sweden
Ed Johnstone, Clinical Senior Lecturer and Consultant (MBChB, PhD, MRCOG)
University of Manchester, UK

PhD Series: Faculty of Medicine, Aalborg University

ISSN (online): 2246-1302
ISBN (online): 978-87-7112-919-9

Published by:
Aalborg University Press
Skjernvej 4A, 2nd floor
DK – 9220 Aalborg Ø
Phone: +45 99407140
aauf@forlag.aau.dk
forlag.aau.dk



Printed in Denmark by Rosendahls, 2017

# ENGLISH SUMMARY

Placental dysfunction is associated with adverse neonatal outcomes including low birth weight. Prenatal identification of placental dysfunction improves the neonatal outcomes and therefore, in vivo markers of placental dysfunction is of high clinical interest. One approach could be the detection of placental hypoxia, which may be associated to placental dysfunction, using T2*-weighted Magnetic Resonance Imaging (MRI). The placental MRI transverse relaxation time, T2*, reflects tissue oxygenation as the presence of deoxyhemoglobin affects the spins of protons thereby creating magnetic field inhomogeneities, which reduce the T2* value. Thus in hypoxic tissue, the T2* value is reduced. Placental Blood Oxygen Level Dependent (BOLD) MRI is a T2*-weighted sequence, in which signal changes are closely correlated to changes in tissue hemoglobin saturation during oxygen-challenge. Therefore, the aim of this project was to investigate the feasibility of T2*-weighted MRI (T2* measurements and BOLD MRI) as non-invasive methods for the detection of placental hypoxia and thereby placental dysfunction.

In this project, we demonstrated that in normal pregnancies, the placental T2* value is reduced as pregnancy advances and in pregnancies complicated by placental dysfunction, the placental T2* value is lower *(Study I)*. In the same study, we assessed the reproducibility of the T2* method and found it to be reasonable robust. In *Study IV,* we revealed strong correlations between placental T2* value and placental perfusion estimated by Doppler ultrasound uterine artery (UtA) pulsatility index (PI) between 20 and 40 weeks' gestation and subsequent birth weight percentiles. The T2* value performed significantly better than the UtA PI in the prediction of low birth weight. Using the BOLD sequence, we demonstrated that in normal pregnancies, the placental BOLD signal increases significantly during maternal oxygen-challenge and in placental dysfunction, the BOLD response is altered *(Study II)*. In contrast to the T2* measurements, the BOLD response can only be measured in relative values as the baseline signals vary among individuals. Therefore, in order to interpret the oxygen-challenge relative BOLD response, we used placental T2* values as markers of placental baseline conditions and absolute changes in placental oxygenation. We concluded that in placental dysfunction, a high BOLD response is caused merely by altered baseline conditions rather than a larger increase in placental oxygenation compared to normal *(Study V)*. Using the BOLD sequence, we also investigated spontaneous uterine contractions. We found that uterine contractions occur regularly in normal pregnancies and that they have a major impact on placental oxygenation, which needs to be considered when interpreting placental MRIs *(Study III)*.

In conclusion, placental T2*-weighted imaging has the potential to detect placental dysfunction in vivo and therefore, the methods deserves further investigations. The perspective may be a clinical tool to be used in the risk stratification of pregnant women.

# DANSK RESUME

Placenta dysfunktion er associeret til dårligt neonatal udkomme herunder lav fødselsvægt. Prænatal identifikation af placenta dysfunktion kan bedre det neonatale udkomme og derfor er udviklingen af in vivo markører for placenta-dysfunktion af høj klinisk interesse. En mulig markør kunne være placenta hypoxi, som er associeret til placenta dysfunktion. Placenta hypoxi kan potentielt detekteres ved hjælp af T2*-vægtet Magnetisk Resonans (MR) scanning. Den transverselle relaxations-tid, T2*, afspejler vævsoxygenering, idet paramagnetisk deoxyghemoglobin påvirker spinnene i naboprotoner og dermed skabes inhomogeniteter i det magnetiske felt, hvilket reducerer vævets T2* værdi. T2* værdien er således reduceret i hypoxisk væv. Blood oxygen level dependent (BOLD) MR er en T2*-vægtet sekvens, der er følsom overfor ændringer i saturation under ilt-test. Formålet med dette projekt var derfor at undersøge om T2*-vægtet MR (T2* måling og BOLD sekvens) kan bruges som in vivo markør for placenta hypoxi og dermed for placenta dysfunktion.

I dette projekt fandt vi, at placenta T2* værdien falder med gestationsalderen i ukomplicerede graviditeter og at T2* værdien er signifikant reduceret i graviditeter kompliceret af placenta dysfunktion *(Studie I).* I samme studie undersøgte vi reproducerbarheden af T2* metoden og fandt at metoden er robust. I *studie IV* fandt vi en stærk korrelation mellem placenta T2* værdien og placenta perfusionen vurderet ud fra ultralyd Doppler pulsatilitet indeks (PI) i arteria uterina (UtA) i gestationsuge 20 til 40 og senere fødselsvægt. Vi fandt ligeledes at T2* værdien var en stærkere prædiktor for lav fødselsvægt end UtA PI.

Ved hjælp af BOLD MR sekvensen, fandt vi at placenta BOLD signalet stiger signifikant under maternel ilt-test i ukomplicerede graviditeter og at BOLD responset i graviditeter kompliceret af placenta dysfunktion er ændret *(Studie II).* I modsætning til T2* værdien kan BOLD responset kun måles i relative værdier. Derfor undersøgte vi BOLD responset ud fra absolutte normoxiske og hyperoxiske T2* værdier, og vi fandt at i graviditeter kompliceret af placenta dysfunktion afspejler et forhøjet BOLD respons blot et ændret udgangs-BOLD signal og ikke en større absolut stigning i placentas oxygenering sammenlignet med ukomplicerede graviditeter *(Studie V).* Vi undersøgte ligeledes spontane uterus kontraktioner under BOLD MR. Her fandt vi at spontane uterus kontraktioner er relativ hyppige og at de i høj grad påvirker placenta BOLD signalet og dermed placentas oxygenering. Det er således en meget væsentlig fejlkilde i T2*-vægtet MR scanning, som man i høj grad skal være opmærksom på, når placenta MR fortolkes.

Vi konkluderer at T2*-vægtet MR scanning af placenta kan detektere placenta dysfunktion og at der derfor bør forskes mere i denne lovende metode. Perspektivet er en klinisk test til anvendelse ved risikostratificeringen af gravide.

# ACKNOWLEDGEMENTS

This thesis was carried out during my time as a PhD student at the Department of Obstetrics and Gynecology, Aalborg University Hospital between April 2014 and March 2017.

Firstly, I would like to thank my four supervisors: Anne N W Sørensen for introducing me into the amazing field of placental MR imaging, for her endless support and encouragement throughout the project and for lots of laughs. I am aware that you went above and beyond the call of duty! Niels Uldbjerg for sharing his experience in fetal medicine and research, for always providing constructive feedback and for the fruitful discussions. David A Peters for patiently teaching me about MRI and for the development of the MRI protocols and Ole B Christiansen for sharing his great knowledge on research and for his important support and friendly encouragement throughout this project. It has been a pleasure and a privilege working with you all.

I also wish to thank Prof. Jens B Frøkjær and research radiographers Carsten W Simonsen and Kenneth K Jensen from the Department of Radiology, Aalborg University Hospital, for their expert assistance in performing the placental MRI scans and for all the advice and support.

Special thanks to Astrid Petersen, pathologist at the Aalborg University Hospital, for the tremendous work on the placental pathological examinations and for sharing her great experience in placental pathology with me.

Thanks go to all my wonderful colleagues at the Department of Obstetrics and Gynecology, Aalborg University Hospital, for friendship and support. I look forward to working with you again in the clinic! Special thanks to Thomas Larsen, Head of Department, for providing working conditions that enabled me to complete this project.

I also wish to express my deepest gratitude to all the pregnant women for dedicating their time to participate in the studies and for sharing their stories. Without you, there would be no studies at all.

Finally, I wish to thank my friends and family, Ivan, my life companion and best friend, and my children, William and Nikoline, for reminding me of what is most important in life.

*Marianne Munk Sinding, March 2017*

**Funding**
The PhD project was financed by Aalborg University Hospital and supported by grants from Region Nordjyllands Sundhedsvidenskabelige Forskningsfond, Speciallæge Heinrich Kopps Legat, Dagmar Marshall Foundation, Fonden til Lægevidenskabens Fremme and from Brødrene Hartmanns Foundation. Moreover, congress participations during the PhD project was financed by Billedfonden, Department of Obstetrics and Gynecology and Reservelæge Fonden, Aalborg University Hospital.

# LIST OF PAPERS

This PhD thesis is based on five studies presented in the following papers, which are referred to in the text by their Roman numerals:

Paper I:
Sinding M, Peters DA, Frokjaer JB, Christiansen OB, Petersen A, Uldbjerg N, Sorensen A. Placental magnetic resonance imaging T2* measurements in normal pregnancies and in those complicated by fetal growth restriction. Ultrasound Obstet Gynecol 2016 Jun;47(6):748-754.

Paper II:
Sorensen A, Sinding M, Peters DA, Petersen A, Frokjaer JB, Christiansen OB, Uldbjerg N. Placental oxygen transport estimated by the hyperoxic placental BOLD MRI response. Physiol Rep 2015 Oct;3(10):10.14814/phy2.12582.

Paper III:
Sinding M, Peters DA, Frokjaer JB, Christiansen OB, Uldbjerg N, Sorensen A. Reduced placental oxygenation during subclinical uterine contractions as assessed by BOLD MRI. Placenta 2016 Mar;39:16-20.

Paper IV:
Sinding M, Peters DA, Frokjaer JB, Christiansen OB, Petersen A, Uldbjerg N, et al. Prediction of low birth weight: Comparison of placental T2* estimated by MRI and uterine artery pulsatility index. Placenta 2017 Jan;49:48-54.

Paper V:
Sinding M, Peters DA, Frokjaer JB, Christiansen OB, Petersen A, Uldbjerg N, Sorensen A. Placental baseline conditions modulate the hyperoxic BOLD-MRI response. *Manuscript in preparation*

# TABLE OF CONTENTS

# ABBREVIATIONS

| | |
|---|---|
| BOLD | Blood oxygen level dependent |
| $CO_2$ | Carbon dioxide |
| CPR | Cerebroplacental ratio |
| DCE | Dynamic contrast-enhanced |
| DV | Ductus venosus |
| DWI | Diffusion weighted imaging |
| EFW | Estimated fetal weight |
| FGR | Fetal growth restriction |
| FIESTA | Fast Imaging Employing Steady-state Acquisition |
| FVM | Fetal vascular malperfusion |
| GRE | Gradient recalled echo |
| ICNIRP | International Commission on Non-Ionizing Radiation Protection |
| MRI | Magnetic resonance imaging |
| MVM | Maternal vascular malperfusion |
| $pCO_2$ | Carbon dioxide partial pressure |
| PI | Pulsatility index |
| $pO_2$ | Oxygen partial pressure |
| PVM | Placental vascular malperfusion |
| RF | Radio frequency |
| ROI | Region of interest |
| SE | Spin echo |
| SGA | Small for gestational age |
| $sO_2$ | Oxygen saturation |
| T1 | Longitudinal relaxation time |
| T2 | Transverse relaxation time (SE MRI) |
| T2* | Transverse relaxation time (GRE MRI) |
| TE | Echo time |
| TR | Repetition time |
| UA | Umbilical artery |
| UtA | Uterine artery |

# CHAPTER 1. INTRODUCTION

Placental dysfunction is associated to adverse pregnancy outcomes including fetal growth restriction (FGR), which may be defined as the failure of the fetus to reach its genetically growth potential (1). Most, but not all, FGR fetuses are small for gestational age (SGA) and placental dysfunction is the leading cause of FGR (2,3). It is a common condition affecting 5-10% of all pregnancies, depending on the definition used (4,5). Placental dysfunction may be classified into two phenotypes termed early-onset and late-onset disease. These phenotypes are characterized by differences in gestational age at disease onset (diagnosis before or after 32-34 week's gestation (6,7)), the association to preeclampsia (8), ultrasound Doppler findings and severity (7,9).

In general, placental dysfunction is a progressive process in which the transfer of nutrients and oxygen to the developing fetus is impaired. This leads to various fetal compensatory adaptations and may progress towards circulatory failure and eventually fetal acidosis and fetal death (10,11). Therefore, growth restricted fetuses are at high risk of perinatal morbidity and mortality (12-15), and they have an increased risk of long term adverse outcomes including impaired neurological development (16,17), cardiovascular disease (18-25), and metabolic syndrome (26).

Prenatal identification improves the perinatal morbidity and mortality through timely delivery and prompt neonatal care (27), whereas a false diagnosis of FGR is associated with higher rates of labor induction, caesarian sections and short-term adverse neonatal outcomes (28). Therefore, correct identification of these fetuses is of enormous importance in the prenatal care. Furthermore, identification of FGR fetuses has the potential to be used in the cardiovascular and metabolic disease risk stratification in adult life. Finally, the adverse effects highlight the need of ongoing research in the development of treatment and prevention of placental dysfunction.

In modern obstetrics, detecting, diagnosing, and predicting placental dysfunction are major challenges due to several factors. The most important factor is that no clinical applicable direct measurement of placental function exists, and therefore, detection and surveillance of pregnancies complicated by placental dysfunction mostly rely on clinical assessments of fetal growth and fetal well-being rather than direct assessment of placental function. During the last decades, extensive research has been conducted in order to develop clinical methods to detect and predict placental dysfunction. These methods may include ultrasound Doppler measurements of the uterine artery (UtA), umbilical artery (UA), and the cerebroplacental ratio (CPR), and measurements of various angiogenetic factors, which together with maternal characteristics and fetal biometry have been combined into predictive models of low birth weight or other adverse outcomes associated to placental dysfunction. Nonetheless, several obstacles as described in this thesis may complicate these predictive models. Therefore, new

strategies are needed in order to detect placental dysfunction, and placental Magnetic Resonance Imaging (MRI) may be an option. As placental dysfunction may be associated to placental hypoxia (29), one approach is the T2*-weighted MR imaging, in which the MRI signal depends on the amount of tissue deoxyhemoglobin (30). Therefore, the aim of this project is to investigate the feasibility of T2*-weighted imaging as a non-invasive in vivo method for estimating placental hypoxia and thereby placental dysfunction.

# CHAPTER 2. BACKGROUND

This chapter contains four parts. The first part holds background information about the normal placenta including the placental structure, development, oxygen environment, and the placental oxygen transport capacity. The second part holds information about placental dysfunction and the related obstacles in clinical practice. The third and fourth parts represent background information for MRI of placental oxygenation, including a short presentation of the previous literature in the field and the ethical considerations regarding MRI in pregnancy.

## 2.1. THE NORMAL PLACENTA

The placenta has a wide range of function being a complex endocrine organ, playing a vital role in the transfer of oxygen and nutrients for the fetus, and acting as an immunological barrier between the mother and the fetus (31).

### 2.1.1. PLACENTAL STRUCTURE

The mature human placenta has a disc-shaped structure and consists of a fetal region (the chorionic plate) and a maternal region (the basal plate) surrounding the intervillous space (Figure 1). Maternal blood enters the intervillous space from the low-resistance spiral arteries and leaves back through the venous orifices in the basal plate. Within the intervillous space, the blood is dispersed through the vascularized fetal villous three, protruding from the chorionic plate. This arrangement of maternal and fetal blood compartments, in which the fetal blood is bathed by a fountain of maternal blood with various flow directions, is termed a *multivillous system* (32,33). Septae protrude from the basal plate into the intervillous spaces dividing the placenta into 15-20 maternal lobes, which can be seen on the maternal surface of the placenta. Each lobe is perfused by one or more spiral arteries and contains one or more fetal villous threes. At the placental margin, the intervillous space is degenerated (the marginal zone) and more peripheral, the chorionic plate and the basal plate fuse and form the chorion leave (34).


***Figure 1.*** *The mature human placenta. CP chorionic plate; BP basal plate; IVS intervillous space; P placental bed; M myometrium; CL chorion leave; A amnion; MZ marginal zone between placenta and fetal membranes; S placental septum; UC umbilical cord (From Kaufmann and Scheffen (35), with permission from publisher (Elsevier)).*

## 2.1.2. PLACENTAL DEVELOPMENT

In early pregnancy, placentation begins with the implantation of the blastocyst at gestational day 6-7. The wall of the blastocyst contains an outer layer of trophoblast and an inner layer of extraembryonic mesoderm. The trophoblast cells start to migrate between the endometrial cells opening up the intercellular spaces, thereby enabling trophoblast protrusions to penetrate. During trophoblast protrusion, the trophoblast cells undergo transformation into syncytiotrophoblast, whereas remaining cells from the blastocyst wall are called the cytotrophoblast. The syncytiotrophoblast rapidly increases and forms a complete mantle around the blastocyst. At day 8$^{th}$ lacunae are formed within the syncytiotrophoblastic mass at the implantation pole. These lacunae are the precursor of the intervillous space and in the first trimester, they are filled with maternal plasma and secretions from endometrial glands. The cytotrophoblast then starts migrating within the trabecula between the lacunae, and eventually they penetrate the syncytiotrophoblast and spread laterally to form a layer between the syncytiotrophoblast mantle and the endometrium. Thereby three layers of the original blastocyst wall exist; 1) the primary chorionic plate facing the cavity of the blastocyst, 2) the lacunar system and 3) the cytotrophoblast facing the endometrium (the initial basal plate) (36). At this stage the fetal villi starts to develop. Cytotrophoblast

proliferation causes side branches on the trabeculae to protrude into the lacunae, which is then transformed into the intervillous space. The branches are termed primary villi until they are invaded by mesenchymal tissue from the extraembryonic mesoderm, forming them into secondary villi. Vasculogensis within the secondary villi begins, and when the first fetoplacental capillaries are present, the villi are termed tertiary villi (3). Thus, at around the 21$^{st}$ day of gestation, the placenta is a vascularized villous organ. A population of the cytotrophoblast cells facing the endometrium in the initial basal plate differentiates and migrates deeper into the endometrium. This is the start of a very important process, known as the trophoblast invasion (37). The trophoblast cells invade into the maternal spiral arteries and form a plug in the lumen thereby preventing maternal blood to enter the intervillous space (38). At the end of the first trimester, the plugs in the spiral arteries disappear, and maternal blood enters the intervillous space. The trophoblast also induces vascular remodeling of the spiral arteries, which lose the smooth muscle in the walls and undergo dilation converting them into low-resistance vessels (39). This dilation is considered to be complete around 20-22 weeks' gestation, whereas the villous trophoblast continues to develop throughout gestation (40). The tertiary villi develop and differentiate into other villous types, which results in an exponential increase of the total villi surface area and a progressive decrease in the thickness of the villous membrane (40,41). These changes increase the placental transfer capacity, thereby meeting the increasing metabolic demand from the fetus and the placenta itself.

### 2.1.3. PLACENTAL OXYGEN ENVIRONMENT

In early gestation, when the trophoblast plugs prohibit the maternal blood flow in the intervillous space, the placenta has a relatively low oxygen level with an oxygen partial pressure ($pO_2$) around 20 mmHg (42-44). This relative hypoxic environment is needed to protect the early developing fetus from oxidative distress (45) and drives ongoing fetal angiogenesis (39). At the end of the first trimester, when the plugs in the spiral arteries disappear, and maternal blood enters the intervillous space, the $pO_2$ rises to around 50 mmHg (43,44,46). In vitro measurements of blood extracted from the intervillous space during cordocentesis performed in 16-20 weeks' gestation (47) and during cordocentesis and cesarean section at 37-40 weeks gestation (47,48) have shown a decrease in placental $pO_2$ as gestational age advances. Likewise, the placental oxygen saturation ($sO_2$) declines from 66.9% at 13-16 weeks' gestation (44) to 52.1% at 37-40 weeks' gestation (48). This decreased $sO_2$ of the intervillous space has also been demonstrated in normal pregnancies at 20 to 36 weeks' gestation using near infrared spectroscopy, in which intervillous space oxygen indexes are used as proxies of intervillous space $sO_2$ (49). The reduction in placental oxygenation can be explained by the increasing oxygen demand from the fetus and the placenta. The development of the intervillous $pO_2$ throughout gestation is summarized in Figure 2.

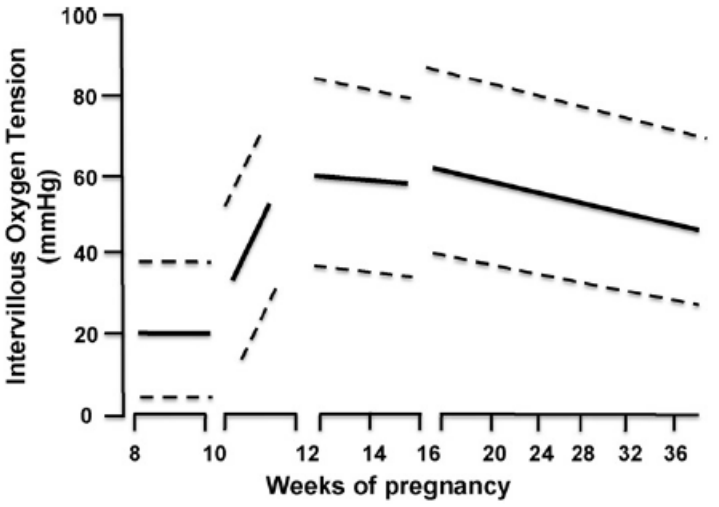


***Figure 2.*** *The mean and 95% confidence intervals of oxygen partial pressure – dashed lines – throughout gestation in the intervillous space in the human. Values are derived from in vivo measurements reported by Rodech et al. (43), Soothill et al. (47,50) and Jauniaux et al (42,44,46) (from Zamudio et al.(51), with permission from publisher (Whiley online library))*

The normal $pO_2$ and $sO_2$ of the umbilical and the uterine blood in the third trimester are presented in Table 1.

| | **$pO_2$ (mmHg)** | **$sO_2$ (%)** |
|---|---|---|
| **Umbilical artery** | 20 | 40 |
| **Umbilical vein** | 30 | 70 |
| **Uterine artery** | 100 | 98-100 |
| **Uterine vein** | 42 | 70 |

***Table 1.*** *The normal $pO_2$ and $sO_2$ of the umbilical and the uterine blood in the third trimester (48,52,53).*

Within the intervillous space, oxygenation of the maternal blood entering from the spiral arteries decreases radially as the blood passes over the villous three and gas-exchange takes place (illustrated in Figure 1 by red and blue arrows). This radial oxygen-gradient has been proposed in primates (54,55) and in the human placenta (56,57). It has also been visualized in human placental MRI studies using BOLD-contrast (58,59), and moreover, it has been evidenced by a higher antioxidant activity in human central villi compared to peripheral once (60).

### 2.1.4. PLACENTAL OXYGEN TRANSPORT

As presented in the beginning of this section, the placenta displays a wide range of function. In this thesis, focus will be on the transfer of oxygen from the mother to the fetus.

The oxygen transport from the mother to the fetus is determined by the rates and patterns of maternal and fetal placental blood flows, the oxygen diffusing capacity of the placenta, and the oxygen capacities and affinities of fetal and maternal blood (61). It is generally accepted that the placental oxygen transfer predominantly occurs by simple diffusion, in which the driving force is the $pO_2$ gradient between maternal blood in the intervillous space and fetal blood in the villi vessels (31). As described by the Ficks law, the simple diffusion of oxygen across the placenta per unit time is determined by the thickness and surface area of the membrane, the placental diffusion coefficient of oxygen and the $pO_2$ difference between uteroplacental and fetoplacental blood (32). $O_2$ is a small hydrophobic molecule, which diffuses readily across the membrane in normal placentas. Hence, as the driving $pO_2$ gradient is maintained by flow within the uteroplacental and the fetoplacental compartments, the oxygen transfer is considered predominantly to be *flow-limited* (32,62,63). However, the observed differences between umbilical vein $pO_2$ and the uterine vein $pO_2$ in normal pregnancy (Table 1) might indicate that oxygen transport to some extend is also limited by the placental diffusion capacity. Nonetheless, other important factors may explain this $pO_2$ difference. Firstly, besides supplying the fetus, the maternal arterial blood supplies the placenta, which has a high metabolic activity, and near term it consumes about 40% of the delivered oxygen. Even when the oxygen availability is reduced, placental oxygen consumption may be maintained at the expense of the fetus (64). Secondly, as the maternal and the fetal blood flow in a multivillous system, in which the fetal vascularized villi are bathed by a fountain of maternal blood with various flow directions, “shunts” may exist, in which maternal blood passes the intervillous space without being in direct contact with the villous tree. Moreover, maternal arteriovenous shunts located in the placental bed (65), fetal arteriovenous shunts (63) and uneven distributions of maternal and fetal blood flows to placental regions also allow blood to bypass areas of gas exchange (32,52,66,67). These nonhomogeneous flow patterns reduce the oxygen transport efficiency and they contribute to the mismatch between umbilical vein $pO_2$ and the uterine vein $pO_2$ in normal pregnancy. In contrast, the passive oxygen diffusion across the placenta is enhanced by differences in hemoglobin oxygen affinities in the maternal and the fetal blood. The fetal hemoglobin (hemoglobin F) has a higher oxygen affinity than maternal hemoglobin (hemoglobin A) (68). Moreover, during gas-exchange the maternal blood receives carbon dioxide ($CO_2$) from the fetal blood thereby increasing the maternal $CO_2$ partial pressure ($pCO_2$). Thereby, the pH of the maternal blood falls, which diminishes the oxygen affinity of maternal hemoglobin. Likewise, as $pCO_2$ is reduced in the fetal blood, the pH rises, which further increases the oxygen affinity of the fetal hemoglobin (the Bohr effect) (63).

Throughout gestation, various adaptations occur in order to meet the increasing oxygen demand from the fetus. Firstly, the total placental size and the total uterine blood flow are increased (69). Uterine blood flow estimates are subjects to many errors; however, the uterine blood flow at term has recently been estimated to be around 800 ml/min or 270 ml/min/kg fetus (70). Although the total uterine blood flow is increased, the flow per unit mass of the placenta (placental perfusion) throughout gestation is a matter of debate. In 1960, Assali et al. (69) found the uterine blood flow per unit weight of pregnant uterus in a constant range between 9 and 40 weeks' gestation. Nowadays, several studies have estimated the placental perfusion using MRI, but the results are varying. The inconsistencies can be explained by the use of different MRI sequences and the use of different regions of interests (ROI) covering the entire placenta or only the basal plate. One should also keep in mind that some MRI techniques do not measure perfusion in a classical manner (net blood flow through a tissue). Rather instead, they measure blood movement within the ROI. Nevertheless, this measurement may be functionally more relevant given the complex architecture of the maternal and fetal vascular network within the placenta, in which blood flows in various directions. Moreover, fetoplacental blood within the ROI may contribute to the MRI result. Some MRI studies report placental perfusion to stay relatively constant throughout gestation (71-74), whereas others have reported a slightly reduction in the placental perfusion fraction as gestational age advances (75,76). These latter studies are in line with a previous histological study on normal placentas reporting slightly reducing intervillous volume fractions as gestational advances (77). On the contrary, in a study using contrast-enhanced ultrasound in the macaques, the rate of perfusion within the intervillous space was increased from the mid-second to early third-trimester (78). Thus, changes in uteroplacental perfusion throughout gestation remain unclear. Nonetheless, these previous study might indicate that the perfusion remains in a relatively constant range. Another adaptation in order to meet the increasing demand from the fetus is the increasing placental diffusion capacity as the villous trophoblast surface area increases and the membrane thickness decreases. Moreover, the total umbilical blood flow is increased as gestational advances; however, the umbilical blood flow per unit fetus is decreased near term (79-81), and so is the $pO_2$ and the $sO_2$ of the umbilical artery and vein (47,82,83). Even though that this decrease is compensated by an increasing fetal hemoglobin concentration in order to maintain the oxygen content relatively constant (47,82), the reduced umbilical blood flow per unit fetus has been proposed to contribute to an adverse intrauterine environment at the very end of gestation (79).

## 2.2. PLACENTAL DYSFUNCTION

Dysfunctional placentas are associated with altered blood flow in the uteroplacental circulation and/or in the fetoplacental circulation, altered placental morphology and altered molecular transport mechanisms (84). The major result of these alterations is reduced delivery of oxygen and nutrients to the fetus.

### 2.2.1. PLACENTAL PATHOLOGICAL FINDINGS

The placental pathological findings associated to placental dysfunction may be classified into signs of maternal vascular malperfusion (MVM) and signs of fetal vascular malperfusion (FVM) (85). In both early-onset and late-onset disease, signs of MVM and FVM may be present at the same time. In early-onset disease, the pathological findings are typically more pronounced than in late-onset disease and they are mainly associated to MVM. Late-onset disease represents a more heterogeneous group (86) with an increasing incidence of pathological findings of MVM and FVM compared to normal pregnancy (87). Moreover, in particular the late-onset cases may be even histological unremarkable (88,89). On the contrary, signs of MVM or FVM may be present in pregnancies with normal outcomes (90). In general, placental dysfunction is associated with a reduced villous volume, reduced villous surface area (91-93), increased thickness of the trophoblast (92,93), and malformed villous capillaries (94). In a recent workshop consensus statement, the placental diagnostic criteria including MVM and FVM were reviewed and agreed upon (85). According to this consensus statement, MVM include several cross morphological and microscopic changes. The former may include reduced placental weight ($< 10^{th}$ percentile), infarction ($> 5\%$) and retroplacental hemorrhage, whereas the latter may include signs of distal villous hypoplasia (long, thin villi), accelerated villous maturation (small, short hypermature villi for gestational age) and decidual arteriopathy including for instance signs of abnormal spiral artery remodeling. Signs of FVM may be focal or global and may contain the presence of avascular villi with or without thrombi, fibrin deposition etc. Moreover, signs of villitis of unknown etiology may be associated to placental dysfunction (85). In this thesis, the term placental vascular malperfusion (PVM) refers to the presence of MVM and/or FVM.

### 2.2.2. PLACENTAL BLOOD FLOWS

A key aspect of the dysfunctional placenta is an impaired conversion of the spiral arteries into low-resistance vessels during early placentation. This impaired placentation is considered the main cause of placental dysfunction in FGR pregnancies as well as in other pregnancy complications such as preeclampsia, spontaneous preterm labor and late spontaneous abortion (95). It is generally accepted that impaired conversion of the spiral arteries limits the maternal blood flow into the intervillous space (96); however, controversies exists regarding the exact hemodynamic consequences of the impaired conversion. Mathematical and in silico models suggest that the impaired conversion of the spiral arteries results in a high-pressure, high-velocity flow of maternal blood into the intervillous space creating turbulent intervillous flow, which may reduce the transport efficiency. Moreover, unstable intervillous flow with subsequent ischemia-reperfusion may induce oxidative damage (97,98). In one of the models, Burton et al. (97) also suggest that the *total* volume of maternal blood flowing to the placenta is not directly affected by the lack of spiral artery conversion. However, secondary changes within the spiral arteries, such as spiral artery atherotic changes and occlusions with infarction of the overlying

placental parenchyma, may restrict the uteroplacental blood flow (29,97) as evidenced by an increased UtA Doppler resistance (99).

The impaired uteroplacental flow may lead to fetal stem vessel vasoconstriction and secondary villous maldevelopment with a subsequent increased resistance in the fetoplacental circulation (100), as evidenced by the increased UA Doppler resistance often observed in FGR pregnancies (99). The pathology underlying the early fetal stem vessel vasoconstriction is unclear. It may be a diminished maternal blood flow and decreased oxygenation in the intervillous space (101,102) or an initial hyperoxic environment (46). It has also been suggested that the stem vessel vasoconstriction is caused by high velocity-flow of the maternal blood in the center of the intervillous space causing perfusion damage of the villi (97,98) and malperfusion of the intervillous space as some blood may short-circle much of the villous three. The degree of malperfusion may explain the different types of secondary villous abnormalities. Thus, low-grade malperfusion may lead to a proliferative villous response (accelerated villous maturation) whereas high-grade malperfusion may lead to villous hypoplasia (103,104). Most often, a high UA Doppler resistance is caused by stem villus vasoconstriction and villous abnormalities secondary to uteroplacental malperfusion as described above. However, in some cases, the primary abnormality may be a primary defect in the terminal villous tree (105). This may explain why some FGR cases exhibit high UA Doppler resistance without abnormal UtA flow. In a recent study, it was demonstrated that such cases were delivered later compared to FGR cases with both abnormal UtA and UA Doppler findings, and that their placentas more often revealed massive perivillous fibrin deposition, chronic intervillositis, and choriangiosis, but significantly lower rates of MVM (106).

### 2.2.3. THE OXYGEN ENVIRONMENT AND OXYGEN TRANSPORT

Decades ago, in vivo cord blood sampling demonstrated that FGR is associated to fetal hypoxemia (82,107). Recently, fetal hypoxemia has also been demonstrated using T2-weighted MRI in late-onset disease (108). However, the cause of fetal hypoxemia is widely debated. In 1997, Kingdom and Kaufmann (96) proposed a model including three categories for the origin of fetal hypoxemia; 1) Preplacental hypoxia, in which the fetus and the placenta are hypoxic due to reduced oxygen content in the maternal blood (high altitude pregnancy or maternal anemia). 2) Uteroplacental hypoxia, in which the maternal blood has a normal oxygen content, but it is restricted to entry the intervillous space due to impaired conversion of spiral arteries or occlusions of the arteries. Thus, the fetus and the placenta are both hypoxic and 3) Postplacental hypoxia, in which oxygenation of the intervillous space is normal (or increased compared to normal), but impaired fetoplacental perfusion prohibits the transfer of oxygen to the fetus, a situation the authors also refer to as “placental hyperoxia”.

It is generally assumed that the lack of spiral artery conversion leads to intervillous hypoxia (95,109,110). However, intervillous hypoxia has never been demonstrated in

pregnancies complicated by placental dysfunction. On favor of intervillous hypoxia is that in preeclampsia, placentas have been shown to have gene expression profiles consistent with hypoxia (111-113). Likewise, in angiotensin-converting enzyme 2 (ACE2) knockout mice associated with small fetal size, uterine artery dysfunction is associated with higher levels of placental pimonidazole, a marker of hypoxia, and hypoxia-inducible factor-2α (114). Most likely, the secondary changes to impaired spiral artery conversion, including for instance acute spiral artery atherosis and thrombosis with infarction of the overlying placental parenchyma, have a major impact on intervillous blood flow resulting in local hypoxia-ischemia (29). This is in accordance with several MRI studies demonstrating reduced placental perfusion in pregnancies complicated by placental dysfunction (74,115-117). In these studies, both changes in the maternal and the fetal compartment may contribute to the MRI findings and therefore, they do not only asses the uteroplacental perfusion. However, in support of reduced intervillous perfusion and thereby reduced oxygen delivery to the intervillous space is a study by Brunelli et al. (118) using dynamic contrast-enhanced (DCE) MRI. Their results, retrospectively obtained from MRI examinations performed in order to exclude placental adhesive disorders, demonstrated significant intervillous hypoperfusion in 14 pregnancies complicated by severe placental dysfunction at 28 weeks' gestation. The 14 pregnancies were compared to 12 controls at the same gestational age without signs of placental dysfunction. In the dysfunctional placentas, they demonstrated a slow MRI signal enhancement and a lower MRI signal intensity within the intervillous space after 2 minutes compared to the controls. Moreover, in the dysfunctional placentas, they did not observe a MRI signal plateau and a culminating negative slope, marking the beginning of contrast washout in the controls. They also found that the signal enhancement was rather uniform distributed within the controls, whereas the dysfunctional placenta displayed many underperfused areas. Finally, it should be noticed that no signal changes were evident in the fetuses, indicating that the observed signal changes arose only from the intervillous circulation. Thus, they demonstrated that in early-onset dysfunctional placentas, the intervillous circulation, and thereby most likely the oxygenation of the intervillous space, is severely impaired. In accordance with these MRI findings is a placental scintigraphy study by Nylund et al. (119). They demonstrated an impaired uteroplacental perfusion in FGR pregnancies using intravenous indium-113m chloride injection. The maximum activity (100%, proportional to the blood volume), the rise time in counts (the time between 5 and 95% of the maximum activity), and the blood flow index (maximum activity/rise time) were significantly reduced in FGR pregnancies compared to normal controls.

Fetal hypoxemia in pregnancies complicated by placental dysfunction may also arise from reduced fetal oxygen extraction, as proposed in the third category in the model by Kaufman and Kingdom. This suggestion is based on the results of a study by Pardi et al. (120). In that study, it was demonstrated that the oxygen contents in the uterine vein obtained during cesarean section was higher in FGR cases, which was interpreted as a reduced fetal oxygen extraction. However, as commented by Burton GJ (121),

oxygen levels were also higher in the maternal arterial blood in those FGR cases. Nonetheless, the findings by Pardi et al. may indicate that in some cases of placental dysfunction, the reduced oxygen delivery to the fetus may be a result of reduced oxygen extraction rather than intervillous hypoxia. Thus, the oxygen transfer in some dysfunctional placentas may be diffusion limited due to reduced surface area and increased thickness of the villous membrane and/or impaired fetoplacental circulation as evidenced by Doppler studies (84,96,122,123). This may also be supported by a study using near infrared spectroscopy, in which intervillous space oxygen indexes used as proxies of intervillous space oxygen $sO_2$ were higher than normal in small for date pregnancies prior to delivery in 37 weeks' gestation (49). Placental pathological examination, however, was not performed in that study, neither were any Doppler findings reported.

In conclusion, controversies exist regarding the placental oxygen environment and the placental transfer of oxygen in pregnancies complicated by placental dysfunction. Whereas it has been demonstrated that the fetoplacental blood is hypoxemic, the oxygenation of the intervillous space and the cause of the fetoplacental hypoxemia may vary. This may, to a great extent, reflect heterogeneities in phenotypes of placental dysfunction regarding gestational age at disease onset, Doppler findings in umbilical and uterine arteries, and placental pathological findings. Nonetheless, in theory, the average oxygenation of the entire placenta should be reduced in pregnancies complicated by placental dysfunction.

### 2.2.4. MANAGEMENT AND OBSTACLES IN CLINICAL PRACTICE

In modern obstetrics, detecting, diagnosing, and predicting placental dysfunction are major challenges due to several factors. The most important factor is that no clinical applicable direct measurement of placental function exist, and therefore, the detection and diagnosis of placental dysfunction rely on indirect estimates. This has led to a wide variety of definitions of placental dysfunction and FGR being used in the literature and in clinical practice (124,125).

**The estimated fetal weight (EFW)**

During pregnancy, the most common indirect estimate of placental function is the ultrasound EFW, in which a low EFW indicates potential placental dysfunction. However, using ultrasound EFW it is not possible to distinguish fetuses that are growth restricted due to placental dysfunction and fetuses that are constitutionally small. Furthermore, EFW fails in detection of the growth restricted fetuses that are not SGA. Low EFW is a known risk factor for stillbirth; however, in approximately two thirds of stillbirths occurring at term, the neonate has a normal birth weight (126). Thus, focusing merely on the EFW does not identify a large proportion of fetuses at risk of stillbirth. Another limitation of the EFW is that the accuracy of the measurement is compromised by large intra- and interobserver variability (127) and errors in the weight-estimating formulas including the use of two-dimension measurements to estimate three-dimension volume, and the use of fetal volume to

estimate fetal weight. There is evidence that the least accurate estimates are in the very small and very large fetuses (128). Furthermore, one should keep in mind that EFW at a single ultrasound scan gives information about fetal size but not about fetal growth velocity. In order to assess fetal growth velocity, the use of longitudinal EFW measurements are required, in which impaired fetal growth can be defined as deceleration in growth between at least two scans two weeks apart. Thus, longitudinal scans are required to detect abnormal fetal growth velocity; however, multiple scans may be limited by the resources available in many clinical settings.

**Cut-of values and growth curves**

The diagnosis of placental dysfunction based on EFW and/or birth weight is complicated by the use of different cut-of values to define FGR. According to the American College of Obstetricians and Gynecologist (ACOG), FGR is diagnosed when the EFW is below the 10$^{th}$ percentile (4); however, other cut-of values may be used including the 3$^{rd}$, 5$^{th}$ or 15$^{th}$ percentile for gestational age or 2 standard deviations below the mean for gestational age. Furthermore, the use of various growth curves in different countries is a matter of debate. Some use growth reference curves representative of an entire population. These reference curves describe how fetuses (and neonates and infants) *have* grown at a particular time and/or place. The reference curves may be based on either ultrasound EFW or birth weights. In the latter case, however, as preterm infants are more likely to be growth-restricted (129,130), population reference curves based on birth weight tend to underestimate SGA in preterm births. Others use population standard curves usually only based on low-risk pregnancies with normal outcomes. Thus, a standard curve describe how fetuses (and neonates and infants) *should* grow when constrains on growth are minimal. Another approach is the use of customized curves, rather than population charts. Using a customized curve, the birth weight is adjusted for maternal characteristics (maternal height, weight, parity, ethnicity etc.). It has been suggested that using a customized curve, the fetuses identified as SGA are at higher risk of adverse outcomes than SGA fetuses identified using population charts (131). However, controversies exist regarding customization, as some of the adjusted factors themselves are risk factors (132,133).

In Denmark, an EFW < -15% based on the intrauterine growth curve by Marsal et al (134) is considered at risk of FGR during pregnancy, whereas low birth weight is defined by a birth weight < -22% using the same reference. The growth curve by Marsal et al. is based on a longitudinal study of 86 uncomplicated pregnancies (759 EFWs) with normal neonatal outcomes from four Scandinavian centers. Using this growth curve, the incidence of low birth weight (< -22%) in Denmark has been estimated to be 2.8% (135).

**Ultrasound Doppler assessments**

During pregnancy, ultrasound Doppler measurements of fetal and maternal vessels are often included in order to risk stratify the pregnancy and to detect placental

dysfunction. Moreover, fetal Doppler measurements are also used to examine fetal well-being and compensatory adaptations to hypoxia (136). Doppler flow velocities of the arteries on both sides of the placenta provide indirect measurements of uteroplacental and fetoplacental circulations and thereby placental function. As absolute blood flow volume measurements are dependent on the insonation angle and diameter of the vessels, the Doppler flow velocity waveform is usually analyzed and characterized by other indices. Often, the waveform is characterized by the pulsatility index (PI), which is a measurement of the blood flow resistance in a vessel ((peak systolic velocity – minimum diastolic velocity)/mean velocity during cardiac cycle)). As opposed to absolute blood flow volume measurements, the PI is an angel independent measurement in which the vessel diameter need not to be known. However, the interpretation of the PI is complex, as it does not directly reflect flow. In arteries, the diastolic flow velocity represents downstream resistance, although other parameters such as fetal heart rate and blood flow viscosity may also affect the flow velocity waveform. These parameters, however, should not be of clinical significance. Moreover, maternal position and fetal breathing movements may affect the velocities. Therefore, the assessment should be performed with the mother in a slightly tilted lateral position in order to avoid vena cava compression and subsequent uteroplacental hypoperfusion. Furthermore, the assessment should not performed during fetal breathing movements. The most frequently used Doppler flow velocity measurements are shortly presented in the following.

**Uterine artery (UtA) Doppler.** In pregnancies complicated by placental dysfunction, the UtA flow may be compromised due to impaired transformation of the spiral arteries into low resistance vessels (29,96). Therefore, the assessment of UtA Doppler flow velocities may be used to distinguish the FGR fetus from the small for date fetus (137,138) or even predict FGR during early pregnancy (139). However, not all pregnancies complicated by placental dysfunction have an elevated UtA PI (106) and the measurement is limited by rather large intra- and interobserver variabilities (140). Hence, the performance of UtA PI varies in the prediction of low birth weight and as a freestanding test, the measurement is inaccurate (141-146). Even in the third trimester, the UtA PI detection rate of low birth weight (< $5^{th}$ percentile) for those delivering < 5 weeks following assessment is only 44% at a false positive rate of 10% (143).

**Umbilical artery (UA) Doppler.** An elevated UA PI reflects increased fetoplacental resistance as it is associated with maldevelopment of the placental terminal villous tree and stem villus vasoconstriction (94,99,104)). FGR pregnancies with preserved end-diastolic UA flow may be associated to a normal or a proliferative villous response (accelerated villous maturation) (3,96,104,147), whereas placentas from pregnancies with an absent or reversed UA flow may be associated to villous hypoplasia (3,94,104). Raised UA PI is an early sign of placental dysfunction, which typically precedes abnormalities in other parameters used in the assessment of fetal well-being, including Doppler findings in the MCA and DV as described below,

changes in biophysical profile and changes in fetal heart rate patterns (148,149). An elevated UA PI may progress towards an absent or even reverse end-diastolic flow velocity and it has been demonstrated that absence of end-diastolic flow velocity is correlated to fetal acidemia (150,151). However, the progression of an elevated UA PI varies (136), and some FGR fetuses have normal UA PI, particular the late gestation FGR fetuses (88).

**Middle cerebral artery (MCA) Doppler and the cerebroplacental ratio (CPR).** Other Doppler flow parameters to be used in the fetal and placental assessment include the PI of the fetal MCA and the CPR, which is the ratio between the UA PI and the MCA PI (152). Brain sparing refers to fetal cerebral vasodilation in response to perceived hypoxemia, which is followed by a decrease in the MCA PI. It is one of the fetal adaptive responses to reduced available oxygen and nutrition, in which the blood is redistributed towards the vital organs including the fetal brain, myocardium and the adrenals (153). In early-onset placental dysfunction, a low MCA PI is typically observed in fetuses with reduced umbilical flow, whereas in late gestations, up to 20% of SGA fetuses with normal UA PI have a low MCA PI (154), which is also associated to adverse neonatal outcomes (155). In case of fetal metabolic acidosis, the ability to maintain the centralization of the fetal blood flow may be lost (156). Thus, normalization of a reduced MCA PI in severely compromised fetuses may occur. A low CPR reflects cardiac redistribution in favor of the brain, which may be observed in milder placental dysfunction (153) with only slight abnormalities in the UA and MCA PI. In early-onset disease, a low CPR may precede abnormal UA PI and MCA PI. On the contrary, in late-onset disease, a low CPR may be the only Doppler sign of fetal adaptive response to reduced oxygen supply (7). In these pregnancies, the fetus may undergo rapid deterioration without any further Doppler signs. Studies have demonstrated that a low CPR is an independent predictor of adverse neonatal outcome regardless of fetal size (157,158).Therefore, in the third trimester, the CPR may be an important tool in the assessment of fetal well-being and it may be able to detect those FGR fetuses that are not SGA.

**Ductus venosus (DV) Doppler.** Alterations of DV flow velocity waveforms are in a closer temporal relationship to intrauterine fetal demise, compared to changes in arterial flows as described above (136,159). Therefore, in severe growth-restricted pregnancies, DV flow velocities in combination with fetal heart rate patterns are used to assess fetal well-being and timing of preterm delivery (160,161). The DV shunts a proportion of the well-oxygenated blood from the umbilical vein towards the fetal heart and brain, thereby bypassing the fetal liver. The degree of shunting depends on the fetal oxygen supply as the DV shunting is increased during hypoxia (162). Increased DV PI and reduced blood flow velocity, which may even be reversed during atrial contractions in case of severe hemodynamic compromise, reflect an increased right ventricular afterload and eventually myocardial dysfunction (159,163,164) and the DV indices are associated to fetal acidemia (163).

**Postpartum diagnosis**

Postpartum diagnosis of placental dysfunction also represents a major challenge. The postpartum diagnosis is often based on the birth weight percentile; however, as is the case of the prenatal EFW, birth weight percentile does not distinguish between small for date neonates and FGR neonates; neither does it include those FGR neonates that are not born small for date. The postpartum diagnosis may be confirmed by placental pathological examinations, in which various pathological signs indicate placental dysfunction (85) as described in Chapter 2.2.1. Nonetheless, in some dysfunctional placentas, no such signs exist, and in placentas from clinical uneventful pregnancies, these signs may be present (90). Furthermore, placental pathological examination is not performed routinely in all pregnancies. Therefore, neither birth weight percentile, nor placental pathological examination may be a perfect proxy of placental dysfunction. Other proxies of placental dysfunction may include adverse outcome measurements including stillbirth, delivery before 32-34 week's gestation etc. or the assessment of catch-up growth in early postnatal life, which may indicate an impaired intrauterine placental environment.

**Prediction of FGR and adverse outcomes**

In clinical practice, prediction of FGR and adverse outcomes due to placental dysfunction is of great importance in the risk stratification of the pregnant women, preferable in early gestation. Several predictive models at various gestations have been proposed. These models may include EFW, Doppler measurements, maternal characteristics and maternal blood pressure, and/or biochemical markers such as placental growth factor (PlGF), soluble Fms-like tyrosin kinase-1 (sFtl-1), pregnancy-associated placental hormone (papp-A) etc. The parameters have been assessed as freestanding tests and in various combinations, but the predictive values are varying (165-171). Moreover, comparison of the different models is difficult due to heterogeneities in study populations, definitions of FGR and outcome measurements. Furthermore, many of the models include a third trimester scan, which is not part of routine practice in many countries.

**Conclusion**

In clinical practice, detecting, diagnosing, and predicting placental dysfunction and the associated adverse outcomes are major challenges due to several factors as discussed above. A direct, reliable measurement of placental function in vivo may overcome these challenges. Therefore, the key to more effective clinical management may be to identify direct placental biomarkers of placental dysfunction rather than indirect estimates of this condition. One potential biomarker is placental hypoxia, which may be detected using MRI.

## 2.3. MAGNETIC RESONANCE IMAGING

MRI was invented in 1972 by the American chemist, Poul C. Lauterburg, while the basic physic fundamentals for MRI were discovered even decades before. Ever since, MRI has undergone a dramatic development and nowadays, MRI has a broad range of applications and it is widely used in the diagnosis of medical disease. In 2003, Poul C. Lauterburg and Sir Peter Mansfield were awarded the Nobel Prize in Physiology or Medicine for their discoveries concerning MRI. Their work has led to the development of modern MRI, which represents a breakthrough in medical diagnostics and research.

### 2.3.1. BASIC MRI PRINCIPLES

MRI is based on the magnetic properties of certain atom nuclei. The most important nuclei is the hydrogen nucleus, being present in water and thus in all tissue. This nucleus has an electrical charge and possesses a spin, creating its own intrinsic magnetic field. Therefore, each nucleus acts like a small magnet and, when placed in an external magnetic field, partially aligns with the external magnetic field. Most nuclei align parallel with the external field (low-energy state), while others align anti-parallel to the external field (high-energy state). In addition to the spin around the nucleus axis, the external magnetic field induces another spin around the axis in the external magnetic field. This spin is also called precession (Figure 1) (172).

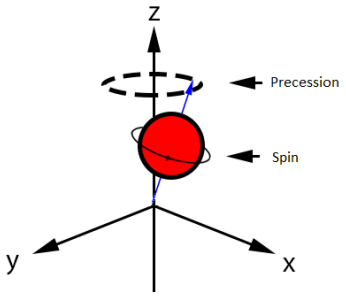


***Figure 3.*** *Illustration of the nucleus spin and precession*

The precession frequency can be described by the Larmor equation:

$$\acute{\omega} = \gamma B_0 \qquad (1)$$

in which ώ is the precession frequency given in Hz (or MHz), γ is the gyromagnetic ratio and $B_0$ is the external magnetic field strength, given in Tesla (T). The sum of the alignment of the nuclei creates a magnetic vector in the direction of $B_0$, creating the Z-axis or the longitudinal magnetization. Applying a radiofrequency (RF) excitation pulse, causes disturbance of the orientation of the nuclei, as some nuclei changes orientation in the opposite direction in the Z-plane (high-energy state), thereby

reducing the longitudinal magnetization. Furthermore, the nuclei starts to precess in phase, thereby creating a magnetic vector that precesses with the precession frequency in the X-Y-plane and a transversal magnetization is created. Thus, the magnetic vector has been "flipped" 90° (Figure 4).

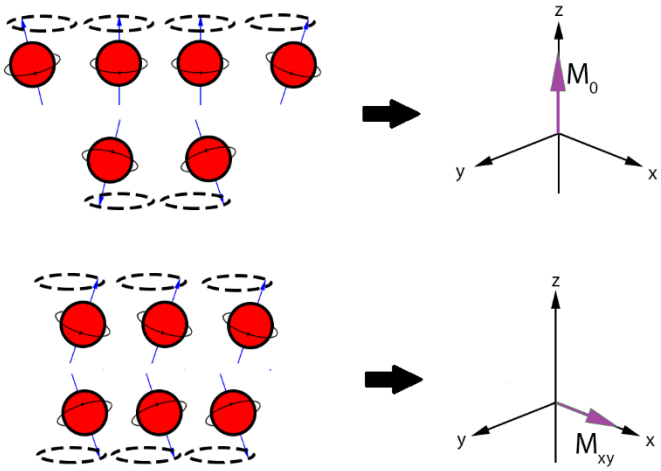


***Figure 4.*** *To the left: nuclei alignment and phase coherence during equilibrium (top) and excitation (bottom). To the right: direction of the magnetic vector (M).*

When the RF excitation pulse has stopped, the nuclei returns to the low-energy equilibrium state by two independent relaxation processes known as T1 and T2 relaxation (Figure 5):

**T1 relaxation**: The nuclei return towards the longitudinal equilibrium state, in which the obtained energy from the excitation pulse exchanged with the surroundings – or *the lattice*, thereby rebuilding the longitudinal magnetization. This exponential process is also known as the *spin-lattice relaxation* or longitudinal relaxation. The speed of this process is described by the tissue longitudinal relaxation time constant, T1, given in milliseconds (ms). The T1 relaxation time is defined as the time when 63% of the longitudinal magnetization has recovered.

**T2 relaxation**: Meanwhile, as the T1 relaxation occur, the nuclei get out of phase, thereby reducing the transversal magnetization, an exponential process also known as *spin-spin relaxation* as it depends the presence of random local magnetic fields created by neighboring nuclei. The speed of transverse magnetization decay is described by the transversal relaxation time constant, T2, given in ms, which is defined as the time when the transverse magnetization is reduced to 37%.

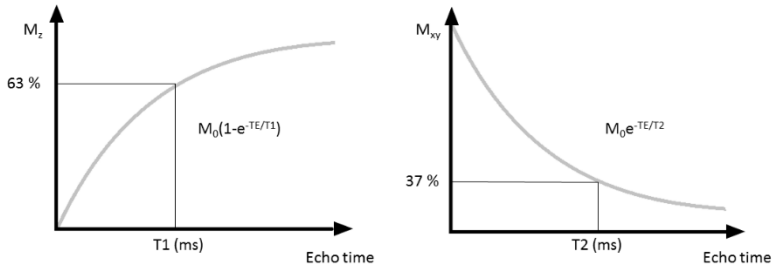


***Figure 5.*** *Left: T1 relaxation. Right: T2 relaxation*

In addition to the spin-spin relaxation, the transverse magnetization decay depends on local magnetic inhomogeneities within the external magnetic field causing the nuclei to get out of phase faster and thereby, shortens the decay of the transverse magnetization. The combined effect of T2 relaxation and relaxation due to magnetic field inhomogeneities is called the **T2* relaxation** (Figure 6). Thus, the T2* relaxation is shorter than the T2 relaxation (30). The relation between T2* relaxation and T2 relaxation can be described by the following equation:

$$1 / T2^* = 1 / T2 + 1 / T2' \qquad (1)$$

In which T2' is the relaxation caused by magnetic field inhomogeneities.

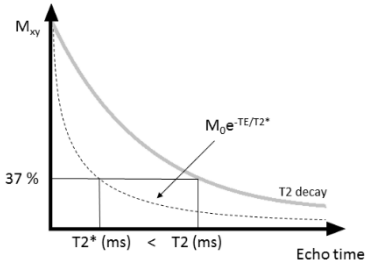


***Figure 6.*** *T2* relaxation (dashed line)*

The longitudinal and transverse relaxations are independent processes; however, they occur parallel thereby leaving a sum magnetizing vector (the sum of the longitudinal and transversal magnetization) to perform a spiraling motion during relaxation in which the obtained energy is released (Figure 7).

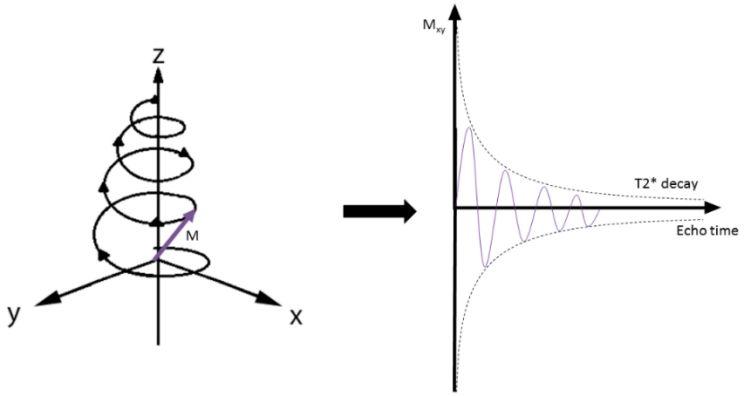


***Figure 7.*** *Left: the spiraling motion of the magnetic vector (M) during relaxation. Right: the corresponding free induction decay curve.*

During relaxation, the energy is released as RF pulses, also known as the *free induction decay* (FID), which represent the exponentially T2* decade of the magnetization. These signals cannot directly be transformed into MR images, as there is no spatial information in FID signals. For this purpose, the exact signal position in the X, Y, Z-plane has to be determine using frequency -, phase - and slice encoding gradients, respectively. Then using Fourier transformation, the signals can be assigned to a certain location, and the MR image can be constructed. In order to enhance the signal, a refocusing gradient (gradient-echo (GRE) MRI) or a 180° refocusing RF pulse (spin-echo (SE) MRI) can be applied, which refocuses the magnetization creating an echo of the signal, which is measured later.

**MRI sequence and sequence parameters**: The relaxation times are tissue specific constants that varies between tissues and pathology and as such, they are the primary source of tissue contrast in a MR image. The dominant source of tissue contrast in an MR image depends on the choice of MRI sequence and sequence parameters. An MRI sequence has a specific number, strength and timing of RF excitation pulses and gradients and the three main sequence parameters are:

- Repetition time (TR): TR is the time between two consecutive RF excitation pulses. A short TR increases the T1-weightning in the MR image.

- Echo time (TE): TE is the time between an RF excitation pulse and the echo. A long TE increases the T2/T2*-weighting in the MR image. In multiple echo sequences, several TE may be used between consecutive RF excitation pulses.

- Flip angle: The RF pulse flips the magnetic vector into the transversal plane, thereby reducing the longitudinal magnetization and increasing the transverse magnetization. The flip angle is the amount of rotation of the magnetic vector into the transversal plane and it can vary between 0 and 180° in MRI sequences depending on the magnitude and duration of the RF excitation pulse. A RF excitation pulse that tips the magnetic vector 90°, as illustrated in Figure 4, is called a 90° pulse. Reducing the flip angle produces less T1-weighting in the image.

### 2.3.2. T2*-WEIGHTED IMAGING

In T2*-weighted MRI, differences in T2* relaxation are the primary source of tissue contrast. As deoxyhemoglobin is a paramagnetic molecule, it induces local constant magnetic field inhomogeneities, which shortens the T2* decay. Therefore, T2*-weighted imaging is sensitive to tissue $sO_2$. This effect is also known as the Blood oxygen level dependent (BOLD) effect, which was discovered in 1990 by Ogawa et al. (173). In 1936, Pauling et al. (174), described the basic magnetic properties of deoxyhemoglobin and oxyhemoglobin. They revealed that the paramagnetic effects of deoxyhemoglobin are caused by the unpaired electrons of the heme groups. The unpaired electrons produce spin, and thereby pronounced magnetic susceptibility, which induces magnetic field inhomogeneities in a magnetic field. Oxyhemoglobin does not contain unpaired electrons, and therefore it does not induce these magnetic field inhomogeneities. Thus, during hyperoxia, the amount of deoxyhemoglobin and thereby the presence of local inhomogeneities, is reduced, which prolongs the T2* decay. On the contrary, during tissue hypoxia, the amount of deoxyhemoglobin is increased, which reduces the T2* decay. Due to these different magnetic properties, deoxyhemoglobin can be regarded as an intrinsic contrast agent.

The BOLD effect can be measured using T2*-weighted imaging and the effect is most pronounced on gradient recalled echo (GRE) sequences. Using these sequences, the imaging can be carried out by measuring signal intensities or by measuring the T2* relaxation time. In this thesis, the BOLD method refers to the dynamic assessment of changes in signal intensities, whereas the T2* method refers to measurement of absolute T2* values. In the following, a GRE sequence is described, and how the sequence is used in the BOLD method and in the T2* method.

**Gradient recalled echo (GRE) MRI sequence**

A GRE sequence is illustrated in Figure 8. In a GRE sequence, the MRI signal is refocused using magnetic field gradients, in which an uneven magnetic field (a gradient field) is superimposed on the existing magnetic field. When the gradient is turned on, the gradient field increases the amount of magnetic field inhomogeneities and the protons dephase, thus the transversal magnetization disappears. Then the gradient is switch off and on again in the opposite direction, thereby rephrasing the protons to some extent and the signal is enhanced. This enhanced signal is called a gradient recalled echo. The magnitude of this echo depends on the tissue T2* decay

as the reversal gradient fields do not neutralize the local magnetic inhomogeneities. Therefore, GRE sequences are sensitive to the presence of paramagnetic substances including deoxyhemoglobin. The extent of T2*-weighting in GRE MRI depends on the sequence parameters. Reducing the flip-angel and increasing the TR produces less T1 weighting, whereas longer TE produces more T2*-weighting.

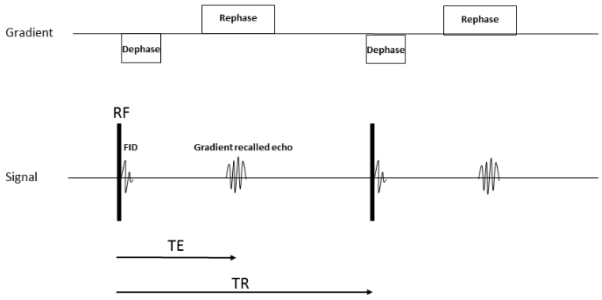


***Figure 8.*** *A GRE MRI sequence. Details are described in the text above.*

**Single-echo GRE – The BOLD method**

The BOLD method is carried out using a single-echo GRE sequence as described above. The magnitude of the echo signal can be simply described by the following equation:

$$S \propto M_0 e^{(-TE/T2^*)} \qquad (2)$$

In which S is the absolute BOLD signal, $M_0$ is the relaxed magnetization (or the equilibrium vector, Figure 4), TE is the echo time and T2* is the transversal relaxation time. The relaxed magnetization depends on multiple factors including 1) technical factors such as the magnetic field strength, sequence parameters, distance to the receiver coil, the shimming effects etc. and 2) baseline physiological factors such as tissue blood flow, blood volume, hydration, temperature, hematocrit, oxygenation and tissue compositions etc. (175,176). As these factors may vary between individuals, the absolute signal (S) cannot be directly inferred into tissue $sO_2$, neither can it be compared between individuals. Dynamic *changes* in the signal, however, as can be induced by varying the tissue $sO_2$ and thereby the T2* value in equation (2), are comparable between individuals. Thus, instead of comparing *absolute* BOLD signals, *relative* BOLD signal changes, given as a percentage of the baseline BOLD signal, are compared between individual.

**Multi-echo GRE – The T2* method**

The T2* value in equation (2) can be measured using a multi-echo GRE sequence. This sequence can be obtained within short breath-holds by reducing the flip-angels and the TR. In multi-echo GRE, additional opposing gradients are applied creating

multiple echo signals at varying echo-times. A multi-echo sequence with three TE's is illustrated in Figure 9.

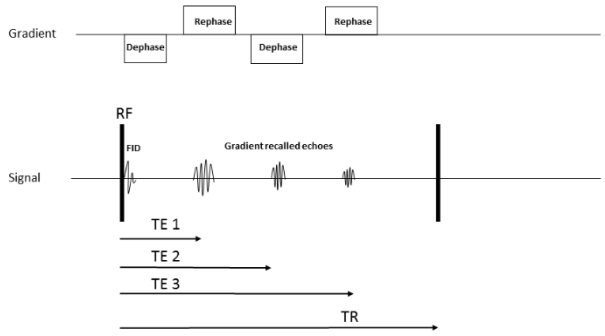


***Figure 9.*** *A Multi-echo GRE sequence. In this figure, three TE's are illustrated. Details are described in the text.*

Using this multi-echo GRE sequence, the T2* value of a tissue can be estimated as follows; for each TE the mean MRI signal of a ROI is plotted, and the mono-exponential decay function (equation (2)) is created as illustrated in Figure 10.

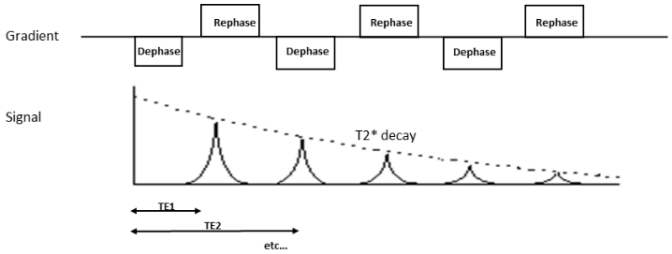


***Figure 10.*** *The mono-exponential decay function achieved using the multiple-echo MRI sequence (five TE's are illustrated).*

Using the multiple values of signal S at the varying TE, the equation (2) can be solved for T2* using a non-linear least squares fitting algorithm (177). Thereby, the tissue specific T2* value can be achieved. As this T2* value is calculated based on multiple signals at varying TE's with $M_0$ being a free parameter, it does not depend on the $M_0$ and therefore it can be compared between individuals. Thus, as opposed to the absolute BOLD signal, *absolute* T2* values can be compared between individuals. However, like the BOLD signal, the T2* value cannot directly be inferred into tissue $sO_2$ as the T2* value also depends on elements of tissue composition such as cell density, water content, surface areas etc. (the intrinsic T2 value, equation (1)) (178).

**Oxygen-challenge during placental T2*-weighted MRI**

As described above, changes in tissue $sO_2$ during oxygen-challenge can be depicted using T2*-weighted imaging. This has been demonstrated in several MRI studies with direct measurements of changes in oxygen contents during hyperoxia/hypoxia (179-184). Oxygen-challenge can be performed using a none-rebreather facial mask, in which exhaled gases are not rebreathed. During oxygen-challenge, the oxygen content of the blood rises. As arterial blood is nearly fully saturated during normoxia, oxygen-challenge increases the arterial $pO_2$ whereas it has little impact on arterial $sO_2$ according to the oxygen hemoglobin dissociation curve (185,186). Thus, the T2*-weighted MRI signal of arterial blood is sparsely affected during oxygen-challenge. On the contrary, in venous low-saturated blood, the additional oxygen binds to deoxyhemoglobin, thereby increasing the venous $sO_2$ whereas the change in venous $pO_2$ is relatively small. Thus, during oxygen-challenge, the T2*-weighted MRI signal within venous, low-saturated blood is increased.

Within the placenta, changes in T2*-weighted MRI signal during maternal oxygen-challenge may arise from increased $sO_2$ within the low-saturated maternal venous blood in the periphery of the intervillous space as well as from increased $sO_2$ of the low-saturated fetoplacental blood. The increased $sO_2$ of the fetoplacental blood can be explained by the increasing $pO_2$ gradient across the placental membrane during oxygen-challenge driving the simple diffusion of oxygen towards the fetoplacental blood, thereby increasing the $sO_2$ (187,188). Different methods have demonstrated increased fetoplacental oxygen content during maternal oxygen-challenge. These methods include for instance invasive studies of the rhesus monkey (188) and the sheep (179,189), blood gas analysis of the human umbilical cord blood obtained by cordocentesis in growth-restricted pregnancies (190) and human MRI methods (191,192). Although, changes in placental T2*-weighted MRI signal during maternal oxygen-challenge may arise from increased placental $sO_2$, one should keep in mind that changes in other parameters during oxygen-challenge may affect the T2* value, and thereby the MRI signal. Such factors may include changes in placental blood flow and blood volume, both of which affect the amount of deoxyhemoglobin within a voxel (183). Therefore, using the BOLD method or the T2* method, MRI changes during oxygen-challenge cannot be directly inferred into quantitative changes in $sO_2$. Moreover, using the dynamic BOLD method, in which signal changes are measured in relative values, baseline conditions affecting the baseline signal, such as baseline oxygenation, blood flow, blood volume, tissue morphology etc., may modulate the BOLD response amplitude (176,193,194). These factors needs to be considered when interpreting changes in placental T2*-weighted signals during oxygen-challenge.

**Previous studies on placental T2*-weighted imaging**

Placental T2*-weighted imaging has been performed in animal studies (58,181,195-198) and in a few human studies (59,199) in order to investigate the placental oxygen environment. Moreover, the T2*-weighted methods have been used in several animal and human fetal studies (179-181,191,192,196,197,200-207). In normal human

pregnancies, Huen et al. (199) demonstrated a significant increase in placental T2* value during maternal oxygen-challenge, whereas neither this increase nor the normoxic T2* value was found to be correlated with gestational age. Using the dynamic BOLD sequence, Sorensen et al (59) demonstrated a significantly increase in placental BOLD response during oxygen-challenge. The authors suggested that the increased BOLD response represented increased fetoplacental $sO_2$. Prior to this thesis, no T2*-weighted placental studies were published in human pregnancies complicated by placental dysfunction. However, in rat FGR models induced by ligation of one uterine artery, it has been demonstrated that the BOLD response during oxygen-challenge is significantly reduced (196,197).

**MRI $B_0$ inhomogeneity and susceptibility artefacts in T2*-weighted imaging**
Several types of MRI artefacts exist and they may interfere with the MRI results. Using T2*-weighted imaging, $B_0$ inhomogeneity and magnetic susceptibility artefacts need to be considered. An exceptionally homogenous static magnetic field is required for MRI, especially at the core of the scanner. Placing a patient within the MRI scanner reduces the overall homogeneity of the magnetic field, especially peripherally. The reduced homogeneity can partly be compensated by shimming of the magnetic field (208). Moreover, local magnetic inhomogeneities near interfaces of tissues may exist due to different magnetic susceptibility within the tissues, i.e. due to differences in the extent to which the tissue becomes magnetized when placed within a magnetic field. Thus, local inhomogeneities may occur near the interface of bone-soft tissues and tissue-air interfaces or by the present of metallic implants etc. Such local inhomogeneities shortens the dephasing of spins and thereby reduce the signal and the T2* value (209). The artefacts may be detected as image distortions or localized signal drop-outs due to this T2* shortening. Susceptibility artifacts increase with the main magnetic field strength; thus, they are more pronounced at 3T compared to 1.5T (210). GRE sequences are especially prone to the susceptibility artefacts, as they do not have a 180° refocusing pulse to compensate for magnetic field inhomogeneities. Moreover, the use of long echo times increases the risk of these artefacts. Different techniques can be used to reduce susceptibility artefact. The use of 1.5T rather than 3T scan system, shorter TE and optimization of the shimming of the magnetic field reduce the presence of these artefacts. In addition, it is also recommended to use a central position of the ROI in the xy- and z-plane.

## 2.4. ETHICAL CONSIDERATIONS

### 2.4.1. SAFETY IN MRI

Identifying potentially hazardous effects of MRI during pregnancy is an ongoing subject of investigation. The main areas of concern are related to the static magnetic field ($B_0$) and the time-varying magnetic field gradients during the MRI acquisitions used for spatially encoding of the MRI signals and the RF pulses used for the

excitation of protons. To date, no human studies have shown any association between MRI and adverse fetal outcome (211-215).

**The static magnetic field**

Potential hazardous effects associated with the exposure of patients to strong static magnetic fields have been investigated in several studies and they have been reviewed comprehensively, among others, by the International Commission on Non-Ionizing Radiation Protection (ICNIRP) (216-218). The static magnetic fields may interact with biological tissues and organisms through various physical mechanisms (219). One important mechanism is magnetic induction, which may originate from the interaction with moving electrolytes in blood vessels, thereby creating electric currents. These currents may induce voltages across the membranes, which potentially may reduce blood flow velocity and affect the heart rate and rhythm (220,221). Studies using cardiotocography during MRI at 1.5T have showed no effects on the fetal heart rate (222,223). Another important mechanism is a magneto-mechanical effect, which induces reorientation of paramagnetic and diamagnetic molecules in order to align their magnetic orientation with the magnetic field. However, as human tissue does not contain strong ferromagnetic components and has extremely small values of magnetic susceptibility, magneto-mechanical forces are considered too small to affect human tissue in vivo. According to a review by the ICNIRP, no consistent effects of static magnetic field exposure on reproduction and development have been seen in mammalian species (218). However, animal studies have been conflicting, as some concerns have been raised regarding fetal growth restriction in mice studies. This adverse effect has never been demonstrated in human pregnancy (224).

**Time-varying magnetic fields**

Like the static magnetic field, the magnetic gradient fields used for spatial encoding of the MRI signal also induce electrical fields and currents with frequencies below 100 kHz. In this frequency range, the currents may induce voltages across the membranes, which potentially may stimulate nerve cells. The primary concern is the potential effect on the heart rate and rhythm. However, as mentioned above, no studies have demonstrated any effects on the fetal heart rate.

The rapid alternations of the magnetic gradient fields during the MRI acquisition produces noises in the range from 80 to 120 dB (225). Therefore, it is recommended to offer hearing protection to the patient. Most likely, the fetus is protected by the maternal abdomen and by the amniotic fluid, which reduces fetal noise exposition with at least 30 dB (226). Follow-up studies of infants exposed to MRI prenatally have demonstrated no adverse effects on hearing (213-215).

**Radiofrequency fields**

The RF pulses used for the excitation the protons typically have frequencies above 10 MHz, and therefore they do not induce voltage across cell membranes. Rather instead, they deposit heat within tissues. During MRI acquisition, a SAR value (Watt/kg) will

estimate the amount of thermal energy conducted to the tissues. According to the recommendations by the ICNIRP the whole body SAR value should be kept below 2 W/kg during a one hour scan, equivalent to a rise in adult tissue temperature of 0.5°C and a rise of fetal temperature to less than 38°C (227). Numerical simulations of SAR and temperature changes in a pregnant human model at 1.5T and 3T MRI scanners have been performed (212). The results suggest that for MRI procedures carried out under normal mode conditions such that the maternal whole-body SAR is ≤2 W/kg, fetal whole-body SAR is 1.24 and 1.14 W/kg at 64 and 128 MHz, respectively. Furthermore, the average temperature of the fetus remains below 38°C. Thus, these results are in line with the recommendations by ICNIRP. Moreover, changes in fetal temperature have been investigated using fiberoptic probes in pregnant pigs during a Fourier single-shot turbo spin-echo (HASTE) sequence (228). This sequence has the potential to generate more heat than traditional sequences; however, no significant changes in temperature were measured in the fetal brain, abdomen or amniotic fluid.

In summary, no evidence of adverse fetal effects to MRI at low field strength has been demonstrated. Nonetheless, proper precautions as stated by the ICNIRP (227) must be taken, in particular in the first trimester in which the rapidly dividing cells are thought to be particular vulnerable.

### 2.4.2. OXYGEN-CHALLENGE

In most obstetric units maternal oxygen supply is standard treatment in case of fetal bradycardia during labor (229,230) and supplementary maternal oxygen is a standard procedure before elective and emergency caesarian section (231,232). One area of concern in relation to these procedures has been the potential vasoconstrictive effect of oxygen. Several Doppler ultrasound studies have shown that short-term oxygen supply has no effect in uncompromised fetuses (233-235). Likewise, using MRI, it has been demonstrated that short-term maternal oxygen supply does not alter fetal brain oxygenation in uncompromised fetuses (191,236). In compromised fetuses, maternal oxygen supply can normalize fetal movements and brain sparring, whereas in severely compromised fetuses, oxygen supply may have no effects on fetal movements or Doppler flows (235,237). Studies on the fetal heart rate in growth-restricted fetuses during maternal oxygen supply has shown an increasing number of accelerations and increasing variability (238,239). Bekedam et al. found a significant increase in number of fetal heart rate deceleration in growth-restricted fetuses after discontinuation of the maternal oxygen supply (239), observations that could not be confirmed by Kyank et al. and Bartnicki et al.(238,240).

# CHAPTER 3. AIM OF THE THESIS

The overall purpose of this project was to investigate the feasibility of T2*-weighted MRI as a non-invasive method for detection of placental hypoxia and thereby placental dysfunction.

The specific aims of the studies in the project were:

Placental T2* measurements:

- To evaluate the reproducibility of placental T2* measurements (*Study I*).
- To investigate the T2* value in normal pregnancy and in those complicated by placental dysfunction (*Study I*).
- To investigate and compare the performance of placental T2* and the UtA PI in the prediction of low birth weight (*Study IV*).

Placental BOLD MRI

- To investigate the relative ΔBOLD response during oxygen-challenge in normal pregnancy and in those complicated by placental dysfunction (*Study II and V*).
- To evaluate the presence of spontaneous uterine contractions during BOLD MRI and their placental physiological effects (*Study III*).
- To interpret the relative ΔBOLD response using placental T2* estimates of placental baseline conditions, including baseline oxygenation and tissue morphology, in normal pregnancies and in those complicated by placental dysfunction (*Study V*).

# CHAPTER 4. MATERIAL AND METHODS

## 4.1. GENERAL STUDY POPULATION

Study I-V are based on an original cohort of 128 singleton pregnancies recruited at the Aalborg University Hospital during 2011 and 2016 (Figure 11). We included women > 18 years of age, carrying singleton pregnancies with no fetal malformation or abnormal karyotype. Women with preexisting diabetes or gestational diabetes, BMI > 34 (for technical reasons), severe claustrophobia or contradictions to MRI were not included. Oral and written informed consents were obtained from all participating women. The project was approved by the Regional Committees on Biomedical Research Ethics (Journal number M-20090006 and N-20090052) and reported to the Danish Data Protection Agency (2008-58-0028).

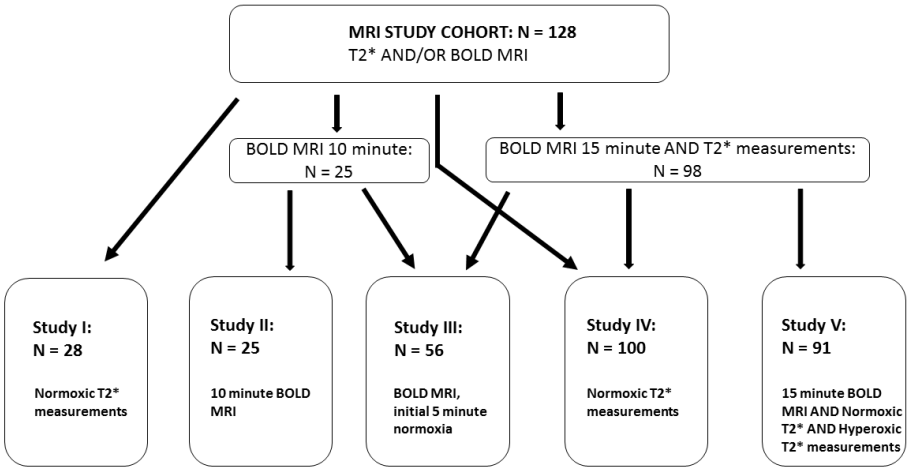


***Figure 11.*** *Flow chart of the MRI study population.*

A subset of the 128 women underwent repeated MRI examination in order to investigate the reproducibility of the T2* method (*study I)*, and another subset of the 128 women underwent repeated MRI examination within weeks in order to obtain longitudinal MRI data (not reported in this thesis).

## 4.2. STUDY DESIGNS AND POPULATIONS IN STUDY I-V

**Study I**
This T2* study was a cross-sectional study, in which placental T2* was investigated in 24 uncomplicated pregnancies at 24 - 40 weeks' gestation. Furthermore, we included four cases with EFW Z-scores < -3.5 (134) at the time of MRI (24-31 weeks' gestation). Case 1 had normal ultrasound Doppler findings, whereas case 2, 3 and 4 had abnormal Doppler PI in the UA (Z-score > 2.0 (241)) and in the MCA (Z-score < -2.0 (241)) and in case 4, even the DV PI was increased (Z-score > 2.0 (242)). Doppler findings were normal in the uncomplicated pregnancies. Placental T2* analysis was performed prospectively at the time of MRI, thus the neonatal outcomes were not known at the time of the T2* analysis. The reproducibility of the T2* methods was also investigated. In the group of uncomplicated pregnancies, a subset of the women (n = 16) underwent repeat T2* scan after 2 minutes while the women remained on the board in the same position. In a subset of these 16 women (n = 8), the placental T2* was repeated in a separate session after a 45-minute interval in which the women left the MRI suite. In this study, normal birth weight was defined by a Z-score > -2.0 (134). Placental pathological examination was performed in the four cases.

**Study II**
This BOLD study was also a cross-sectional study, in which placental BOLD MRI was investigated in 21 uncomplicated pregnancies at 24 - 40 weeks' gestation (33 ± 5, mean ± SD). Moreover, we included four cases with EFW Z-score < -3.5 at the time of MRI (24-31 weeks' gestation). These pregnancies also participated in *Study I*. Unfortunately, the case numbering was changed. Thus, in this study, case 1, 2 and 3 had abnormal UA and MCA Doppler findings at the time of MRI. In case 1, the DV PI was also increased, whereas this figure was normal in case 2 and 3. Case 4 and the 21 uncomplicated pregnancies had normal Doppler findings. Placental BOLD MRI analysis was performed by one single observer, who was not blinded to the neonatal outcomes. Normal birth weight was defined by a Z-score > -2.0. Placental pathological examination was performed in the four cases.

**Study III**
In this BOLD study, we aimed to investigate the presence of spontaneous uterine contractions during BOLD MRI scans. It was a cross-sectional study, in which we analyzed the 5-minute normoxic placental BOLD MRI of 56 uncomplicated pregnancies with normal neonatal outcomes including normal birth weight defined by a Z–score > -2.0. At the time of MRI (23 - 40 weeks' gestation), ultrasound EFW and Doppler findings were normal.

**Study IV**
In this T2* study, we investigated the relation between placental T2*, UtA PI and birth weight, and we compared the performance of T2* and UtA PI in the prediction of low birth weight defined by a Z-score ≤ - 2.0. Secondary outcome was abnormal

placental pathological findings. It was a prospectively observational study, in which 100 pregnancies attending for routine or specialist examination were included at 20 - 40 week's gestation. The study population was mixed regarding the risk of low birth weight based on the ultrasound EFW. At the time of inclusion, 68 out the 100 pregnancies had an EFW > -15%, whereas 32 had an EFW ≤ - 15%. Out of these 32 pregnancies, five had an elevated UA PI. At the day of MRI (20-40 week's gestation), an additional ultrasound examination was performed, including measurement of the UtA PI.

**Study V**

In this study, we aimed to interpret the relative ΔBOLD response by using placental T2* estimates of placental baseline conditions in normal pregnancies and in those complicated by placental dysfunction. Originally, we included 68 normal, uneventful pregnancies with normal neonatal outcome including normal birth weight at term defined by a Z-score > -1.28 (> - 15%), and 23 cases defined by a birth weight Z-score ≤ -1.28. In order to reduce the risk of mixing normal and dysfunctional placentas, the results of placental pathological examinations were included. In 17 out of the 23 cases, placental examination revealed signs of PVM, whereas the remaining six placentas were normal, and therefore these six cases were excluded. As a part of the study protocol, placental pathological examination was also performed in 31 of the 68 normal pregnancies. In four of these, signs of PVM was demonstrated and consequently, those were excluded. Thus, 64 normal pregnancies and 17 cases remained in the study for further analysis.

## 4.3. METHODS

### 4.3.1. STUDY I–V: ULTRASOUND EXAMINATION

At the time of MRI (+/- 1 day), an ultrasound examination was performed using a Voluson E10 ultrasound system (GE Healthcare, Kretz Ultrasound, Zipf. Austria). The examination included an EFW, measurement of the amniotic deepest vertical pocket and Doppler assessment of the UtA, UA and the MCA including the CPR. In cases with abnormal UA PI and MCA PI, the DV flow velocity was also assessed. The EFW was calculated based on the head circumference, abdominal circumference and femur length (243). The UtA PI was measured at the point where the UtA crosses the external iliac artery. The mean PI of the left and right UtA and the presence of diastolic notch was reported. The UA PI was measured in a free-floating mid-portion of the umbilical cord, and the MCA PI was obtained in the proximal section at the level of the circle of Willis. The DV flow velocity was assessed either in a mid-sagittal longitudinal plane of the fetal trunk or in an oblique transverse plane through the upper abdomen.

### 4.3.2. STUDY I-V: MRI EXAMINATION

The placental MRI examinations were all performed in a GE Discovery MR450 1.5-Tesla MRI System (GE Healthcare, Milwaukee,WI, USA). The pregnant women were placed in left lateral position in order to avoid aortocaval compressions by the uterus. Hearing protection was provided for the women and a cardiac receiver coil was placed on the abdomen, covering the uterus. Initially, T2-weighted localizer images in three planes were obtained in order to determine the anatomical position of the placenta. In order to obtain the placental imaging near the center of the magnet, the women was repositioned if the placenta was not located near the magnetic isocenter. From the localizer images, placement of placental slices was determined in order to obtain a transversal view of the placenta (Figure 12). This orientation of placental slices was used in all the MRI sequences in the MRI protocol.

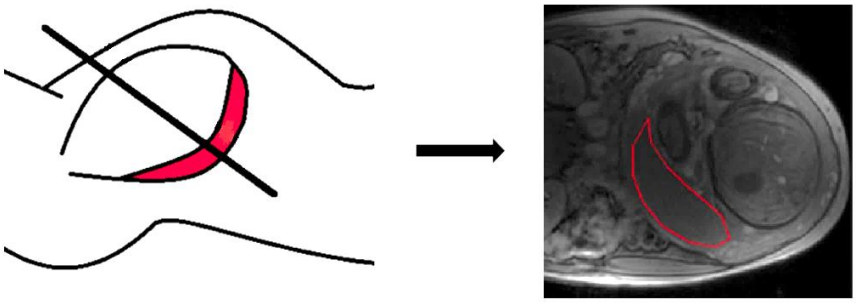

***Figure 12.*** *Placement of a placental slice. To the right: T2*-weighted image. Placenta marked in red.*

After the localizer images and slice set-up, the MRI acquisition was performed according to the protocol as illustrated in Figure 13. A FIESTA sequence (Fast Imaging Employing Steady-state Acquisition) and a diffusion-weighted MRI (DWI) were obtained for other studies not reported in this thesis. The average scan time was 35 minutes, which was well tolerated by the women. In a minor subset of the women, the BOLD sequence and T2* map during oxygen-challenge were not performed due to time constraints.

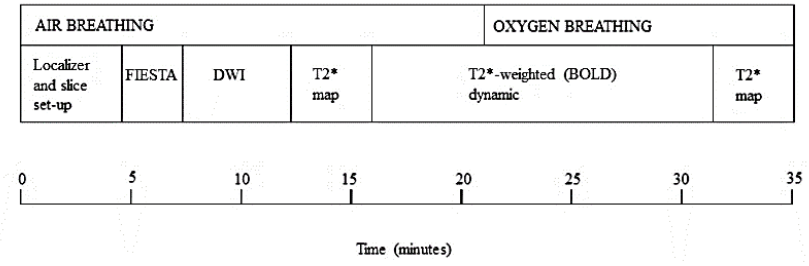


***Figure 13.*** *The MRI acquisition protocol.*

**T2* acquisition (Study I, IV-V)**
Placental T2* measurements were performed using a multi-echo GRE sequence with the following parameters: TR = 70.9ms; 16 echoes ranging from 3.0 to 67.5ms in steps of 4.3ms; flip-angel 30°, field of view, 350×350 mm; and matrix, 256×128 mm. The size of the matrix resulted in an in-plane resolution of 1.37×2.73 mm. In *Study I*, two 8 mm central placental slices with a slice gap of approximately 2 cm were obtained. As the reproducibility of the T2* values was increased by averaging the T2* values in each slice (*Study I)*, the MRI protocol was changed, and thus three placental slices were obtained in *Study IV-V*. Each slice was acquired in a single breath-hold of 12 seconds during normoxia and during oxygen-challenge.

**BOLD MRI acquisition (Study II-III, V)**
The BOLD MRI was acquired using a dynamic single-echo GRE MRI sequence with the following parameters: TR = 8000 ms, TE = 50 ms, flip-angle = 90. Field-of-view of 36x36 cm with a matrix of 128x128 which resulted in an in plane spatial resolution of 3.6x3.6 mm. Multiple slices (thickness of 6 mm, no spacing) covering the entire uterus were obtained, thus the number of slices varied according to the size of the uterus. Each slice was repeated every eighth second.

During the initial 5-minute BOLD MRI, the women breathed normoxic air. Then a non-rebreather facial mask (Hudson Respratoty Care, Durham, NC) was applied, while the women remained in the same position on the board, followed by medical oxygen challenge (100% $O_2$) delivered at a flow rate of 12 L/min. In *Study II, a* 5-minute oxygen-challenge was performed. However, these data indicated that this time period was too short in order to achieve steady state hyperoxic levels in some dysfunctional placentas. Therefore, the oxygen-challenge period was prolonged to 10 minutes in the *Study V.*

### 4.3.3. MRI ANALYSIS
The MRI Dicom data were processed using an in-house developed program written in MatLab (The MathWorks Inc., Natick, MA, USA).

**T2* analysis (Study I, IV-V)**
In each placental slice, a ROI covering the entire placenta was drawn and the placental T2* values were estimated from the mean signal intensities within the placental ROI as a function of echo time using a non-linear least squares fitting algorithm (Figure 14).

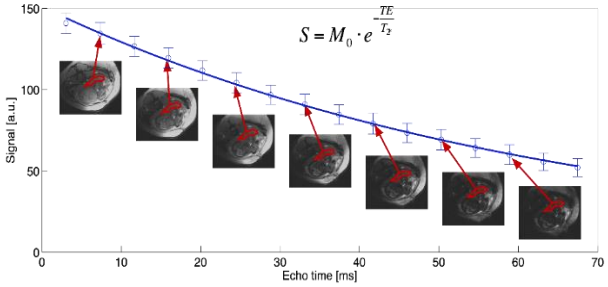


***Figure 14.*** *The T2* analysis (244)*

The T2* value was reported as the mean of the acquired placental slices. In case of placental susceptibility artefacts (Figure 15), the T2* dataset was excluded.

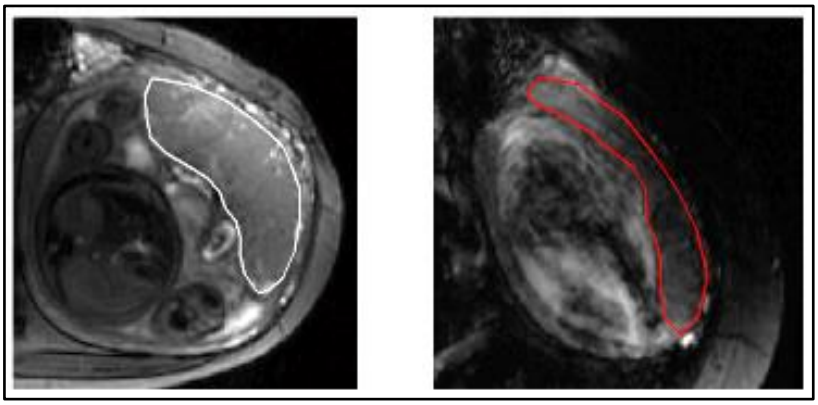

***Figure 15.*** *Placental T2*-weighted images at TE 30. To the left: no placental artefacts, placenta marked in grey. To the right: severe susceptibility artefact (dark blurring) covering a large part of the placenta (marked in red).*

In *Study I*, the reproducibility of the T2* method was assessed including repeat T2* measurements as described in the Chapter 4.2. In that study, we also assessed the inter-observer reproducibility of the ROI drawings as the ROIs were drawn by two independent observers. Furthermore, we investigated the variation of T2* values between two parallel placental slices.

In *Study V*, changes in placental T2* values during oxygen-challenge (ΔT2*) were estimated and used in the interpretation of the oxygen-challenge ΔBOLD response. The ΔT2* was estimated as:

$$\Delta T2^* = T2^*_{\text{hyperoxic}} - T2^*_{\text{baseline}} \quad (3)$$

Other T2* MRI analysis methods were investigated (unpublished). As the placenta has varying fractions of maternal and fetal compartments, we considered if division of the MRI ROI into two layers, would improve the accuracy. However, in these T2*-weighted images, often it was difficult to distinguish between the two compartments, especially in dysfunctional placentas and in early normal pregnancy. Thus, we experienced that separate ROIs reduced the accuracy of the method. Furthermore, we considered calculation of T2* as an average of the ROI based on pixel by pixel T2*. However, we experienced that low signal-to-noise ratio as well as minor movements made these calculations less accurate as compared to the T2* value based on the signal average of the ROI.

**BOLD MRI analysis (Study II, III, V)**

Placenta BOLD signal was investigated in three placental slices evenly distributed in the placenta. Within each slice, a ROI covering the entire placenta was drawn. In each frame, this ROI was adjusted in order to correct for maternal movements including uterine contractions ensuring that the placental borders were not crossed. BOLD signal (mean of the three slices) versus time curves were made. As discussed in Chapter 2.3.2, the *absolute* BOLD signal cannot be compared between individuals. Therefore, we then normalized the BOLD signal using a 2-3 minute normoxic steady state BOLD signal levels ($S_{baseline}$):

$$\text{Normalized BOLD Signal (X)} = S_x/S_{baseline} \times 100\% \quad (4)$$

In case of a uterine contraction reducing the BOLD signal during the normoxic period, the steady state level was defined from a steady state time interval prior to or after the contraction. Normalized BOLD signal versus time curves were then created (mean of the three slices), and the oxygen-challenge steady state level was defined as a 2-3 minute steady state level during the final 5-minute oxygen-challenge. The relative change in BOLD signal (ΔBOLD response) was then calculated as

$$\Delta\text{BOLD response} = (S_{hyperoxic} - S_{baseline}) / S_{baseline} \times 100\% \quad (5)$$

In case of uterine contractions preventing estimation of normoxic or hyperoxic steady state levels (steady state period < 1 minute), the BOLD dataset was excluded.

In *Study III*, only the initial 5-minute normoxic BOLD MRI was analyzed. Using equation (4), we created normalized placenta BOLD signal versus time curves (mean of the three slices). Moreover, we assessed the MR images regarding changes in the uterine shape and placental volume during the 5-minute MRI. Figure 16 illustrates the placental slices used for these analyses.

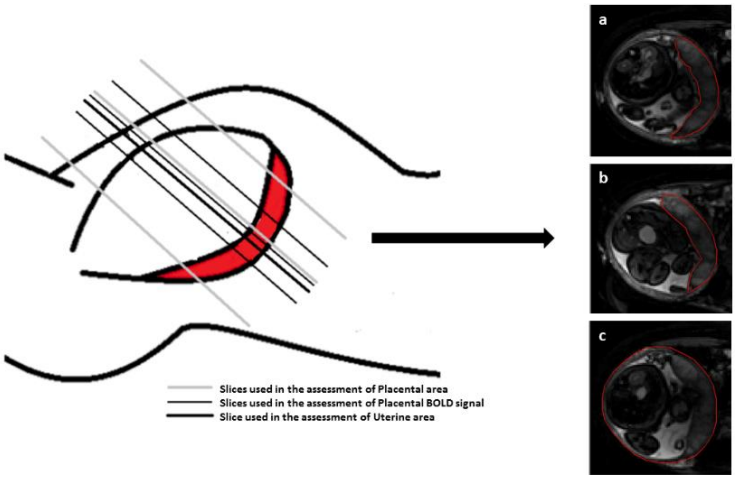


***Figure 16.*** *Slice placements during MRI. To the left: slices used for the assessment of placental area, placental BOLD signal and uterine area. To the right: examples of ROIs onto BOLD MR images: a) placental area ROI, b) placental BOLD signal ROI, c) uterine area ROI (245)*

In order to assess changes in the uterine shape and placental volume during the MRI scan, we used a manual segmentation method. In the 56 MRI scans, ROIs were drawn covering the outer border of the uterus and the placenta. In each frame, the ROIs were manually adjusted in order to correct for movements. The area of the ROI could then be estimated by the number and size of the pixels within the ROIs. In the placenta, three ROIs (one central and two peripherally, Figure 16) were assessed enabling an estimation of changes in placental volume rather than placental area. Due to time-constraints, only one central slice was used in the assessment of changes in the uterine shape. Time curves of the normalized BOLD signal and pixel numbers within the uterine and the placental ROIs were then created in order to investigate the timely relation between changes in the three figures.

In *Study V*, the relative changes in BOLD signal during oxygen-challenge was interpreted using the T2* measurements based on the following approximation:

$$\Delta\text{BOLD response} \approx \Delta T2^* / T2^*_{\text{baseline}} \qquad (6)$$

### 4.3.4. PLACENTAL PATHOLOGICAL EXAMINATION

The original project protocol did not include placental pathological examination in uncomplicated pregnancies, as pathological examination in these pregnancies is not a part of our routine practice. Thus, in *Study I-III* placental pathological examination was only performed in pregnancies complicated by placental dysfunction. However, during the project period, the protocol was changed, thereby also including placental pathological examination in the uncomplicated pregnancies. Thus, in *Study IV and V*, placental pathological examination was also performed in a large proportion of the uncomplicated pregnancies. An experienced placental pathologist, who was blinded

to any MRI results but not to the clinical information, performed the examinations. They were performed according to the standard protocol described in Chapter 2.2.1 including standard sections taken for microscopy (85). Placental trimmed weights were measured after removing the membranes, the umbilical cord and excessive blood (246). In the studies in this thesis, only pathological signs of PVM, defined as signs of MVM and/or FVM (85), were reported.

## 4.4. STATISTICAL ANALYSIS IN STUDY I-V

In each study, the assumptions behind the statistical tests were assessed, including the distributions of variables, which were examined using probability plots and Shapiro-Wilk test. Gestational age-adjusted Z-scores of MRI variables were calculated by subtracting the expected MRI value from the measured value and divided by the standard deviation at the given time in gestation. The statistical software package Stata®14 (StataCorp LP, College Station, TX, USA) was used for the data analysis. P-values $< 0.05$ were considered statistically significant.

**Study I**
In the 24 normal pregnancies, the association between placental T2* and gestational age was examined using a regression analysis. From this model, the T2* values of the four cases were converted into Z-scores. The inter-observer reproducibility, the T2* variation between two parallel placental slices, and the reproducibility of repeat measurements were investigated using Bland Altman plots.

**Study II**
In each of the 25 pregnancies, the significance of the increase in BOLD signal was tested using a paired t test. In the normal group ($n = 21$), the mean ΔBOLD response was estimated (mean ± SD).

**Study III**
In the uterine contraction study, the significance of a reduction in normalized placenta BOLD signal was tested against the steady state BOLD signal level using a paired t test. We defined the maximum reduction in BOLD signal as the lowest measured signal value. Likewise, we tested the maximum reductions in the number of pixels in the uterine and placental ROIs against the steady state levels, defining the maximum reductions as the lowest measured number of pixels within the ROIs. The mean timely delay between changes in the three figures were also assessed (mean ± SD).

**Study IV**
Placental T2* values were converted into gestational age-adjusted Z-scores using the T2* regression model obtained in *Study I*. The associations between Z-scores of birth weight, placental T2* and UtA PI were investigated using linear regression models.

The performance of T2* and UtA PI in prediction of low birth weight were assessed and compared using receiver operating characteristics curve (ROC) analyses (247).

**Study V**

In the normal pregnancies, the associations between the ΔBOLD response and T2* figures and gestational age were assessed using linear regression analysis, and from the obtained regression models, the MRI figures were converted into gestational age-adjusted Z-scores. The mean Z-score values of the MRI figures were compared between groups using a Student's t test or unequal variance t test. Among all the pregnancies, the ΔBOLD response was not normally distributed, and therefore this figure was logarithmically transformed which achieved normality. We then investigated the association between the logarithmically transformed ΔBOLD response ($Log_{10}$BOLD) and normoxic T2* value using a regression analysis.

# CHAPTER 5. SUMMARY OF RESULTS

In the following section, a summary of main results in each study is presented. Detailed descriptions of results are available in the published papers.

## 5.1. STUDY I

In this T2* study, the 24 normal pregnancies were all clinically uneventful and had normal neonatal outcomes including birth weight Z-score > -2.0, and gross placental findings were normal. In the four cases, birth weight Z-scores were below -2.0. In the three cases with abnormal Doppler findings, placental pathological examination revealed signs of PVM, whereas no signs of PVM were demonstrated in the fourth case (further description of the four cases are available in Table 1, Paper I).

In normal pregnancies, a significant positive linear association between placental T2* and gestational age was observed ($r = 0.83$, $p < 0.001$), with a reduction in placental T2* of 4.6 ms per gestational week (Figure 17). In the three cases with abnormal Doppler findings and placenta pathological signs of PVM, the placental T2* Z-scores were significantly lower (Z-scores < -3.8), whereas the T2* Z-score in the fourth case with normal Doppler flows and no signs of PVM, was normal (Z-score of – 0.34).

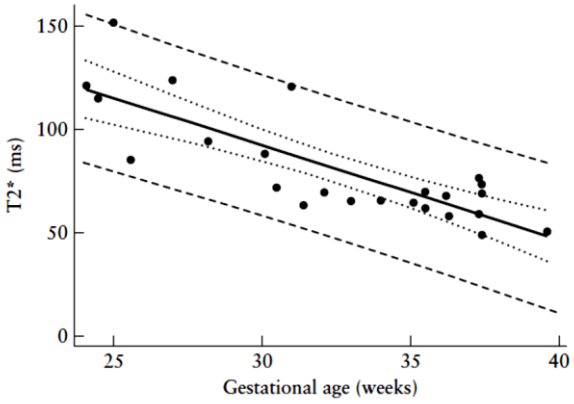


***Figure 17.*** *The linear relation between placental T2* (mean of two slices) and gestational week. Thick line is ordinary least squares fit (P < 0.001. $R^2 = 0.68$). Dotted lines indicate 95% confidence interval while dashed lines indicate 95% prediction interval (244).*

The reproducibility assessment of the method, investigated in the normal pregnancies, revealed 95% limits of agreement for the within- and between-session variation for a single slice of -2.1 ± 10.4ms and -0.6 ± 22.6ms, respectively. For the mean value of

two slices, the agreements were -1.1 ± 7.0ms and -0.0 ± 17.8ms. The agreement between two paralleled placental slices was -1.1 ± 17ms (Bland Altman plots illustrated in Figure 3, Paper I) and the inter-observer agreements of the ROI drawings were -0.1 ± 4.6ms.

## 5.2. STUDY II

In this BOLD study, the 21 normal pregnancies were all clinically uneventful and had normal neonatal outcomes including normal birth weights and normal gross placental findings. Case 1 with abnormal Doppler flows, including an increased DV PI, resulted in still birth at 26 weeks' gestation. Case 2 and 3 with abnormal UA and MCA Doppler findings resulted in acute cesarean section at 29 and 31 weeks' gestation due to fetal distress. In case 4, with the normal Doppler findings, an elective cesarean section was performed in gestational week 34 due to a very small EFW of -39%. Placental pathological examination demonstrated signs of PVM in case 1, 2 and 3, whereas no signs of PVM were demonstrated in case 4. In the four cases, birth weight Z-score was < -2.0. (Further description of the four cases are available in Table 1, Paper II).

In each of the 21 normal pregnancies, we observed a significant increase in the BOLD signal during oxygen-challenge. In this group, the mean ΔBOLD response was 12.6 ± 5.4%, $p < 0.0001$. Figure 18 illustrates the differences in placental BOLD signal during normoxia and hyperoxia. During oxygen-challenge, the placenta appeared brighter and more homogenous.

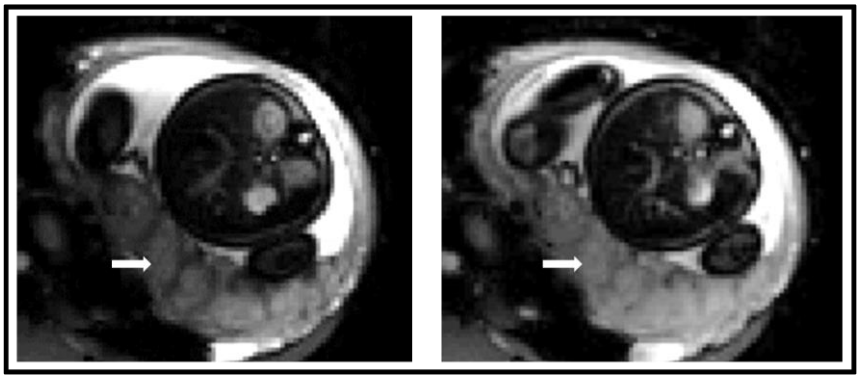

***Figure 18.*** *Placenta BOLD MR images in a normal pregnancy at 36 weeks' gestation. Cross-section through the central part of the placenta during normoxia (left) and during maternal oxygen-challenge (right). Placenta marked with white arrows.*

In the four cases, opposing BOLD results were demonstrated (Figure 19). In case 1, with the increased DV PI, we could not demonstrate a significant increase in the

BOLD signal during the oxygen challenge (ΔBOLD response of 0.1%). In case 2 and 3, we observed very high ΔBOLD responses of 26.8% and 29.5%, respectively. In case 4, with the normal Doppler findings, the ΔBOLD response was 13.4%.

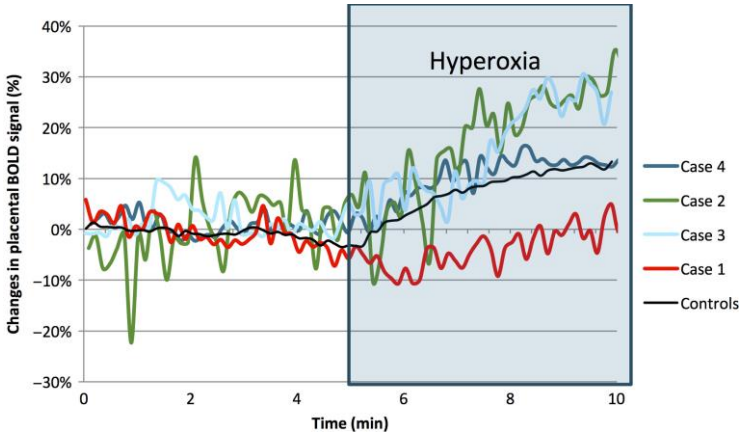


***Figure 19.*** *The mean ΔBOLD response in 21 normal pregnancies and the ΔBOLD response in each of the four cases (248).*

## 5.3. STUDY III

Spontaneous uterine contractions were observed in eight out the 56 5-minute BOLD MRIs (14.2%). These eight pregnancies were between 23 and 37 weeks' gestation at the time of MRI. During the contractions, the BOLD signal was significantly reduced by 17 ± 5%. This was clearly visible in the MRI scan as the placenta appeared darker. In each case, the reduction in BOLD signal was preceded by a remarkably change in the uterine shape, which could be assessed by a reduction of the number of pixels within the uterine ROI area of 8 ± 2%. The mean duration of the contraction was 189 ± 66 seconds. During the contractions, we also observed a reduced placental area in the three separate slices, as assessed by a reduced number of pixels within in the ROI of the slices of 17 ± 7%. Figure 20 illustrates these main three observations during a uterine contraction.

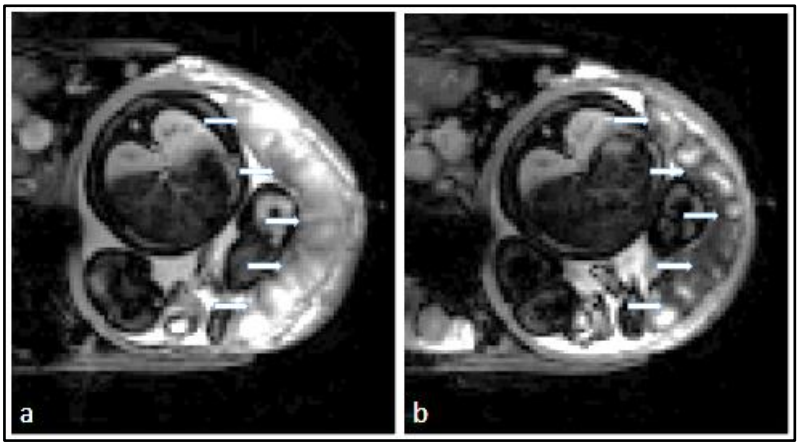


***Figure 20.*** *T2*-weighted images during uterine relaxation (a) and uterine contraction (b). Placenta marked with white arrows. During the contraction, the placenta is darker and the uterine and placental areas are reduced (245).*

In the eight uterine contractions, the manual segmentation revealed a significant temporal delay between the change in the uterine shape, the reduction in placental volume and in the reduction of BOLD signal (illustrated in Figure 21).

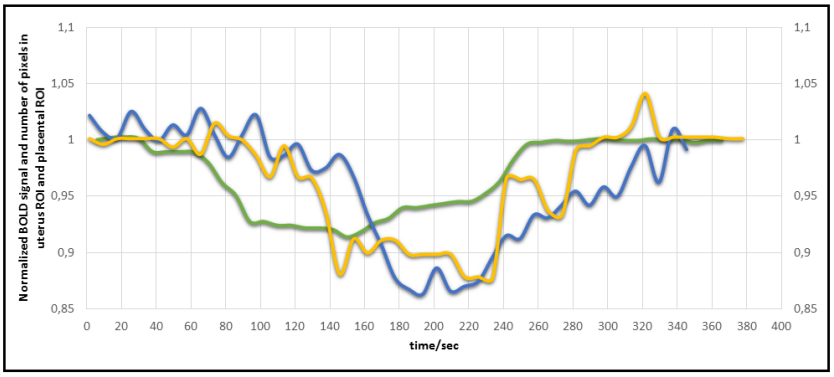


***Figure 21.*** *The timeline of changes in normalized BOLD signal (blue line) and changes in the number of pixels within the uterine (green line) and the placental ROIs (yellow line) in a uterine contraction (245)*

In the remaining 48 BOLD MRI scans, we observed no remarkably change in the uterine shape followed by reductions in the BOLD signal.

## 5.4. STUDY IV

Of the 100 pregnancies originally included in this T2* study, three uncomplicated pregnancies were excluded because of placental susceptibility artifacts, leaving 97 pregnancies for further analysis. Fifteen of these 97 pregnancies (15%) resulted in a neonate with a birth weight Z-score ≤ 2.0.

The study demonstrated significant associations between Z-scores of placental T2* and UtA PI (r = -0.56, p < 0.0001), birth weight and T2* (r = 0.68, p < 0.0001), and birth weight and UtA PI (r = -0.43, p < 0.0001), (Figure 22).

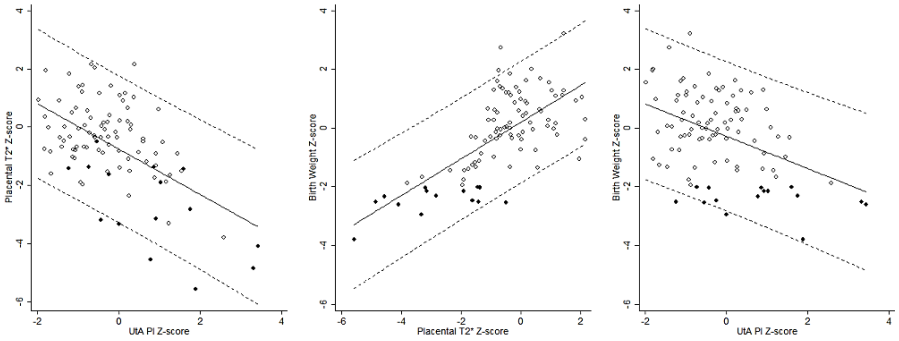


***Figure 22.*** *The associations between Z-scores of placental T2* and UtA PI (left), birth weight and T2* (middle) and birth weight and UtA PI (right). Black lines present ordinary least squares fits, dashed lines 95% prediction intervals. Black hollow circles represent the normal pregnancies. Black closed circles represent neonates with low birth weight (249)*

The ROC analysis revealed a significant higher performance of the T2* value (AUC = 0.92, 95% CI, 0.85-0.98) than the UtA PI (AUC = 0.74; 95% CI, 0.60-0.89) in the prediction of low birth weight (p = 0.010). The performance was not improved by combining the two methods (p = 0.438). The optimal Z-score T2* cut-off in detecting low birth weight was -1.3. Using this cut-of, the sensitivity and specificity of the T2* method were 93% (95% CI, 68-100) and 80 % (95 CI, 73-90), respectively. Likewise, the optimal UtA PI cut-off was 0.7 with a sensitivity of 60% (95% CI, 32-84) and specificity of 87% (95% CI, 77-93). The distribution of cases at the T2* Z-score cut-off of -1.3 and birth weight Z-score cut-off of -2.0 is illustrated in Figure 23.

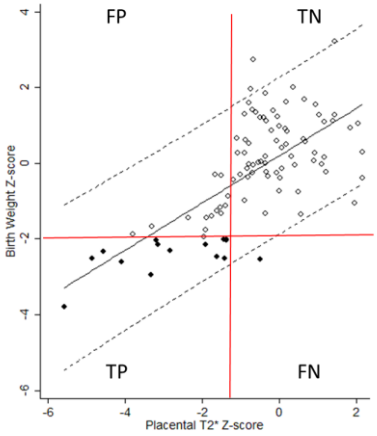


***Figure 23.*** *The distribution of cases: FP, false positive; TN, true negatives; TP, true positive; FN false negative. Vertical red line represents the estimated optimal T2* Z-score cut-off value of -1.3. Horizontal red line represent the birth weight Z-score cut-off of -2. Closed circles representing low birth weight, open circles normal birth weight. The association between Z-scores of placental T2* and birth weight is illustrated. Black line presents ordinary least squares fit, dashed lines 95% prediction intervals.*

Placental pathological examination was performed in 57 out of the 97 pregnancies. The examinations revealed signs of MVM and/or FVM in 13 out of 14 cases with low T2* value and low birth weight (“true positives”, TP), and in 8 out 11 examined cases with low T2* value but normal birth weight (“false positive”, FP). Furthermore, signs of PVM were demonstrated in 6 out of 32 examined pregnancies with normal T2* value as well as normal birth weight (“true negatives”, TN). In the remaining examined pregnancies, including the single case with normal T2* value and low birth weight (“false negative”, FN), no signs of PVM were revealed. The results of the placental pathological examination are further highlighted in Figure 24.

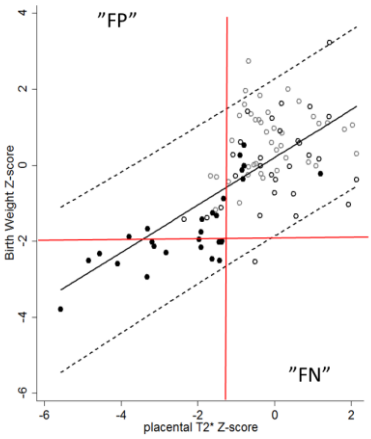


***Figure 24.*** *Results of placental pathological examination: signs of PVM (black closed circles), normal examination (black open circles), no examination (gray open circles dots). Vertical red line represents the estimated optimal T2* Z-score cut-off value of -1.3. Horizontal red line represent the birth weight Z-score cut-off of -2.0. FP, false positive; FN, false negative. The association between Z-scores of placental T2* and birth weight is illustrated. Black line presents ordinary least squares fit, dashed lines 95% prediction intervals.*

The 14 TP cases were all clinical complicated pregnancies with clinical signs of placental dysfunction including abnormal Doppler ultrasound findings and/or abnormal CTG and/or abnormal biophysical profile. Likewise, most of the FP cases had clinical signs of placental dysfunction, whereas the TN cases and the single FN case showed no such signs. One of the six TN cases with placental signs of PVM, however, delivered spontaneously at 33 weeks' gestation. (Further characteristics of each pregnancy including the major placental pathological findings are presented in Table 2 and in Supplementary Data in Paper IV).

## 5.5. STUDY V

Of the 64 normal pregnancies and 17 cases complicated by placental dysfunction, 16 were excluded due to uterine contraction preventing estimation of steady state BOLD signal levels (12 normal pregnancies, 4 cases). Figure 25 presents a BOLD signal curve from such an excluded pregnancy. Furthermore, three normal pregnancies were excluded due to placental susceptibility artefact. Thus, 62 pregnancies remained in the study for further analyses (49 normal pregnancies at 15 – 41 weeks' gestation at MRI and 13 cases at 22 – 37 week's gestation at MRI). Four of the 13 cases had an increased UA PI at the time of MRI.

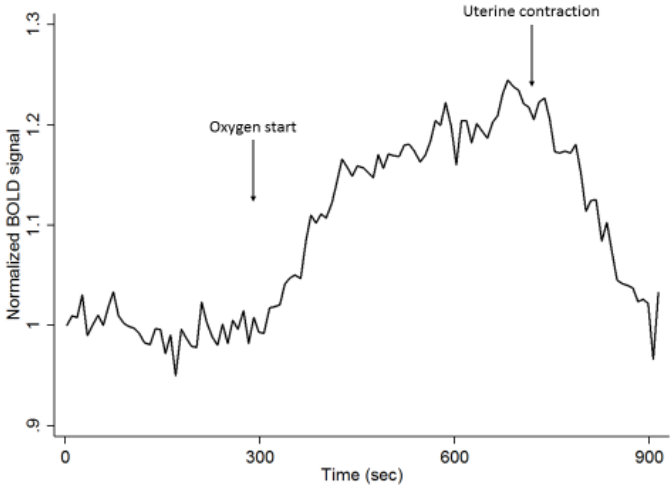


***Figure 25.*** *BOLD signal versus time plot from a MRI scan complicated by a placental uterine contraction.*

In the normal group, there was a significantly positive linear association between the ΔBOLD response and gestational age ($r = 0.81$, $p < 0.0001$) and in the group of cases, the ΔBOLD response was significantly higher (median Z-score = 4.94, $p = 0.0001$; Figure 26).

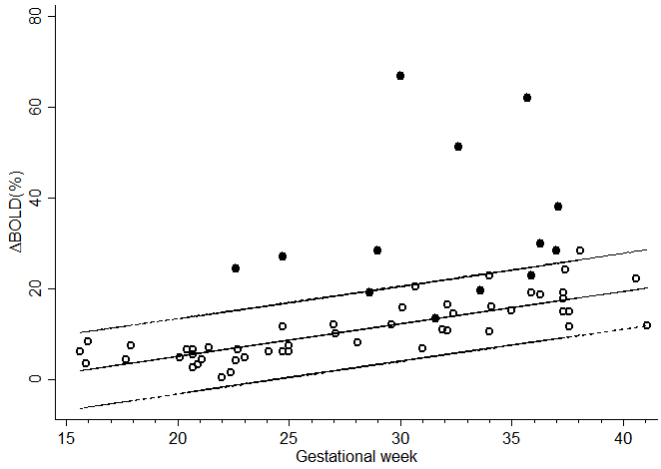


***Figure 26.*** *The association between placental ΔBOLD response and gestational age in normal pregnancies (open circles). Black line indicate the least square fit, dashed lines indicate 95% prediction interval. Black closed circles indicate the 13 cases.*

Figure 27 presents the BOLD signal curve from a normal pregnancy and a case, both at 32 weeks' gestation.

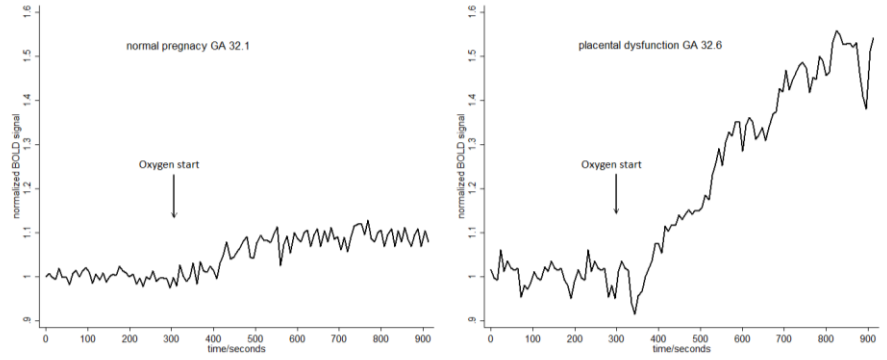


***Figure 27.*** *Normalized BOLD signal intensity curves in a normal pregnancy (left) and in a pregnancy complicated by placental dysfunction (right). GA, gestational age.*

The results of the T2* measurements are illustrated in Figure 28. In the normal group, there was a significantly negative linear association between gestational age and baseline T2* ($r = -0.90$, $p < 0.0001$). In the case group, baseline T2* (mean Z-score = -3.13) was significantly lower when compared to normal group ($p < 0.0001$). In the normal group, the absolute $\Delta$T2* was increased with gestational age ($r = 0.47$, $p = 0.0009$), whereas $\Delta$T2* did not differ between groups ($p = 0.37$).

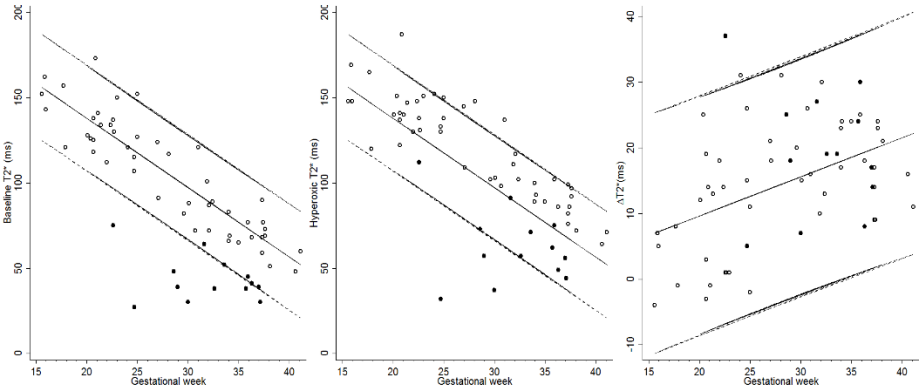


***Figure 28.*** *The association between placental T2* measurements and gestational age in normal pregnancies (open circles). Black lines indicate least square fit, dashed lines indicate 95% prediction interval (PI). Left: Baseline T2*. Middle: Hyperoxic T2* (baseline T2* least square fit and 95% PI superimposed on the graph). Right: $\Delta$T2*. Black closed circles indicate the 13 cases complicated by placental dysfunction.*

In the 62 pregnancies, there was a strong linear association between $Log_{10}$ $\Delta$BOLD and normoxic T2* ($r = -0.88$, $p < 0.0001$), (Figure 29).

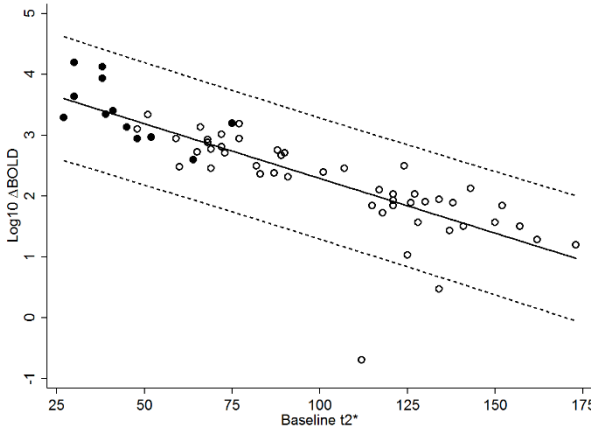


***Figure 29.*** *The association between Log10 ΔBOLD and normoxic T2*. Black line indicates least square fit, dashed lines indicate 95% prediction interval (PI). Open circles, normal pregnancies; closed circles, cases.*

# CHAPTER 6. DISCUSSION

This chapter contains a detailed discussion of each of the five studies, including methodological considerations as well as general discussions of the placenta T2* value and the placenta ΔBOLD response when relevant. Furthermore, at the end, the chapter contains a short discussion of some general aspects of the studies.

## 6.1. STUDY I

In this study, we assessed the reproducibility of the placental T2* measurements and we investigated the T2* value in 24 normal pregnancies and in 4 FGR cases.

A limitation of this study was the very few cases, in which however, placental pathological examination was performed. Moreover, placental pathological examination was not performed in the normal pregnancies, and in theory, some of these might have had abnormal placental findings. Nonetheless, these pregnancies were clinical uneventful with normal Doppler findings, normal birth weights at term (Z-score > -2.0), and normal gross placental findings, indicating normal placental function.

The assessment of the within session, between sessions and inter-observer reproducibility showed the T2* method to be reasonable robust. Averaging two slices improved the reproducibility, which most likely reflects the heterogeneous nature of the placenta. Based on this observation, we recommend averaging of two or more slices in future studies.

In the 24 normal pregnancies, the T2* value was reduced as gestational age advanced. This can be explained by reduced placental oxygenation within both the intervillous blood and the fetoplacental blood as demonstrated by previous invasive studies (44,48). Nonetheless, the maturation of the normal placenta, including the continuous development of the trophoblast throughout gestation and the deposition of fibrin, may reduce the intrinsic T2 relaxation (178,250,251) and thereby reduce the placental T2* value. From our data it is not possible to assess which of these parameters contribute the most to the reduced T2* value. Moreover, changes in placental blood volume fraction (the ratio of vascular volume to total placental volume) could affect the intrinsic T2 value. However, this fraction seems to be constant throughout gestation (252). Our findings are in contrast to a study by Huen et al. (199) who could not demonstrate any correlation between placental T2* and gestational age in 14 uncomplicated pregnancies at 23 to 37 weeks' gestation. One explanation might be that we used a higher number of echo-times at a wider range, which may have improved our T2* fits. Moreover, our findings are in accordance with previous MRI studies demonstrating reduced placental T2 values (250,251) and reduced placental perfusion fractions (75,76) as gestational advances.

In the case with normal Doppler findings and normal placental pathological findings, the T2* value was normal, indicating that this fetus was SGA but not growth restricted. In the three cases with abnormal Doppler findings and placental pathological signs of PVM, the T2* values were markedly lower. Thus, these fetuses were small for date due to placental dysfunction. The low T2* value may be explained by placental hypoxia and abnormal tissue morphology associated to placental dysfunction. As discussed in Chapter 2.2, it is well known that the $sO_2$ of the fetoplacental blood may be reduced in placental dysfunction (82,107,108); however, controversies exist regarding the $sO_2$ of the maternal blood. In addition to placental hypoxia, placental morphological changes such as infarction and fibrosis may reduce the intrinsic T2 relaxation (253) and thereby the T2* value. Previous studies have demonstrated lower placental T2 values in FGR pregnancies (74,251,254). Moreover, changes in blood volume fractions in the dysfunctional placenta might affect the T2* value. However, opposing results are presented in the literature regarding the blood volume fractions in dysfunctional placentas (93,252). Thus, as the ROIs covered the entire placenta in transverse section, the low T2* value may reflect abnormal placental morphology, low $sO_2$ of maternal blood as well as low $sO_2$ of the fetoplacental blood. Which of these parameters contributes the most to the low T2* value, cannot be elucidated from our data. Even so, for the purpose of a diagnostic test of placental dysfunction, this distinction may not be of clinical interest.

## 6.2. STUDY II

In this study, we investigated the ΔBOLD response in 21 normal pregnancies and in 4 FGR cases.

Limitations of the study were the same as discussed in *Study I* regarding the small number of cases and lack of placental pathological examination in the normal pregnancies. In addition, we did not assess the reproducibility of the ΔBOLD response including assessment of inter-observer variation of the ROI drawings.

In each of the 21 normal pregnancies, we observed a significant increase in placenta BOLD signal (mean of 12.6 ± 5.4%) during the 5-minute oxygen-challenge. This finding was in accordance with a previous study by Sorensen et al. (59), in which they demonstrated a mean ΔBOLD response of 15.2 ± 3.2% in 8 uncomplicated pregnancies at the same mean gestational age. The interpretation of the increased BOLD signal is complex. In the following, the origin of the changes in BOLD signal is discussed, including $sO_2$ changes and the potential contributions from changes in blood flow and blood volume during oxygen-challenge.

Changes in placental BOLD signal during oxygen-challenge may reflect changes in maternal and fetoplacental blood $sO_2$, as discussed in Chapter 2.3.2. The MRI ROIs were drawn in cross sections of the placental, thereby containing both maternal and

fetal blood compartments. In order to assess the separate contribution from each of these compartments, separate ROIs should have been drawn. Nevertheless, as previously described, we experienced such separation of the two compartments to be very challenging in the BOLD MRI image. Therefore, in order to assess the relative contributions from these blood compartments, the in vivo ratio of maternal versus fetal blood volume in the placental ROI should be considered. Previous postpartum morphometric analysis studies have estimated the ratio of maternal versus fetal blood volume within the placenta to be around 4:1 at term (93,255,256). In vivo, the intrauterine total placental volume as assessed by MRI has been estimated to be around 450 ml at 27 week's gestation (257,258) and 1000 ml (258,259) near term. In contrast, the postpartum placental volume has been estimated to be only around 250 ml at 23-31 weeks' gestation (40) and 450 ml at term (40,256). Thus, a large proportion of the in vivo placental volume consists of maternal and fetal blood. In vivo, the total amount of blood in the fetoplacental circulation is about 110 ml/kg fetal weight (260). At 30 week's gestation, nearly half of the fetoplacental blood volume is within the placenta (261), whereas at term, one third of the blood volume is within the placenta (260). Thus at term, if 15 ml umbilical cord blood is subtracted (260), the in vivo placenta contains approximately 100 ml fetal blood at a fetal weight of 3000 g. From these estimates, an approximation of the in vivo amount of maternal blood in the intervillous space at term is around 450 ml (1000 ml subtracted by 450 ml + 100 ml) given the assumption that the postpartum placental volume is blood empty. Thus at term, the in vivo ratio of maternal versus fetal blood volume within the placenta may be at least 4:1, which is in accordance with the postpartum estimates. Thereby, when considering this in vivo ratio, maternal blood may be a larger contributor to changes in BOLD signal than the fetoplacental blood.

Nonetheless, in addition to the in vivo blood volume ratio, the normoxic $sO_2$ of the maternal and fetoplacental blood should also be considered in the assessment of the contribution to BOLD signal changes. As the maternal arterial blood entering the intervillous space is almost fully saturated during normoxia, only the binding of additional oxygen within the maternal venous blood in the periphery of the intervillous space contributes to the increase in BOLD signal during oxygen-challenge. On the contrary, during normoxia, the entire fetoplacental blood volume is low-saturated and therefore during oxygen-challenge, the entire fetoplacental blood volume may contribute to the BOLD signal changes. These considerations are well in line with the observed changes in the BOLD MR image. During normoxia (Figure 18, left), the placenta in cross-section appears rather heterogeneous with several regional areas with high signal intensity centrally and low signal intensities peripherally and towards the fetal site of the placenta. These areas most likely represent the placental lobes containing the intervillous space and the villous three protruding from the chorion plate, with high-saturated maternal arterial blood centrally (high BOLD signal intensity) and low-saturated venous blood peripherally and towards the fetoplacental side (low BOLD signal intensity). This interpretation of the BOLD image is supported by a study by Schabel et al, who demonstrated that local maxima in T2* maps were strongly correlated with entering spiral arteries identified using DCE MRI in the rhesus macaque (58). During oxygen-challenge (Figure 18, right), the placenta

appears more homogeneous as the signal intensity in the darker areas increases, reflecting an increased saturation of the maternal venous blood and the fetoplacental blood. Thus, the increased BOLD signal during oxygen-challenge may reflect increased $sO_2$ of the maternal venous blood as well as the placental oxygen transport from the mother to the fetus (188). The distinction between maternal and fetal blood contributions cannot be further elucidated from our data.

In addition to changes in blood $sO_2$ during oxygen-challenge, changes in placental blood perfusion and blood volume should be considered as both of these parameters may affect the amount of deoxyhemoglobin within a voxel and thereby the BOLD signal. The potential vasocontrictory effects of oxygen might reduce the placental blood flow during maternal oxygen-challenge. This remains to be investigated; however, using MRI arterial spin labelling, preliminary data from the thesis by Huen (262) indicated that changes in placental perfusion during oxygen-challenge is sparse. Therefore, placenta BOLD signal changes observed during oxygen-challenge most likely primary reflects changes in $sO_2$. Moreover, in a previous study using a rat brain model, Kennan et al (183) presented a model for separating the effects of changes in blood volume and blood oxygenation during respiratory challenges (hyperoxia and hypoxia). They demonstrated that during respiratory challenge, the BOLD signal change is dominated by changes in blood oxygenation rather than changes in regional blood volume. This is accordance with the well-described close correlation between BOLD signal changes and changes in tissue oxygenation as demonstrated by previous invasive studies (179,180,263).

In the four cases, divergent ΔBOLD responses were observed. In case number 4, the ΔBOLD response was normal, thereby indicating normal placental function. This BOLD finding was in accordance with the normal Doppler findings and the normal placental pathological findings in this case. This fetus was SGA, however, not growth restricted. In case 2 and 3 (with abnormal UA and MCA Doppler findings and placental signs of PVM), we observed a ΔBOLD hyper-response. As the ΔBOLD response can only be assessed in relative values, this hyper-response may be explained by 1) altered baseline conditions, including a lower baseline oxygenation and abnormal placental morphology, reducing the baseline signal, and/or 2) an increased absolute oxygenation during oxygen-challenge compared to normal. Previously, it has been demonstrated that baseline oxygenation in cerebral MRI studies is a significant modulator of the ΔBOLD response, in which lower baseline oxygenation is associated with a higher ΔBOLD response (176). Baseline oxygenation of the placenta may have the same effect on the placental ΔBOLD response. This hypothesis is further elaborated on in the discussion of *Study V*. In the remaining case number 1 (in which even the DV flow velocity was abnormal and placental examination revealed signs of PVM), we observed no significant increase in BOLD signal during the 5-minute oxygen-challenge. This finding may reflect a severely impaired placental oxygen transport capacity in line with the “non-responder” theory as proposed by Arduini et al. (237) and Nicolaides et al.(190). Nonetheless, we speculate that the BOLD signal may have increased during prolonged oxygen-challenge as we observed a small - yet

insignificant - increase in BOLD signal towards the end of the 5-minute oxygen-challenge (Figure 19). For this reasons, the oxygen-challenge was prolonged from 5 to 10 minutes in *Study V*. Furthermore, in the dynamic BOLD MRI and in the BOLD signal intensity curve, signs of a uterine contraction starting prior to the oxygen-challenge was observed, which may have biased the BOLD result. The presence of uterine contractions during BOLD MRI and their effect on the BOLD signal is discussed in *Study III.*

## 6.3. STUDY III

In this study, we investigated the presence of spontaneous reductions in placental BOLD signal during dynamic BOLD MRI in 56 normal pregnancies. Spontaneous reduction in BOLD signal was observed in eight out of these pregnancies at a broad range of gestations. As each case was preceded by a change in the uterine shape, which was only observed in these cases, we suggest that the reductions in BOLD signal are due to spontaneous uterine contractions.

This study had limitations. Firstly, considerations regarding the lack of placental pathological examination are the same as discussed in *Study I*. Another limitation was the lack of contraction intensity registrations. Nonetheless, the use of intrauterine pressure assessment during these MRI scans would never be an option in our setting. The women were informed to report if they felt spontaneous uterine contractions during the MRI acquisition, but none of them did and therefore, we assume that the observed contractions were generally low-intensity contractions. Moreover, a limitation of the study was that we did not assess intra- or interobserver reproducibility of the ROI drawings due to time constraints. However, in collaboration with Health Science and Technology, Aalborg University, methods for automatic segmentations of the uterus are being developed, and the results of an unpublished pilot study were highly in accordance with the manual segmentations.

We observed a temporal association between the uterine contraction, the reduction in placental volume and the reduction in placental oxygenation (Figure 21). At the very beginning of the contraction, the placental volume and oxygenation are unaffected. However, within approx. 30 seconds, the placental volume and placental oxygenation start to decrease. During uterine relaxation, the placental volume and placental oxygenation slowly recover, notable the placental oxygenation fully recovers later than the placental volume.

The interpretation of the observed reductions in placenta BOLD signal is complex as several factors may affect the signal. These factors include changes in placental blood flows, blood volumes and fetal oxygen extraction as described below.

The temporal delay between the beginning of the contraction and the reduction in placental volume and placental oxygenation may represent a gradual increased resistance in the spiral arteries and thereby an impaired uteroplacental blood flow. This increased resistance may be caused by the contracting myometrium and/or the increased intrauterine pressure. The finding is in accordance with previous Doppler ultrasound studies, which have also revealed this temporal association between the UtA blood flow velocities and provoked uterine contractions (264) and between the UtA blood flow velocities and Braxton Hicks contractions (265) with increasing resistance of the uterine arteries during contraction. This impaired uteroplacental blood flow reduces the BOLD signal. On the contrary, several studies have demonstrated that fetoplacental circulation during uterine contractions is unaffected in normal pregnancies. This may be explained by that, the increased intrauterine pressure is transmitted equally to the umbilical vein and arteries without changes in blood flow, or that an increased fetal preload enables the uncompromised fetus to maintain a constant fetoplacental blood flow (266-268).

Changes in blood volumes during contractions may also affect the BOLD signal. We observed a reduced placental volume during the contractions. Thus, this finding suggests that during low amplitude uterine contractions, the maternal blood is squeezed out of the intervillous space like a sponge. If so, the ratio between well-oxygenated maternal and low-oxygenated fetal blood within the placental MRI ROI is decreased. This may contribute to the observed reduction in placental BOLD signal during uterine contractions. The observed reduction in placental blood volume is in conflict with a previous study by Bleker et al (269). In that study, using ultrasound, a distention of the intervillous space during labor contraction was suggested, thereby indicating initial venous obstruction, leaving more maternal blood available for exchange with the fetal compartment during contraction. However, the contractions investigated by Bleker et al were labor contractions, which may explain the opposing results.

Increased fetal oxygen extraction may also contribute to the reduction in BOLD signal. This is supported by the slower recovery of placental oxygenation compared to the recovery of placental volume (Figure 21), which was observed in each of the eight contractions. The slower recovery of placental oxygenation may be explained as follows: During a uterine contraction, maternal blood is squeezed out of the intervillous space reducing the maternal blood volume in the placenta. Therefore, increased oxygen extraction occurs in order to avoid fetal hypoxia as described in previous studies (187). During uterine relaxation, the blood volume is regained, and the delayed recovery of the BOLD signal may represent a gradually washout of intervillous blood, from which the increased oxygen extraction has occurred. Thus, due to this delay between the recovery of the placental volume and the placental BOLD signal, our data indicate that during uterine contractions, the BOLD signal is reduced not only because of impaired uteroplacental blood flow and reduced maternal

blood volume, but also because of an increased oxygen extraction, and thereby a reduced $sO_2$ within the intervillous blood.

This study demonstrates that the presence of uterine contractions needs to be considered when interpreting placental MRI results. In placental BOLD MRI, a uterine contraction during oxygen-challenge may lead to an underestimation of the ΔBOLD response.

## 6.4. STUDY IV

In this study, we investigated the association between placental T2* measurements, UtA PI and birth weight, and we compared the performance of the T2* with the UtA PI in the prediction of low birth weight. Significantly associations were revealed between birth weight and both T2* and UtA PI as well as between T2* and UtA PI. The study indicated that T2* may be a strong predictor of low birth weight and it performed significantly better than the UtA. Furthermore, the T2* values were closely related to the presence of pathological signs of PVM.

One major limitation of this study was the mixed population regarding the risk of low birth weight. Thus, relevant predictive values of the T2* measurements could not be estimated. The mixed population was chosen in order to increase the number of low birth weight infants, as the incidence of low birth weight in our population is only around 3%. Nonetheless, the mixed population did not prevent comparison of the T2* and UtA PI. Moreover, a major limitation was that we did not perform a cross-validation of our data. Thus, the performance of placental T2* in the prediction of low birth weight should be validated in a larger clinical cohort study with randomly division of the data into training and validation sets.

A strength of the study was that placental pathological examination was performed in a large subset of the pregnancies. The results of the examinations were highly in accordance with the measured T2* values. Interestingly, the only false negative case (normal T2*, low birth weight) revealed no signs of PVM which was in accordance with the lack of clinical signs of placental dysfunction during pregnancy. Moreover, in 8 out of 11 examined false positive cases (low T2*, normal birth weight), pathological signs of PVM were revealed. This was also well in line with the presence of clinical signs of placental dysfunction during pregnancy. These results of the placental pathological examinations highlight the limitations in using low birth weight as a freestanding marker of placental dysfunction as described in Chapter 2.2.4.

In this study, we observed a negative association between the T2* measurements and the UtA PI, which may be explained by a lower placental $sO_2$ when the placental perfusion is impaired. Moreover, as discussed in *Study I,* morphological changes

associated to placental dysfunction, including changes in placental blood fractions, may contribute to the observed association. This is supported by a study by Derwig et al. (254), who demonstrated significant associations between placental T2 and UtA PI. Our data indicated that the T2* method performed significantly better than the UtA PI in the prediction of low birth weight. The low T2* value in cases with pathology only on the fetoplacental site, may contribute to the higher performance of the T2* method as the UtA PI only estimates the placental vasculature on the maternal site. Another explanation may be a higher reproducibility of the T2* than the UtA PI. In the latter, rather poor intra- and interobserver reproducibilities have been demonstrated (140). In our study, specialists in fetal medicine performed the UtA PI measurements, and the performance was comparable to previous studies (141-144,146).

## 6.5. STUDY V

In this study, we aimed to interpret the relative ΔBOLD response in normal pregnancies and in those complicated by placental dysfunction by using placental T2* measurements.

A strength of this study was that we included the results of placental pathological examinations in the distinction between normal pregnancies and those complicated by placental dysfunction. Thereby, we reduced the risk of mixing normal and dysfunctional placentas. The pathological examination, however, was not performed in a subset of the normal pregnancies, yet these were clinical uneventful with normal gross placental examination. Another strength was the exclusion of pregnancies in which uterine contractions interfered with the estimation of steady state BOLD signal levels, which could have biased the results as described in *Study III*.

In the 49 normal pregnancies, we observed an increasing ΔBOLD response as gestational age advances. The T2* findings indicated that this can be explained by a combination of a reduced baseline T2* and an increasing hyper-oxygenation (ΔT2*). The reduced T2* value may represent the well-described decline in placental oxygenation within the maternal and the fetoplacental blood as well as morphological maturation of the placenta throughout gestation as discussed in *Study I*. The increasing ΔT2* may be explained by the decline in placental $sO_2$ throughout gestation, leaving more of the additional oxygen during oxygen-challenge to be bound in later gestations. Moreover, an increased placental blood volume fraction within the placental ROI throughout gestation would increase the ΔT2*, although previous studies suggest the placental blood volume fraction to stay relatively constant throughout gestation (252,270).

In the group of 13 cases, the ΔBOLD response was significantly higher compared to normal. In these pregnancies, the baseline T2* value was significantly lower, whereas the absolute change in placental oxygenation (ΔT2*) during oxygen-challenge did not differ from normal. The low baseline T2* value may represent reduced oxygenation within the maternal and/or fetoplacental blood as well as abnormal placental morphology, as described in *Study I*. These placental morphological abnormalities, including a lower placental blood volume fraction (93), may prevent the average hyperoxic T2* value to reach normal levels during oxygen-challenge (Figure 28, middle). This may explain why the ΔT2* did not differ from the normal pregnancies, and thereby it may illustrate the baseline intrinsic T2 effect on the T2* value. Thus, in the dysfunctional placenta, the high ΔBOLD response is caused merely by altered baseline conditions (reduced baseline T2*) rather than an absolute increase in placental oxygenation (ΔT2*). This is also supported by the strong negative association between baseline T2* and the oxygen-challenge ΔBOLD response; and our findings are in accordance with a previous cerebral BOLD MRI study demonstrating that baseline oxygenation modulates the cerebral ΔBOLD response (176). Thus, according to our results, the placenta baseline state modulates the hyperoxic ΔBOLD amplitude.

As the ΔT2* did not differ between the two groups, one could speculate whether the oxygen environment in dysfunctional placentas differs from normal and whether the low baseline T2* value simple reflects morphological abnormalities within the dysfunctional placenta. Nonetheless, it is well documented that the fetoplacental blood $sO_2$ is reduced in pregnancies complicated by placental dysfunction (82,107,108). As the ROIs covered the entire placenta, this reduced fetoplacental $sO_2$ would contribute to the low placental T2* values, at least in the cases with abnormal UA Doppler. Nonetheless, whether the maternal blood within the intervillous space is hypoxic or not cannot be elucidated from our data.

The pathophysiological explanation of the slow response observed in some of the dysfunctional placentas (as illustrated in Figure 27) is unclear. One explanation may be that the simple diffusion across the villous membrane is impaired in the dysfunctional placentas. Thus, oxygenation of the fetoplacental blood during the oxygen-challenge is delayed compared to normal. Another explanation may be an impaired perfusion in the intervillous space, including hypoperfused local areas (8), and thereby a slow replacement of relatively low-saturated maternal blood within these areas. This latter explanation is in accordance with the previous placental study by Brunelli et al. (118) using DCE MRI as described in Chapter 2.2.3. In that study, they demonstrated significant intervillous hypoperfusion and many patchy underperfused areas in pregnancies complicated by placental dysfunction, representing the different degrees of occlusion within the spiral arteries (39). In our study, we did not assess the ΔBOLD variation between placental slices, which may be higher in cases compared to normal. In order to elaborate on the slow response in our BOLD MRIs, the ΔBOLD response should be correlated to the results of the

placental pathological findings, as the response rate might differ between placentas with signs of MVM and those with signs of FVM.

Because of the placental "non-responder" observed in *Study II*, the oxygen-challenge was prolonged from 5 to 10 minutes in the current study. The prolonged oxygen-challenge may explain why we did not observe any cases with a ΔBOLD hypo-response in this study. Even thought that the oxygen-challenge was prolonged, in several dysfunctional placentas, we observed that the steady state level was not reach until the final minutes during the 10-minute oxygen-challenge. In some of these cases, one could even speculate whether the hyperoxic steady state level was reached (as in the case illustrated in Figure 27). Thus, we might have underestimated the ΔBOLD response. The observed ΔBOLD hyper-response is in conflict with two studies in rat FGR models, in which low ΔBOLD/ΔT2* responses were observed in placentas within the ligated horn (196,197). The opposing results may be due to differences in rat FGR models and human FGR pregnancies, or a too short oxygen-challenge in the rat studies. Nonetheless, further human placenta BOLD studies in severe dysfunctional placentas are needed in order to assess whether placental "non-responders" exist.

## 6.6. GENERAL ASPECTS

**Placental ROIs**
As described in the method section, placental ROIs covered the entire placenta in transverse section. Thus, the ROIs contained both the maternal and the fetal blood compartments. We used this method, as we experienced that it was extremely challenging to distinguish between the two compartments in the MR images. Thereby, as mentioned above, our data were limited in terms of the interpretations of the T2* values and BOLD responses. As the trophoblast protrudes into the intervillous space, complete separation of the two compartments using MRI is challenging. Methods to be used may include DCE MRI but for safety reasons in human pregnancies, this is not possible in most settings. Other MRI sequences and post-processing tools might be useful in the distinction between the two placental compartments.

**Low birth weight as a proxy of placental dysfunction**
In this project, we used low birth as a proxy of placental dysfunction. As previously described, this estimate is not a perfect marker of placental dysfunction as not all FGR neonates are SGA and not all SGA neonates are FGR. Therefore, a major strength of this project was that placental pathological examination was performed in the FGR cases (*Study I, II, IV, V*) and in a large subset of the normal pregnancies (*Study IV* and *V*). Although, placental pathological findings may be present in normal pregnancies and absent in some pathological pregnancies, in theory we thereby improved the diagnosis of "true" placental dysfunction. *Study IV* highlighted the issue of using low

birth weight as a freestanding marker of placental dysfunction as several false positive cases (normal birth weight, low T2* value) exhibited clinical and placental pathological signs of placental dysfunction. The T2* value was indeed in accordance with the results of placental pathological examinations regardless of the birth weight. In general, the studies could have been improved if placental pathological examination had been performed in all the pregnancies. Even after the updated protocol, unfortunately, not all placentas in the uncomplicated pregnancies were collected post-partum. Thus, in some of the uncomplicated pregnancies, placental pathological examination might have revealed abnormal findings. This could in particular have been the case in study I-IV, in which we defined normal birth weight by a Z-score > -2. In study V, we defined normal birth weight by a Z-score > - 1.28 and therefore, in that study it was more unlikely that the "normal" neonates had suffered from placental dysfunction.

**Subgroup analyses**

In *Study I-II* and *IV-V*, subgroup analysis based on the placental pathological findings of MVM and/or FVM may have revealed interesting differences in ΔBOLD response and T2* values. Likewise, subgroup analysis of early-onset versus late-onset placental disease should be elaborated on due to the potential different placental phenotypes as described in Chapter 2.2.1. Preeclampsia was present in a small number (two) of our cases, and subgroup analysis may reveal interesting MRI differences between cases with and without preeclampsia. Moreover, subgroup analysis based on Doppler findings should be examined. Because of the small sample sizes of pregnancies complicated by placental dysfunction, such subgroup analyses were not performed in this project.

**Placental MRI bias**

In this project, we focused on two types of placental MRI bias that could potentially interfere with the MRI results, namely placental susceptibility artefacts, as discussed in Chapter 2.3.2, and the presence of spontaneous uterine contractions as discussed in *Study III*.

The presence of placental susceptibility artefacts was a minor problem in this project and the artefacts only excluded very few participants. Several actions were done in order to prevent the occurrence of these artefacts. Firstly, we used a 1.5 T system rather than a 3T system. Secondly, we aimed to place the placenta, as isocentric within the MRI scanner as possible, were the magnetic field is most homogenous. Moreover, we used a maximum TE of 67.5 ms during the T2* acquisition. In addition, prior to the MRI scan, we carefully evaluated the participants clothing etc. in order to remove any magnetic material.

The presence of uterine contraction during the BOLD scans was a major problem as they often interfered with the estimation of the steady state BOLD signal levels and therefore, they excluded rather many participants. Nonetheless, they were often

clearly visible during the dynamic BOLD MRI scans. This is in contrast to uterine contractions during the rather static T2* acquisitions, during which it was not possible to assess the characteristic dynamic changes in the shape of the uterus and the placenta as well as characteristic changes in placental signal. A uterine contraction during the T2* acquisition may reduce the T2* value thereby creating false positive results. MRI-compatible tocography might be used in order to detect the uterine contractions; however, it remains to be investigated whether such equipment would be able to detect these low-amplitude contractions. Rather instead, the T2* acquisition could be repeated during the MRI session, and then the highest mean should be reported.

# CHAPTER 7. CONCLUSIONS

The overall conclusion of this thesis is that placental T2*-weighted imaging can be used as a non-invasively method to detect placental hypoxia and thereby placental dysfunction.

The conclusions of each of the five studies are as follows:

**Study I**

- Placental T2* measurements are reproducible between MRI sessions and the reproducibility can be further improved by averaging two placental slices.
- In normal pregnancies, the placental T2* value is reduced as gestational age advances.
- In pregnancies complicated by placental dysfunction, the T2* value is significantly lower.

**Study II**

- During 5-minute oxygen-challenge, the placenta BOLD signal is increased in normal pregnancies.
- In pregnancies complicated by placental dysfunction, the ΔBOLD response is altered; in pregnancies with mild/moderate placental dysfunction, the ΔBOLD response is higher than normal, while the response might be absent in case of severe placental dysfunction ("non-responder").

**Study III**

- Subclinical uterine contractions occur frequently throughout pregnancy and they markedly reduce placental oxygenation.
- Spontaneous subclinical uterine contractions need to be considered when interpreting placental MRI as these contractions may interfere with the MRI results.

**Study IV**

- Placental T2* may be used as a predictor of low birth weight. In this study, it performed significantly better than the UtA PI.
- Placental T2* is closely related to placental pathological findings.

**Study V**

- In normal pregnancies, the ΔBOLD response increases as gestational age advances.
- In pregnancies complicated by placental dysfunction, the ΔBOLD response is higher than normal.
- The ΔBOLD hyper-response is caused merely by altered baseline conditions, including a lower baseline oxygenation and altered placental morphology.

# CHAPTER 8. PERSPECTIVES AND FUTURE WORK

## 8.1. THE FUTURE MRI PROTOCOL

The overall purpose of this project was to investigate the feasibility of T2*-weighted Magnetic Resonance Imaging (MRI) as a non-invasive method for detection of placental hypoxia and thereby placental dysfunction. It was concluded that both the BOLD method as well as the T2* method were able to detect placental dysfunction. However, in *Study V*, we concluded that both methods estimate placental baseline conditions. Therefore, one should consider whether the MRI protocol should include both methods in future works. For this purpose, strength and limitations of each method need to be considered as well as their performance in the prediction of low birth weight.

**Strengths and limitations of the BOLD and the T2* methods**
Strengths of the T2* method are the very short acquisition time (12 sec. per slice) and the simple and easy MRI analysis, which makes it suitable to be combined with other easy-obtained MRI biomarkers. Moreover, the reproducibility of the T2* measurements is acceptable, although between scanner reproducibility remains to be investigated. Limitations are the presence of susceptibility artefacts and spontaneous uterine contractions – both of which may reduce the T2* value creating false positive results. Strengths of the BOLD method is the dynamic assessment, which could be useful in the investigation of placental and/or fetal physiological phenomena. Major limitations of the BOLD method is the rather long acquisition time (15 minutes) in which even 10 minute of oxygen-challenge may not be enough in order to reach steady state level in some dysfunctional placental. If the BOLD signal does not reach the state-state level, the BOLD response is underestimated leading to a false negative result. Moreover, uterine contractions often interfere with the estimation of the steady state BOLD signal levels and this may also potentially lead to false negative results. The extremely time-consuming MRI analysis is also a major limitation of the BOLD method, and for this method ever to become a clinical tool, automatic placental segmentation tools need to be developed. Finally, the reproducibility of the BOLD methods remains to be investigated. The strengths and limitations of the two methods are summarized in Table 2.

| | **T2*** | **BOLD** |
|---|---|---|
| + | Short acquisition time<br>Short analysis time<br>Reproducible | Dynamic assessment of the placenta (and the fetus)<br>Reproducibility? |
| - | Susceptibility artefacts → false positives<br>Uterine contractions → false positives | Long acquisition time<br>Time-consuming MRI analysis<br>Uterine contractions → false negatives |

***Table 2.*** *Strengths and limitations of the T2* method and in the BOLD method.*

**The performance of the BOLD and T2* methods in detecting low birth weight.** In an unpublished study, we have investigated and compared the performance of each methods in detecting low birth weight. This was in a mixed population of 104 pregnancies, in which 1/3 had an EFW < - 15% at the time of MRI. The primary outcome was low birth weight (Z-score < - 2.0). Twenty pregnancies were excluded due to uterine contractions preventing estimation of steady state BOLD signal levels, leaving 84 pregnancies in the study for further analysis. Eleven of these 84 pregnancies resulted in a neonate with low birth weight. The performance in the prediction of low birth weight did not differ statistically between the BOLD and the T2* method, although there was a trend towards a higher performance of the T2* method (BOLD AUC = 0.82 versus T2* AUC of 0.90, p = 0.157). Combining the methods did not improve the performance compared to the T2* performance.

In conclusion, given the strengths and limitation of each methods and the test performances as illustrated above, the oxygen-challenge BOLD sequence could be excluded from the placental MRI protocol.

## 8.2. THE CLINICAL PERSPECTIVE

The clinical perspective of T2*-weighted imaging is a none-invasive in-vivo test of placental dysfunction. Nonetheless, clinical implementation would depend on several factors. The cost and availability of MRI scanners would be a limiting factor in most centers. For this reason, MRI may only be used in selected cases; however, the question is which cases should be selected? According to our local data, 66% of pregnant women attend for at least one ultrasound EFW scan after 24 weeks' gestation. In 19% of these women, the EFW is below -15% and thereby they are considered at risk of FGR and receive additional scans throughout pregnancy. However, in our population, less than 3% of all singletons are born with low birth weight. Thus, a clinical implication of the T2* method in our setting could be in the risk-stratification of pregnancies with an EFW < -15%. For this purpose, the performance of the T2* method in a population of pregnancies with an EFW < -15% should be investigated. The perspective would be a reduced number of late second and third trimester scans as pregnancies with normal placental T2* need no further

controls. This would lead to more attention on the true high-risk fetuses suffering from placental dysfunction. Nonetheless, as not all FGR fetuses are SGA, other markers could be included in order to decide whom to scan. Such markers could be the maternal characteristics, the UtA PI or angiogenetic factors – depending on the surveillance program in the center. The T2* performance in such high-risk populations should be investigated, although one should keep in mind that a large proportion of adverse outcomes including low birth weight occurs within the low-risk population.

## 8.3. FUTURE WORK

Several aspects of the T2* method need to be further investigated. In this project, we investigated the reproducibility between MRI sessions; however, the reproducibility between different MRI scanners needs to be assessed. Longitudinal studies of the placental T2* values should also be conducted in order to examine the development of the T2* value within the same pregnancy. Moreover, the relation between the T2* value and time to delivery should be investigated as the T2* value might provide predictive information on delivery day, which would be of high clinical interest. Likewise, other adverse outcome measurements could be included in future studies. Furthermore, as previous mentioned, the correlation between placental T2* values and specific placental pathological findings, Doppler findings and gestational age at disease onset (early versus late onset) should be elaborated on.

The performance of the T2* method in combination with other easy-obtained placental MRI biomarkers should also be examined. Such MRI biomarkers could include the T2/T2*-ratio and the T1 relaxation time, the latter being sensitive to tissue $pO_2$ levels. In our MRI protocol, we included a multi-slice 2D FIESTA and a DWI sequence. From these sequences, the placental volume, the ADC map and/or the perfusion fraction can be obtained, and they could be other MRI biomarkers to be combined with the T2* value. In addition to a clinical perspective of these combined MRI biomarkers, they could also be applied in future animal and human FGR studies in order to assess intervention effects directly within the placenta.

Various MRI techniques are continuously being developed and technical improved, and they provide us new tools to be used in the understanding and the in vivo assessment of placental function.

# LITERATURE LIST

(1) Bamberg C, Kalache KD. Prenatal diagnosis of fetal growth restriction. Semin Fetal Neonatal Med 2004 Oct;9(5):387-394.

(2) Alberry M, Soothill P. Management of fetal growth restriction. Arch Dis Child Fetal Neonatal Ed 2007 Jan;92(1):F62-7.

(3) Kingdom J, Huppertz B, Seaward G, Kaufmann P. Development of the placental villous tree and its consequences for fetal growth. Eur J Obstet Gynecol Reprod Biol 2000 Sep;92(1):35-43.

(4) American College of Obstetricians and Gynecologists. ACOG Practice bulletin no. 134: fetal growth restriction. Obstet Gynecol 2013 May;121(5):1122-1133.

(5) Bamfo JE, Odibo AO. Diagnosis and management of fetal growth restriction. J Pregnancy 2011;2011:640715.

(6) Savchev S, Figueras F, Sanz-Cortes M, Cruz-Lemini M, Triunfo S, Botet F, et al. Evaluation of an optimal gestational age cut-off for the definition of early- and late-onset fetal growth restriction. Fetal Diagn Ther 2014;36(2):99-105.

(7) Figueras F, Gratacos E. Update on the diagnosis and classification of fetal growth restriction and proposal of a stage-based management protocol. Fetal Diagn Ther 2014;36(2):86-98.

(8) Ness RB, Sibai BM. Shared and disparate components of the pathophysiologies of fetal growth restriction and preeclampsia. Am J Obstet Gynecol 2006 Jul;195(1):40-49.

(9) Baschat AA. Integrated fetal testing in growth restriction: combining multivessel Doppler and biophysical parameters. Ultrasound Obstet Gynecol 2003 Jan;21(1):1-8.

(10) Gagnon R. Placental insufficiency and its consequences. Eur J Obstet Gynecol Reprod Biol 2003 Sep 22;110 Suppl 1:S99-107.

(11) Baschat AA. Fetal growth restriction - from observation to intervention. J Perinat Med 2010 May;38(3):239-246.

(12) Gilbert WM, Danielsen B. Pregnancy outcomes associated with intrauterine growth restriction. Am J Obstet Gynecol 2003 Jun;188(6):1596-9; discussion 1599-601.

(13) Kramer MS, Olivier M, McLean FH, Willis DM, Usher RH. Impact of intrauterine growth retardation and body proportionality on fetal and neonatal outcome. Pediatrics 1990 Nov;86(5):707-713.

(14) Divon MY, Haglund B, Nisell H, Otterblad PO, Westgren M. Fetal and neonatal mortality in the postterm pregnancy: the impact of gestational age and fetal growth restriction. Am J Obstet Gynecol 1998 Apr;178(4):726-731.

(15) Froen JF, Gardosi JO, Thurmann A, Francis A, Stray-Pedersen B. Restricted fetal growth in sudden intrauterine unexplained death. Acta Obstet Gynecol Scand 2004 Sep;83(9):801-807.

(16) Pallotto EK, Kilbride HW. Perinatal outcome and later implications of intrauterine growth restriction. Clin Obstet Gynecol 2006 Jun;49(2):257-269.

(17) Zubrick SR, Kurinczuk JJ, McDermott BM, McKelvey RS, Silburn SR, Davies LC. Fetal growth and subsequent mental health problems in children aged 4 to 13 years. Dev Med Child Neurol 2000 Jan;42(1):14-20.

(18) Leon DA, Lithell HO, Vagero D, Koupilova I, Mohsen R, Berglund L, et al. Reduced fetal growth rate and increased risk of death from ischaemic heart disease: cohort study of 15 000 Swedish men and women born 1915-29. BMJ 1998 Jul 25;317(7153):241-245.

(19) Barker DJ, Osmond C, Golding J, Kuh D, Wadsworth ME. Growth in utero, blood pressure in childhood and adult life, and mortality from cardiovascular disease. BMJ 1989 Mar 4;298(6673):564-567.

(20) Visentin S, Grumolato F, Nardelli GB, Di Camillo B, Grisan E, Cosmi E. Early origins of adult disease: low birth weight and vascular remodeling. Atherosclerosis 2014 Dec;237(2):391-399.

(21) Sehgal A, Skilton MR, Crispi F. Human fetal growth restriction: a cardiovascular journey through to adolescence. J Dev Orig Health Dis 2016 Jul 7:1-10.

(22) Demicheva E, Crispi F. Long-term follow-up of intrauterine growth restriction: cardiovascular disorders. Fetal Diagn Ther 2014;36(2):143-153.

(23) Juonala M, Cheung MM, Sabin MA, Burgner D, Skilton MR, Kahonen M, et al. Effect of birth weight on life-course blood pressure levels among children born premature: the Cardiovascular Risk in Young Finns Study. J Hypertens 2015 Aug;33(8):1542-1548.

(24) Cruz-Lemini M, Crispi F, Valenzuela-Alcaraz B, Figueras F, Sitges M, Bijnens B, et al. Fetal cardiovascular remodeling persists at 6 months in infants with intrauterine growth restriction. Ultrasound Obstet Gynecol 2016 Sep;48(3):349-356.

(25) Crispi F, Bijnens B, Figueras F, Bartrons J, Eixarch E, Le Noble F, et al. Fetal growth restriction results in remodeled and less efficient hearts in children. Circulation 2010 Jun 8;121(22):2427-2436.

(26) Hales CN, Barker DJ, Clark PM, Cox LJ, Fall C, Osmond C, et al. Fetal and infant growth and impaired glucose tolerance at age 64. BMJ 1991 Oct 26;303(6809):1019-1022.

(27) Lindqvist PG, Molin J. Does antenatal identification of small-for-gestational age fetuses significantly improve their outcome? Ultrasound Obstet Gynecol 2005 Mar;25(3):258-264.

(28) Gabbay-Benziv R, Aviram A, Hadar E, Chen R, Bardin R, Wiznitzer A, et al. Pregnancy outcome after false diagnosis of fetal growth restriction. J Matern Fetal Neonatal Med 2016 Sep 21:1-4.

(29) Parks WT. Placental hypoxia: The lesions of maternal malperfusion. Semin Perinatol 2015 Feb;39(1):9-19.

(30) Chavhan GB, Babyn PS, Thomas B, Shroff MM, Haacke EM. Principles, techniques, and applications of T2*-based MR imaging and its special applications. Radiographics 2009 Sep-Oct;29(5):1433-1449.

(31) Fox H, Sebire N. Physiology of the placenta. Pathology of the placenta. third ed.: Saunders elsevier; 2007. p. 57-68.

(32) Schroder HJ. Comparative aspects of placental exchange functions. Eur J Obstet Gynecol Reprod Biol 1995 Nov;63(1):81-90.

(33) BORELL U, FERNSTROM I, WESTMAN A. Arteriographic study of placental circulation. Geburtshilfe Frauenheilkd 1958 Jan;18(1):1-9.

(34) Benirschke K, Burton GJ, Baergen RN. Placental Types. Pathology of the human placenta: Springer; 2012. p. 27-37.

(35) Kaufmann P, Scheffen I. Placental development. In: Polin R, Fox W, editors. Neonatal and fetal medicine-physiology and pathophysiology. vol 1 ed.: Saunders, Orlando; 1992. p. 47-55.

(36) Benirschke K, Burton GJ, Baergen RN. Early development of the human placenta. Pathology of the human placenta: Springer; 2012. p. 41-53.

(37) Brosens I, Robertson WB, Dixon HG. The physiological response of the vessels of the placental bed to normal pregnancy. J Pathol Bacteriol 1967 Apr;93(2):569-579.

(38) Hustin J, Schaaps JP, Lambotte R. Anatomical studies of the utero-placental vascularization in the first trimester of pregnancy. Placental Vascularization and Blood Flow: Springer; 1988. p. 49-60.

(39) Kaufmann P, Black S, Huppertz B. Endovascular trophoblast invasion: implications for the pathogenesis of intrauterine growth retardation and preeclampsia. Biol Reprod 2003 Jul;69(1):1-7.

(40) Jackson MR, Mayhew TM, Boyd PA. Quantitative description of the elaboration and maturation of villi from 10 weeks of gestation to term. Placenta 1992 Jul-Aug;13(4):357-370.

(41) Jauniaux E, Burton GJ, Moscoso GJ, Hustin J. Development of the early human placenta: a morphometric study. Placenta 1991 May-Jun;12(3):269-276.

(42) Jauniaux E, Watson A, Ozturk O, Quick D, Burton G. In-vivo measurement of intrauterine gases and acid-base values early in human pregnancy. Hum Reprod 1999 Nov;14(11):2901-2904.

(43) Rodesch F, Simon P, Donner C, Jauniaux E. Oxygen measurements in endometrial and trophoblastic tissues during early pregnancy. Obstet Gynecol 1992 Aug;80(2):283-285.

(44) Jauniaux E, Watson A, Burton G. Evaluation of respiratory gases and acid-base gradients in human fetal fluids and uteroplacental tissue between 7 and 16 weeks' gestation. Am J Obstet Gynecol 2001 Apr;184(5):998-1003.

(45) Schneider H. Oxygenation of the placental-fetal unit in humans. Respir Physiol Neurobiol 2011 Aug 31;178(1):51-58.

(46) Jauniaux E, Watson AL, Hempstock J, Bao YP, Skepper JN, Burton GJ. Onset of maternal arterial blood flow and placental oxidative stress. A possible factor in human early pregnancy failure. Am J Pathol 2000 Dec;157(6):2111-2122.

(47) Soothill PW, Nicolaides KH, Rodeck CH, Campbell S. Effect of gestational age on fetal and intervillous blood gas and acid-base values in human pregnancy. Fetal Ther 1986;1(4):168-175.

(48) Fujikura T, Yoshida J. Blood gas analysis of placental and uterine blood during cesarean delivery. Obstet Gynecol 1996 Jan;87(1):133-136.

(49) Hasegawa J, Nakamura M, Matsuoka R, Mimura T, Ichizuka K, Sekizawa A, et al. Evaluation of placental function using near infrared spectroscopy during fetal growth restriction. J Perinat Med 2010;38(1):29-32.

(50) Soothill PW, Nicolaides KH, Campbell S. Prenatal asphyxia, hyperlacticaemia, hypoglycaemia, and erythroblastosis in growth retarded fetuses. Br Med J (Clin Res Ed) 1987 Apr 25;294(6579):1051-1053.

(51) Zamudio S. Hypoxia and the placenta. The Placenta: From Development to Disease, From Development to Disease 2011:43-49.

(52) Goplerud JM, Delivoria-Papadopoulos M. Physiology of the placenta--gas exchange. Ann Clin Lab Sci 1985 Jul-Aug;15(4):270-278.

(53) Gregg AR, Weiner CP. "Normal" umbilical arterial and venous acid-base and blood gas values. Clin Obstet Gynecol 1993 Mar;36(1):24-32.

(54) RAMSEY EM, CORNER GW,Jr, DONNER MW. Serial and cineradioangiographic visualization of maternal circulation in the primate (hemochorial) placenta. Am J Obstet Gynecol 1963 May 15;86:213-225.

(55) RICHART RM, DOYLE GB, RAMSAY GC. Visualization of the Entire Maternal Placental Circulation in the Rhesus Monkey. Am J Obstet Gynecol 1964 Oct 1;90:334-339.

(56) Wigglesworth JS. Vascular anatomy of the human placenta and its significance for placental pathology. J Obstet Gynaecol Br Commonw 1969 Nov;76(11):979-989.

(57) Lin M, Mauroy B, James JL, Tawhai MH, Clark AR. A multiscale model of placental oxygen exchange: The effect of villous tree structure on exchange efficiency. J Theor Biol 2016 Nov 7;408:1-12.

(58) Schabel MC, Roberts VH, Lo JO, Platt S, Grant KA, Frias AE, et al. Functional imaging of the nonhuman primate Placenta with endogenous blood oxygen level-dependent contrast. Magn Reson Med 2015 Nov 24.

(59) Sorensen A, Peters D, Frund E, Lingman G, Christiansen O, Uldbjerg N. Changes in human placental oxygenation during maternal hyperoxia estimated by blood oxygen level-dependent magnetic resonance imaging (BOLD MRI). Ultrasound Obstet Gynecol 2013 Sep;42(3):310-314.

(60) Hempstock J, Bao YP, Bar-Issac M, Segaren N, Watson AL, Charnock-Jones DS, et al. Intralobular differences in antioxidant enzyme expression and activity reflect the pattern of maternal arterial bloodflow within the human placenta. Placenta 2003 May;24(5):517-523.

(61) Carter AM. Evolution of factors affecting placental oxygen transfer. Placenta 2009 Mar;30 Suppl A:S19-25.

(62) Sibley CP, Boyd RD. Control of transfer across the mature placenta. Oxf Rev Reprod Biol 1988;10:382-435.

(63) Metcalfe J, Bartels H, Moll W. Gas exchange in the pregnant uterus. Physiol Rev 1967 Oct;47(4):782-838.

(64) Carter AM. Placental Gas Exchange and the Oxygen Supply to the Fetus. Compr Physiol 2015 Jul 1;5(3):1381-1403.

(65) Schaaps JP, Tsatsaris V, Goffin F, Brichant JF, Delbecque K, Tebache M, et al. Shunting the intervillous space: new concepts in human uteroplacental vascularization. Am J Obstet Gynecol 2005 Jan;192(1):323-332.

(66) Frias AE, Schabel MC, Roberts VH, Tudorica A, Grigsby PL, Oh KY, et al. Using dynamic contrast-enhanced MRI to quantitatively characterize maternal vascular organization in the primate placenta. Magn Reson Med 2015 Apr;73(4):1570-1578.

(67) Power GG, Dale PS, Nelson PS. Distribution of maternal and fetal blood flow within cotyledons of the sheep placenta. Am J Physiol 1981 Oct;241(4):H486-96.

(68) Bauer C, Ludwig M, Ludwig I, Bartels H. Factors governing the oxygen affinity of human adult and foetal blood. Respir Physiol 1969 Oct;7(3):271-277.

(69) ASSALI NS, RAURAMO L, PELTONEN T. Measurement of uterine blood flow and uterine metabolism. VIII. Uterine and fetal blood flow and oxygen consumption in early human pregnancy. Am J Obstet Gynecol 1960 Jan;79:86-98.

(70) Battaglia FC, Meschia G. Review of studies in human pregnancy of uterine and umbilical blood flows. Med Wieku Rozwoj 2013 Oct-Dec;17(4):287-292.

(71) Derwig I, Lythgoe DJ, Barker GJ, Poon L, Gowland P, Yeung R, et al. Association of placental perfusion, as assessed by magnetic resonance imaging and uterine artery Doppler ultrasound, and its relationship to pregnancy outcome. Placenta 2013 Aug 9.

(72) Gowland PA, Francis ST, Duncan KR, Freeman AJ, Issa B, Moore RJ, et al. In vivo perfusion measurements in the human placenta using echo planar imaging at 0.5 T. Magn Reson Med 1998 Sep;40(3):467-473.

(73) Moore RJ, Ong SS, Tyler DJ, Duckett R, Baker PN, Dunn WR, et al. Spiral artery blood volume in normal pregnancies and those compromised by pre-eclampsia. NMR Biomed 2008 May;21(4):376-380.

(74) Duncan KR, Gowland P, Francis S, Moore R, Baker PN, Johnson IR. The investigation of placental relaxation and estimation of placental perfusion using echo-planar magnetic resonance imaging. Placenta 1998 Sep;19(7):539-543.

(75) Sohlberg S, Mulic-Lutvica A, Lindgren P, Ortiz-Nieto F, Wikstrom AK, Wikstrom J. Placental perfusion in normal pregnancy and early and late preeclampsia: a magnetic resonance imaging study. Placenta 2014 Mar;35(3):202-206.

(76) Moore RJ, Issa B, Tokarczuk P, Duncan KR, Boulby P, Baker PN, et al. In vivo intravoxel incoherent motion measurements in the human placenta using echo-planar imaging at 0.5 T. Magn Reson Med 2000 Feb;43(2):295-302.

(77) Mayhew TM, Wadrop E. Placental morphogenesis and the star volumes of villous trees and intervillous pores. Placenta 1994 Feb-Mar;15(2):209-217.

(78) Roberts VH, Lo JO, Salati JA, Lewandowski KS, Lindner JR, Morgan TK, et al. Quantitative assessment of placental perfusion by contrast-enhanced ultrasound in macaques and human subjects. Am J Obstet Gynecol 2016 Mar;214(3):369.e1-369.e8.

(79) Link G, Clark KE, Lang U. Umbilical blood flow during pregnancy: evidence for decreasing placental perfusion. Am J Obstet Gynecol 2007 May;196(5):489.e1-489.e7.

(80) Lingman G, Marsal K. Fetal central blood circulation in the third trimester of normal pregnancy--a longitudinal study. I. Aortic and umbilical blood flow. Early Hum Dev 1986 Apr;13(2):137-150.

(81) Acharya G, Wilsgaard T, Rosvold Berntsen GK, Maltau JM, Kiserud T. Reference ranges for umbilical vein blood flow in the second half of pregnancy based on longitudinal data. Prenat Diagn 2005 Feb;25(2):99-111.

(82) Nicolaides KH, Economides DL, Soothill PW. Blood gases, pH, and lactate in appropriate- and small-for-gestational-age fetuses. Am J Obstet Gynecol 1989 Oct;161(4):996-1001.

(83) Lazarevic B, Ljubic A, Stevic R, Sulovic V, Rosic B, Radunovic N, et al. Respiratory gases and acid base parameter of the fetus during the second and third trimester. Clin Exp Obstet Gynecol 1991;18(2):81-84.

(84) Sibley CP, Turner MA, Cetin I, Ayuk P, Boyd CA, D'Souza SW, et al. Placental phenotypes of intrauterine growth. Pediatr Res 2005 Nov;58(5):827-832.

(85) Khong TY, Mooney EE, Ariel I, Balmus NC, Boyd TK, Brundler MA, et al. Sampling and Definitions of Placental Lesions: Amsterdam Placental Workshop Group Consensus Statement. Arch Pathol Lab Med 2016 Jul;140(7):698-713.

(86) Mifsud W, Sebire NJ. Placental pathology in early-onset and late-onset fetal growth restriction. Fetal Diagn Ther 2014;36(2):117-128.

(87) Kovo M, Schreiber L, Ben-Haroush A, Cohen G, Weiner E, Golan A, et al. The placental factor in early- and late-onset normotensive fetal growth restriction. Placenta 2013 Apr;34(4):320-324.

(88) Parra-Saavedra M, Crovetto F, Triunfo S, Savchev S, Peguero A, Nadal A, et al. Placental findings in late-onset SGA births without Doppler signs of placental insufficiency. Placenta 2013 Dec;34(12):1136-1141.

(89) Parra-Saavedra M, Simeone S, Triunfo S, Crovetto F, Botet F, Nadal A, et al. Correlation between histological signs of placental underperfusion and perinatal morbidity in late-onset small-for-gestational-age fetuses. Ultrasound Obstet Gynecol 2015 Feb;45(2):149-155.

(90) Pathak S, Lees CC, Hackett G, Jessop F, Sebire NJ. Frequency and clinical significance of placental histological lesions in an unselected population at or near term. Virchows Arch 2011 Dec;459(6):565-572.

(91) Egbor M, Ansari T, Morris N, Green CJ, Sibbons PD. Morphometric placental villous and vascular abnormalities in early- and late-onset pre-eclampsia with and without fetal growth restriction. BJOG 2006 May;113(5):580-589.

(92) Mayhew TM. A stereological perspective on placental morphology in normal and complicated pregnancies. J Anat 2009 Jul;215(1):77-90.

(93) Mayhew TM, Ohadike C, Baker PN, Crocker IP, Mitchell C, Ong SS. Stereological investigation of placental morphology in pregnancies complicated by pre-eclampsia with and without intrauterine growth restriction. Placenta 2003 Feb-Mar;24(2-3):219-226.

(94) Krebs C, Macara LM, Leiser R, Bowman AW, Greer IA, Kingdom JC. Intrauterine growth restriction with absent end-diastolic flow velocity in the umbilical artery is associated with maldevelopment of the placental terminal villous tree. Am J Obstet Gynecol 1996 Dec;175(6):1534-1542.

(95) Brosens I, Pijnenborg R, Vercruysse L, Romero R. The "Great Obstetrical Syndromes" are associated with disorders of deep placentation. Am J Obstet Gynecol 2011 Mar;204(3):193-201.

(96) Kingdom J, Kaufmann P. Oxygen and placental villous development: origins of fetal hypoxia. Placenta 1997;18(8):613-621.

(97) Burton GJ, Woods AW, Jauniaux E, Kingdom JC. Rheological and physiological consequences of conversion of the maternal spiral arteries for uteroplacental blood flow during human pregnancy. Placenta 2009 Jun;30(6):473-482.

(98) Roth CJ, Haeussner E, Ruebelmann T, Koch FV, Schmitz C, Frank HG, et al. Dynamic modeling of uteroplacental blood flow in IUGR indicates vortices and elevated pressure in the intervillous space - a pilot study. Sci Rep 2017 Jan 19;7:40771.

(99) Sebire NJ, Sepulveda W. Correlation of placental pathology with prenatal ultrasound findings. J Clin Pathol 2008 Dec;61(12):1276-1284.

(100) Sebire NJ. Umbilical artery Doppler revisited: pathophysiology of changes in intrauterine growth restriction revealed. Ultrasound Obstet Gynecol 2003 May;21(5):419-422.

(101) Ramasubramanian R, Johnson RF, Downing JW, Minzter BH, Paschall RL. Hypoxemic fetoplacental vasoconstriction: a graduated response to reduced oxygen conditions in the human placenta. Anesth Analg 2006 Aug;103(2):439-42, table of contents.

(102) Howard RB, Hosokawa T, Maguire MH. Hypoxia-induced fetoplacental vasoconstriction in perfused human placental cotyledons. Am J Obstet Gynecol 1987 Nov;157(5):1261-1266.

(103) Benirschke K, Burton GJ, Baergen RN. Villous Maldevelopment. Pathology of the Human Placenta: Springer; 2012. p. 411-427.

(104) Todros T, Sciarrone A, Piccoli E, Guiot C, Kaufmann P, Kingdom J. Umbilical Doppler waveforms and placental villous angiogenesis in pregnancies complicated by fetal growth restriction. Obstet Gynecol 1999 Apr;93(4):499-503.

(105) Kohnen G, Kingdom J. Villous development and the pathogenesis of IUGR. In: Kingdom J, Baker P, editors. Intrauterine growth restriction: aetiology and management: London: Springer; 2000. p. 131-147.

(106) Levytska K, Higgins M, Keating S, Melamed N, Walker M, Sebire NJ, et al. Placental Pathology in Relation to Uterine Artery Doppler Findings in Pregnancies with Severe Intrauterine Growth Restriction and Abnormal Umbilical Artery Doppler Changes. Am J Perinatol 2016 Sep 20.

(107) Pardi G, Cetin I, Marconi AM, Lanfranchi A, Bozzetti P, Ferrazzi E, et al. Diagnostic value of blood sampling in fetuses with growth retardation. N Engl J Med 1993 Mar 11;328(10):692-696.

(108) Zhu MY, Milligan N, Keating S, Windrim R, Keunen J, Thakur V, et al. The hemodynamics of late-onset intrauterine growth restriction by MRI. Am J Obstet Gynecol 2016 Mar;214(3):367.e1-367.e17.

(109) Huppertz B, Peeters LL. Vascular biology in implantation and placentation. Angiogenesis 2005;8(2):157-167.

(110) Veerbeek JH, Nikkels PG, Torrance HL, Gravesteijn J, Post Uiterweer ED, Derks JB, et al. Placental pathology in early intrauterine growth restriction associated with maternal hypertension. Placenta 2014 Sep;35(9):696-701.

(111) Soleymanlou N, Jurisica I, Nevo O, Ietta F, Zhang X, Zamudio S, et al. Molecular evidence of placental hypoxia in preeclampsia. J Clin Endocrinol Metab 2005 Jul;90(7):4299-4308.

(112) Caniggia I, Winter JL. Adriana and Luisa Castellucci Award lecture 2001. Hypoxia inducible factor-1: oxygen regulation of trophoblast differentiation in normal and pre-eclamptic pregnancies--a review. Placenta 2002 Apr;23 Suppl A:S47-57.

(113) Nevo O, Soleymanlou N, Wu Y, Xu J, Kingdom J, Many A, et al. Increased expression of sFlt-1 in in vivo and in vitro models of human placental hypoxia is mediated by HIF-1. Am J Physiol Regul Integr Comp Physiol 2006 Oct;291(4):R1085-93.

(114) Yamaleyeva LM, Pulgar VM, Lindsey SH, Yamane L, Varagic J, McGee C, et al. Uterine artery dysfunction in pregnant ACE2 knockout mice is associated with placental hypoxia and reduced umbilical blood flow velocity. Am J Physiol Endocrinol Metab 2015 Jul 1;309(1):E84-94.

(115) Francis ST, Duncan KR, Moore RJ, Baker PN, Johnson IR, Gowland PA. Non-invasive mapping of placental perfusion. Lancet 1998 May 9;351(9113):1397-1399.

(116) Moore RJ, Strachan BK, Tyler DJ, Duncan KR, Baker PN, Worthington BS, et al. In utero perfusing fraction maps in normal and growth restricted pregnancy measured using IVIM echo-planar MRI. Placenta 2000 Sep;21(7):726-732.

(117) Sohlberg S, Mulic-Lutvica A, Olovsson M, Weis J, Axelsson O, Wikstrom J, et al. MRI estimated placental perfusion in fetal growth assessment. Ultrasound Obstet Gynecol 2015 Jan 14.

(118) Brunelli R, Masselli G, Parasassi T, De Spirito M, Papi M, Perrone G, et al. Intervillous circulation in intra-uterine growth restriction. Correlation to fetal well being. Placenta 2010 Dec;31(12):1051-1056.

(119) Nylund L, Lunell NO, Lewander R, Sarby B. Uteroplacental blood flow index in intrauterine growth retardation of fetal or maternal origin. Br J Obstet Gynaecol 1983 Jan;90(1):16-20.

(120) Pardi G, Cetin I, Marconi AM, Bozzetti P, Buscaglia M, Makowski EL, et al. Venous drainage of the human uterus: respiratory gas studies in normal and fetal growth-retarded pregnancies. Am J Obstet Gynecol 1992 Feb;166(2):699-706.

(121) Burton G. On ‘Oxygen and placental villous development: Origins of fetal hypoxia’fetal hypozxia’. Placenta 1997;18(8):625-626.

(122) Macara L, Kingdom JC, Kaufmann P, Kohnen G, Hair J, More IA, et al. Structural analysis of placental terminal villi from growth-restricted pregnancies with abnormal umbilical artery Doppler waveforms. Placenta 1996 Jan;17(1):37-48.

(123) Sibley CP, Pardi G, Cetin I, Todros T, Piccoli E, Kaufmann P, et al. Pathogenesis of intrauterine growth restriction (IUGR)-conclusions derived from a European Union Biomed 2 Concerted Action project 'Importance of Oxygen Supply in Intrauterine Growth Restricted Pregnancies'-a workshop report. Placenta 2002 Apr;23 Suppl A:S75-9.

(124) Unterscheider J, Daly S, Geary MP, Kennelly MM, McAuliffe FM, O'Donoghue K, et al. Optimizing the definition of intrauterine growth restriction: the multicenter prospective PORTO Study. Am J Obstet Gynecol 2013 Apr;208(4):290.e1-290.e6.

(125) Zhang J, Merialdi M, Platt LD, Kramer MS. Defining normal and abnormal fetal growth: promises and challenges. Am J Obstet Gynecol 2010 Jun;202(6):522-528.

(126) Poon LC, Volpe N, Muto B, Syngelaki A, Nicolaides KH. Birthweight with gestation and maternal characteristics in live births and stillbirths. Fetal Diagn Ther 2012;32(3):156-165.

(127) Dudley NJ. A systematic review of the ultrasound estimation of fetal weight. Ultrasound Obstet Gynecol 2005 Jan;25(1):80-89.

(128) Chauhan SP, Hendrix NW, Magann EF, Morrison JC, Kenney SP, Devoe LD. Limitations of clinical and sonographic estimates of birth weight: experience with 1034 parturients. Obstet Gynecol 1998 Jan;91(1):72-77.

(129) Ott WJ. Intrauterine growth retardation and preterm delivery. Am J Obstet Gynecol 1993 Jun;168(6 Pt 1):1710-5; discussion 1715-7.

(130) Secher NJ, Kern Hansen P, Thomsen BL, Keiding N. Growth retardation in preterm infants. Br J Obstet Gynaecol 1987 Feb;94(2):115-120.

(131) Gardosi J, Figueras F, Clausson B, Francis A. The customised growth potential: an international research tool to study the epidemiology of fetal growth. Paediatr Perinat Epidemiol 2011 Jan;25(1):2-10.

(132) Hutcheon JA, Zhang X, Cnattingius S, Kramer MS, Platt RW. Customised birthweight percentiles: does adjusting for maternal characteristics matter? BJOG 2008 Oct;115(11):1397-1404.

(133) Zhang X, Platt RW, Cnattingius S, Joseph KS, Kramer MS. The use of customised versus population-based birthweight standards in predicting perinatal mortality. BJOG 2007 Apr;114(4):474-477.

(134) Maršál K, Persson P, Larsen T, Lilja H, Selbing A, Sultan B. Intrauterine growth curves based on ultrasonically estimated foetal weights. Acta Paediatrica 1996;85(7):843-848.

(135) Westergaard HB, Langhoff-Roos J. Doppler ultrasonography in singleton pregnancies at risk of intrauterine growth retardation-- a national estimate. Acta Obstet Gynecol Scand 2002 Jun;81(6):534-539.

(136) Turan OM, Turan S, Gungor S, Berg C, Moyano D, Gembruch U, et al. Progression of Doppler abnormalities in intrauterine growth restriction. Ultrasound Obstet Gynecol 2008 Aug;32(2):160-167.

(137) Parra-Saavedra M, Crovetto F, Triunfo S, Savchev S, Peguero A, Nadal A, et al. Association of Doppler parameters with placental signs of underperfusion in late-

onset small-for-gestational-age pregnancies. Ultrasound Obstet Gynecol 2014 Sep;44(3):330-337.

(138) Cruz-Martinez R, Savchev S, Cruz-Lemini M, Mendez A, Gratacos E, Figueras F. Clinical utility of third-trimester uterine artery Doppler in the prediction of brain hemodynamic deterioration and adverse perinatal outcome in small-for-gestational-age fetuses. Ultrasound Obstet Gynecol 2015 Mar;45(3):273-278.

(139) Khalil A, Thilaganathan B. Role of uteroplacental and fetal Doppler in identifying fetal growth restriction at term. Best Pract Res Clin Obstet Gynaecol 2016 Sep 23.

(140) Ferreira AE, Mauad Filho F, Abreu PS, Mauad FM, Araujo Junior E, Martins WP. Reproducibility of first- and second-trimester uterine artery pulsatility index measured by transvaginal and transabdominal ultrasound. Ultrasound Obstet Gynecol 2015 Nov;46(5):546-552.

(141) Familiari A, Bhide A, Morlando M, Scala C, Khalil A, Thilaganathan B. Mid-pregnancy fetal biometry, uterine artery Doppler indices and maternal demographic characteristics: role in prediction of small-for-gestational-age birth. Acta Obstet Gynecol Scand 2016 Feb;95(2):238-244.

(142) Papageorghiou AT, Yu CK, Bindra R, Pandis G, Nicolaides KH, Fetal Medicine Foundation Second Trimester Screening Group. Multicenter screening for pre-eclampsia and fetal growth restriction by transvaginal uterine artery Doppler at 23 weeks of gestation. Ultrasound Obstet Gynecol 2001 Nov;18(5):441-449.

(143) Bakalis S, Stoilov B, Akolekar R, Poon LC, Nicolaides KH. Prediction of small-for-gestational-age neonates: screening by uterine artery Doppler and mean arterial pressure at 30-34 weeks. Ultrasound Obstet Gynecol 2015 Jun;45(6):707-714.

(144) Fadigas C, Guerra L, Garcia-Tizon Larroca S, Poon LC, Nicolaides KH. Prediction of small-for-gestational-age neonates: screening by uterine artery Doppler and mean arterial pressure at 35-37 weeks. Ultrasound Obstet Gynecol 2015 Jun;45(6):715-721.

(145) Yu CK, Khouri O, Onwudiwe N, Spiliopoulos Y, Nicolaides KH, Fetal Medicine Foundation Second-Trimester Screening Group. Prediction of pre-eclampsia by uterine artery Doppler imaging: relationship to gestational age at delivery and small-for-gestational age. Ultrasound Obstet Gynecol 2008 Mar;31(3):310-313.

(146) Cnossen JS, Morris RK, ter Riet G, Mol BW, van der Post JA, Coomarasamy A, et al. Use of uterine artery Doppler ultrasonography to predict pre-eclampsia and

intrauterine growth restriction: a systematic review and bivariable meta-analysis. CMAJ 2008 Mar 11;178(6):701-711.

(147) Sagol S, Sagol O, Ozdemir N. Stereological quantification of placental villus vascularization and its relation to umbilical artery Doppler flow in intrauterine growth restriction. Prenat Diagn 2002 May;22(5):398-403.

(148) Baschat AA, Gembruch U, Harman CR. The sequence of changes in Doppler and biophysical parameters as severe fetal growth restriction worsens. Ultrasound Obstet Gynecol 2001 Dec;18(6):571-577.

(149) Bekedam DJ, Visser GH, van der Zee AG, Snijders RJ, Poelmann-Weesjes G. Abnormal velocity waveforms of the umbilical artery in growth retarded fetuses: relationship to antepartum late heart rate decelerations and outcome. Early Hum Dev 1990 Oct;24(1):79-89.

(150) Yoon BH, Romero R, Roh CR, Kim SH, Ager JW, Syn HC, et al. Relationship between the fetal biophysical profile score, umbilical artery Doppler velocimetry, and fetal blood acid-base status determined by cordocentesis. Am J Obstet Gynecol 1993 Dec;169(6):1586-1594.

(151) Bilardo CM, Nicolaides KH, Campbell S. Doppler measurements of fetal and uteroplacental circulations: relationship with umbilical venous blood gases measured at cordocentesis. Am J Obstet Gynecol 1990 Jan;162(1):115-120.

(152) Baschat AA, Gembruch U. The cerebroplacental Doppler ratio revisited. Ultrasound Obstet Gynecol 2003 Feb;21(2):124-127.

(153) Baschat AA. Arterial and venous Doppler in the diagnosis and management of early onset fetal growth restriction. Early Hum Dev 2005;81(11):877-887.

(154) Hershkovitz R, Kingdom JC, Geary M, Rodeck CH. Fetal cerebral blood flow redistribution in late gestation: identification of compromise in small fetuses with normal umbilical artery Doppler. Ultrasound Obstet Gynecol 2000 Mar;15(3):209-212.

(155) Severi FM, Bocchi C, Visentin A, Falco P, Cobellis L, Florio P, et al. Uterine and fetal cerebral Doppler predict the outcome of third-trimester small-for-gestational age fetuses with normal umbilical artery Doppler. Ultrasound Obstet Gynecol 2002 Mar;19(3):225-228.

(156) Rowlands DJ, Vyas SK. Longitudinal study of fetal middle cerebral artery flow velocity waveforms preceding fetal death. Br J Obstet Gynaecol 1995 Nov;102(11):888-890.

(157) Khalil AA, Morales-Rosello J, Morlando M, Hannan H, Bhide A, Papageorghiou A, et al. Is fetal cerebroplacental ratio an independent predictor of intrapartum fetal compromise and neonatal unit admission? Am J Obstet Gynecol 2015 Jul;213(1):54.e1-54.10.

(158) Khalil A, Morales-Rosello J, Townsend R, Morlando M, Papageorghiou A, Bhide A, et al. Value of third-trimester cerebroplacental ratio and uterine artery Doppler indices as predictors of stillbirth and perinatal loss. Ultrasound Obstet Gynecol 2016 Jan;47(1):74-80.

(159) Hecher K, Campbell S, Doyle P, Harrington K, Nicolaides K. Assessment of fetal compromise by Doppler ultrasound investigation of the fetal circulation. Arterial, intracardiac, and venous blood flow velocity studies. Circulation 1995 Jan 1;91(1):129-138.

(160) Lees CC, Marlow N, van Wassenaer-Leemhuis A, Arabin B, Bilardo CM, Brezinka C, et al. 2 year neurodevelopmental and intermediate perinatal outcomes in infants with very preterm fetal growth restriction (TRUFFLE): a randomised trial. Lancet 2015 May 30;385(9983):2162-2172.

(161) Visser GH, Bilardo CM, Derks JB, Ferrazzi E, Fratelli N, Frusca T, et al. The TRUFFLE study; fetal monitoring indications for delivery in 310 IUGR infants with 2 year's outcome delivered before 32 weeks of gestation. Ultrasound Obstet Gynecol 2016 Nov 11.

(162) Kiserud T, Kessler J, Ebbing C, Rasmussen S. Ductus venosus shunting in growth-restricted fetuses and the effect of umbilical circulatory compromise. Ultrasound Obstet Gynecol 2006 Aug;28(2):143-149.

(163) Hecher K, Snijders R, Campbell S, Nicolaides K. Fetal venous, intracardiac, and arterial blood flow measurements in intrauterine growth retardation: relationship with fetal blood gases. Am J Obstet Gynecol 1995 Jul;173(1):10-15.

(164) Kiserud T, Eik-Nes SH, Blaas HG, Hellevik LR, Simensen B. Ductus venosus blood velocity and the umbilical circulation in the seriously growth-retarded fetus. Ultrasound Obstet Gynecol 1994 Mar 1;4(2):109-114.

(165) Bakalis S, Silva M, Akolekar R, Poon LC, Nicolaides KH. Prediction of small-for-gestational-age neonates: screening by fetal biometry at 30-34 weeks. Ultrasound Obstet Gynecol 2015 May;45(5):551-558.

(166) Akolekar R, Machuca M, Mendes M, Paschos V, Nicolaides KH. Prediction of stillbirth from placental growth factor at 11-13 weeks. Ultrasound Obstet Gynecol 2016 Nov;48(5):618-623.

(167) Lesmes C, Gallo DM, Saiid Y, Poon LC, Nicolaides KH. Prediction of small-for-gestational-age neonates: screening by uterine artery Doppler and mean arterial pressure at 19-24 weeks. Ultrasound Obstet Gynecol 2015 Sep;46(3):332-340.

(168) Yerlikaya G, Akolekar R, McPherson K, Syngelaki A, Nicolaides KH. Prediction of stillbirth from maternal demographic and pregnancy characteristics. Ultrasound Obstet Gynecol 2016 Aug 26.

(169) Miranda J, Triunfo S, Rodriguez-Lopez M, Sairanen M, Kouru H, Parra-Saavedra M, et al. Performance of a third trimester combined screening model for the prediction of adverse perinatal outcome. Ultrasound Obstet Gynecol 2016 Oct 5.

(170) Poon LC, Lesmes C, Gallo DM, Akolekar R, Nicolaides KH. Prediction of small-for-gestational-age neonates: screening by biophysical and biochemical markers at 19-24 weeks. Ultrasound Obstet Gynecol 2015 Oct;46(4):437-445.

(171) Seravalli V, Block-Abraham DM, Turan OM, Doyle LE, Blitzer MG, Baschat AA. Second-trimester prediction of delivery of a small-for-gestational-age neonate: integrating sequential Doppler information, fetal biometry, and maternal characteristics. Prenat Diagn 2014 Nov;34(11):1037-1043.

(172) Currie S, Hoggard N, Craven IJ, Hadjivassiliou M, Wilkinson ID. Understanding MRI: basic MR physics for physicians. Postgrad Med J 2013 Apr;89(1050):209-223.

(173) Ogawa S, Lee TM, Nayak AS, Glynn P. Oxygenation-sensitive contrast in magnetic resonance image of rodent brain at high magnetic fields. Magn Reson Med 1990 Apr;14(1):68-78.

(174) Pauling L, Coryell CD. The Magnetic Properties and Structure of Hemoglobin, Oxyhemoglobin and Carbonmonoxyhemoglobin. Proc Natl Acad Sci U S A 1936 Apr;22(4):210-216.

(175) Ugurbil K, Adriany G, Andersen P, Chen W, Gruetter R, Hu X, et al. Magnetic resonance studies of brain function and neurochemistry. Annu Rev Biomed Eng 2000;2:633-660.

(176) Lu H, Zhao C, Ge Y, Lewis-Amezcua K. Baseline blood oxygenation modulates response amplitude: Physiologic basis for intersubject variations in functional MRI signals. Magn Reson Med 2008 Aug;60(2):364-372.

(177) Marquardt DW. An algorithm for least-squares estimation of nonlinear parameters. Journal of the Society for Industrial & Applied Mathematics 1963;11(2):431-441.

(178) Cameron IL, Ord VA, Fullerton GD. Characterization of proton NMR relaxation times in normal and pathological tissues by correlation with other tissue parameters. Magn Reson Imaging 1984;2(2):97-106.

(179) Sorensen A, Pedersen M, Tietze A, Ottosen L, Duus L, Uldbjerg N. BOLD MRI in sheep fetuses: a non-invasive method for measuring changes in tissue oxygenation. Ultrasound Obstet Gynecol 2009 Dec;34(6):687-692.

(180) Wedegartner U, Popovych S, Yamamura J, Kooijman H, Adam G. DeltaR2* in fetal sheep brains during hypoxia: MR imaging at 3.0 T versus that at 1.5 T. Radiology 2009 Aug;252(2):394-400.

(181) Wedegartner U, Tchirikov M, Schafer S, Priest AN, Kooijman H, Adam G, et al. Functional MR imaging: comparison of BOLD signal intensity changes in fetal organs with fetal and maternal oxyhemoglobin saturation during hypoxia in sheep. Radiology 2006 Mar;238(3):872-880.

(182) Li D, Wang Y, Waight DJ. Blood oxygen saturation assessment in vivo using T2* estimation. Magn Reson Med 1998 May;39(5):685-690.

(183) Kennan RP, Scanley BE, Gore JC. Physiologic basis for BOLD MR signal changes due to hypoxia/hyperoxia: separation of blood volume and magnetic susceptibility effects. Magn Reson Med 1997 Jun;37(6):953-956.

(184) Schoennagel BP, Yamamura J, Fischer R, de Sousa MT, Weyhmiller M, Birkelbach M, et al. BOLD MRI in the brain of fetal sheep at 3T during experimental hypoxia. J Magn Reson Imaging 2013 Dec 18.

(185) Severinghaus JW. Blood gas calculator. J Appl Physiol 1966 May;21(3):1108-1116.

(186) Collins JA, Rudenski A, Gibson J, Howard L, O'Driscoll R. Relating oxygen partial pressure, saturation and content: the haemoglobin-oxygen dissociation curve. Breathe (Sheff) 2015 Sep;11(3):194-201.

(187) Carter AM. Factors affecting gas transfer across the placenta and the oxygen supply to the fetus. J Dev Physiol 1989 Dec;12(6):305-322.

(188) Jackson BT, Piasecki GJ, Novy MJ. Fetal responses to altered maternal oxygenation in rhesus monkey. Am J Physiol 1987 Jan;252(1 Pt 2):R94-101.

(189) Sonesson SE, Fouron JC, Teyssier G, Bonnin P. Effects of increased resistance to umbilical blood flow on fetal hemodynamic changes induced by maternal oxygen

administration: a Doppler velocimetric study on the sheep. Pediatr Res 1993 Dec;34(6):796-800.

(190) Nicolaides KH, Campbell S, Bradley RJ, Bilardo CM, Soothill PW, Gibb D. Maternal oxygen therapy for intrauterine growth retardation. Lancet 1987 Apr 25;1(8539):942-945.

(191) Sorensen A, Peters D, Simonsen C, Pedersen M, Stausbol-Gron B, Christiansen OB, et al. Changes in human fetal oxygenation during maternal hyperoxia as estimated by BOLD MRI. Prenat Diagn 2013 Feb;33(2):141-145.

(192) Sorensen A, Holm D, Pedersen M, Tietze A, Stausbol-Gron B, Duus L, et al. Left-right difference in fetal liver oxygenation during hypoxia estimated by BOLD MRI in a fetal sheep model. Ultrasound Obstet Gynecol 2011 Dec;38(6):665-672.

(193) Cohen ER, Ugurbil K, Kim SG. Effect of basal conditions on the magnitude and dynamics of the blood oxygenation level-dependent fMRI response. J Cereb Blood Flow Metab 2002 Sep;22(9):1042-1053.

(194) Buxton RB. The physics of functional magnetic resonance imaging (fMRI). Rep Prog Phys 2013 Sep;76(9):096601-4885/76/9/096601. Epub 2013 Sep 4.

(195) Girsh E, Plaks V, Gilad AA, Nevo N, Schechtman E, Neeman M, et al. Cloprostenol, a prostaglandin F(2alpha) analog, induces hypoxia in rat placenta: BOLD contrast MRI. NMR Biomed 2007 Feb;20(1):28-39.

(196) Chalouhi GE, Alison M, Deloison B, Thiam R, Autret G, Balvay D, et al. Fetoplacental Oxygenation in an Intrauterine Growth Restriction Rat Model by Using Blood Oxygen Level-Dependent MR Imaging at 4.7 T. Radiology 2013 May 21.

(197) Aimot-Macron S, Salomon LJ, Deloison B, Thiam R, Cuenod CA, Clement O, et al. In vivo MRI assessment of placental and foetal oxygenation changes in a rat model of growth restriction using blood oxygen level-dependent (BOLD) magnetic resonance imaging. Eur Radiol 2013 May;23(5):1335-1342.

(198) Avni R, Golani O, Akselrod-Ballin A, Cohen Y, Biton I, Garbow JR, et al. MR Imaging-derived Oxygen-Hemoglobin Dissociation Curves and Fetal-Placental Oxygen-Hemoglobin Affinities. Radiology 2016 Jan 14:150721.

(199) Huen I, Morris DM, Wright C, Parker GJ, Sibley CP, Johnstone ED, et al. R(1) and R(2) * changes in the human placenta in response to maternal oxygen challenge. Magn Reson Med 2012 Dec 27.

(200) Hykin J, Moore R, Duncan K, Clare S, Baker P, Johnson I, et al. Fetal brain activity demonstrated by functional magnetic resonance imaging. the Lancet 1999;354(9179):645-646.

(201) Semple SI, Wallis F, Haggarty P, Abramovich D, Ross JA, Redpath TW, et al. The measurement of fetal liver T(*)(2) in utero before and after maternal oxygen breathing: progress towards a non-invasive measurement of fetal oxygenation and placental function. Magn Reson Imaging 2001 Sep;19(7):921-928.

(202) Wedegartner U, Tchirikov M, Koch M, Adam G, Schroder H. Functional magnetic resonance imaging (fMRI) for fetal oxygenation during maternal hypoxia: initial results. Rofo 2002 Jun;174(6):700-703.

(203) Fulford J, Vadeyar SH, Dodampahala SH, Ong S, Moore RJ, Baker PN, et al. Fetal brain activity and hemodynamic response to a vibroacoustic stimulus. Hum Brain Mapp 2004;22(2):116-121.

(204) Fulford J, Vadeyar SH, Dodampahala SH, Moore RJ, Young P, Baker PN, et al. Fetal brain activity in response to a visual stimulus. Hum Brain Mapp 2003;20(4):239-245.

(205) Wedegartner U, Tchirikov M, Schafer S, Priest AN, Walther M, Adam G, et al. Fetal sheep brains: findings at functional blood oxygen level-dependent 3-T MR imaging--relationship to maternal oxygen saturation during hypoxia. Radiology 2005 Dec;237(3):919-926.

(206) Morris DM, Ross JA, McVicar A, Semple SI, Haggarty P, Gilbert FJ, et al. Changes in foetal liver T2* measurements by MRI in response to maternal oxygen breathing: application to diagnosing foetal growth restriction. Physiol Meas 2010 Sep;31(9):1137-1146.

(207) Cahill LS, Zhou YQ, Seed M, Macgowan CK, Sled JG. Brain sparing in fetal mice: BOLD MRI and Doppler ultrasound show blood redistribution during hypoxia. J Cereb Blood Flow Metab 2014 Apr 9.

(208) Dietrich O, Reiser MF, Schoenberg SO. Artifacts in 3-T MRI: physical background and reduction strategies. Eur J Radiol 2008 Jan;65(1):29-35.

(209) Haacke EM, Tkach JA, Parrish TB. Reduction of T2* dephasing in gradient field-echo imaging. Radiology 1989 Feb;170(2):457-462.

(210) Bernstein MA, Huston J,3rd, Ward HA. Imaging artifacts at 3.0T. J Magn Reson Imaging 2006 Oct;24(4):735-746.

(211) Expert Panel on MR Safety, Kanal E, Barkovich AJ, Bell C, Borgstede JP, Bradley WG,Jr, et al. ACR guidance document on MR safe practices: 2013. J Magn Reson Imaging 2013 Mar;37(3):501-530.

(212) Hand JW, Li Y, Hajnal JV. Numerical study of RF exposure and the resulting temperature rise in the foetus during a magnetic resonance procedure. Phys Med Biol 2010 Feb 21;55(4):913-930.

(213) Kok RD, de Vries MM, Heerschap A, van den Berg PP. Absence of harmful effects of magnetic resonance exposure at 1.5 T in utero during the third trimester of pregnancy: a follow-up study. Magn Reson Imaging 2004 Jul;22(6):851-854.

(214) Clements H, Duncan KR, Fielding K, Gowland PA, Johnson IR, Baker PN. Infants exposed to MRI in utero have a normal paediatric assessment at 9 months of age. Br J Radiol 2000 Feb;73(866):190-194.

(215) Baker PN, Johnson IR, Harvey PR, Gowland PA, Mansfield P. A three-year follow-up of children imaged in utero with echo-planar magnetic resonance. Am J Obstet Gynecol 1994 Jan;170(1 Pt 1):32-33.

(216) Schenck JF. Safety of strong, static magnetic fields. J Magn Reson Imaging 2000 Jul;12(1):2-19.

(217) Yamaguchi-Sekino S, Sekino M, Ueno S. Biological effects of electromagnetic fields and recently updated safety guidelines for strong static magnetic fields. Magn Reson Med Sci 2011;10(1):1-10.

(218) Matthes R, International Commission on Non-Ionizing Radiation Protection. Exposure to Static and Low Frequency Electromagnetic Fields, Biological Effects and Health Consequences (0-100 KHz): Review of the Scientific Evidence on Dosimetry, Biological Effects, Epidemiological... : International Commission on Non-ionizing Radiation Protection; 2003.

(219) International Commission on Non-Ionizing Radiation Protection. Guidelines on limits of exposure to static magnetic fields. Health Phys 2009;96(4):504-514.

(220) Tenforde TS, Gaffey CT, Moyer BR, Budinger TF. Cardiovascular alterations in Macaca monkeys exposed to stationary magnetic fields: experimental observations and theoretical analysis. Bioelectromagnetics 1983;4(1):1-9.

(221) Tenforde TS. Magnetically induced electric fields and currents in the circulatory system. Prog Biophys Mol Biol 2005 Feb-Apr;87(2-3):279-288.

(222) Poutamo J, Partanen K, Vanninen R, Vainio P, Kirkinen P. MRI does not change fetal cardiotocographic parameters. Prenat Diagn 1998 Nov;18(11):1149-1154.

(223) Michel SC, Rake A, Keller TM, Huch R, Konig V, Seifert B, et al. Original report. Fetal cardiographic monitoring during 1.5-T MR imaging. AJR Am J Roentgenol 2003 Apr;180(4):1159-1164.

(224) Myers C, Duncan KR, Gowland PA, Johnson IR, Baker PN. Failure to detect intrauterine growth restriction following in utero exposure to MRI. Br J Radiol 1998 May;71(845):549-551.

(225) Price DL, De Wilde JP, Papadaki AM, Curran JS, Kitney RI. Investigation of acoustic noise on 15 MRI scanners from 0.2 T to 3 T. J Magn Reson Imaging 2001 Feb;13(2):288-293.

(226) Glover P, Hykin J, Gowland P, Wright J, Johnson I, Mansfield P. An assessment of the intrauterine sound intensity level during obstetric echo-planar magnetic resonance imaging. Br J Radiol 1995 Oct;68(814):1090-1094.

(227) International Commission on Non-Ionizing Radiation Protection. Medical magnetic resonance (MR) procedures: protection of patients. Health Phys 2004;87(2):197-216.

(228) Levine D, Zuo C, Faro CB, Chen Q. Potential heating effect in the gravid uterus during MR HASTE imaging. J Magn Reson Imaging 2001 Jun;13(6):856-861.

(229) Haydon ML, Gorenberg DM, Nageotte MP, Ghamsary M, Rumney PJ, Patillo C, et al. The effect of maternal oxygen administration on fetal pulse oximetry during labor in fetuses with nonreassuring fetal heart rate patterns. Am J Obstet Gynecol 2006 Sep;195(3):735-738.

(230) Bartnicki J, Saling E. The influence of maternal oxygen administration on the fetus. Int J Gynaecol Obstet 1994 May;45(2):87-95.

(231) Khaw KS, Wang CC, Ngan Kee WD, Tam WH, Ng FF, Critchley LA, et al. Supplementary oxygen for emergency Caesarean section under regional anaesthesia. Br J Anaesth 2009 Jan;102(1):90-96.

(232) Van de Velde M. Emergency Caesarean delivery: is supplementary maternal oxygen necessary? Br J Anaesth 2009 Jan;102(1):1-2.

(233) Polvi HJ, Pirhonen JP, Erkkola RU. The hemodynamic effects of maternal hypo- and hyperoxygenation in healthy term pregnancies. Obstet Gynecol 1995 Nov;86(5):795-799.

(234) Meyenburg M, Bartnicki J, Saling E. The effect of maternal oxygen administration on fetal and maternal blood flow values using Doppler ultrasonography. J Perinat Med 1991;19(3):185-190.

(235) Arduini D, Rizzo G, Mancuso S, Romanini C. Short-term effects of maternal oxygen administration on blood flow velocity waveforms in healthy and growth-retarded fetuses. Am J Obstet Gynecol 1988 Nov;159(5):1077-1080.

(236) Huen I, Morris D, Wright C, Sibley C, Naish J, Johnstone E. Absence of Po change in fetal brain despite Po increase in placenta in response to maternal oxygen challenge. BJOG 2014 May 12.

(237) Arduini D, Rizzo G, Romanini C, Mancuso S. Fetal haemodynamic response to acute maternal hyperoxygenation as predictor of fetal distress in intrauterine growth retardation. BMJ 1989 Jun 10;298(6687):1561-1562.

(238) Bartnicki J, Saling E. Influence of maternal oxygen administration on the computer-analysed fetal heart rate patterns in small-for-gestational-age fetuses. Gynecol Obstet Invest 1994;37(3):172-175.

(239) Bekedam DJ, Mulder EJ, Snijders RJ, Visser GH. The effects of maternal hyperoxia on fetal breathing movements, body movements and heart rate variation in growth retarded fetuses. Early Hum Dev 1991 Dec;27(3):223-232.

(240) Kyank HR, Seidenschnur G. Intrauterine growth retardation--CTG findings in pre-partum oxygen respiration and transcutaneous nerve stimulation. Zentralbl Gynakol 1988;110(22):1407-1415.

(241) Parra-Cordero M, Lees C, Missfelder-Lobos H, Seed P, Harris C. Fetal arterial and venous Doppler pulsatility index and time averaged velocity ranges. Prenat Diagn 2007 Dec;27(13):1251-1257.

(242) Hecher K, Campbell S, Snijders R, Nicolaides K. Reference ranges for fetal venous and atrioventricular blood flow parameters. Ultrasound Obstet Gynecol 1994 Sep 1;4(5):381-390.

(243) Hadlock FP, Harrist RB, Carpenter RJ, Deter RL, Park SK. Sonographic estimation of fetal weight. The value of femur length in addition to head and abdomen measurements. Radiology 1984 Feb;150(2):535-540.

(244) Sinding M, Peters DA, Frokjaer JB, Christiansen OB, Petersen A, Uldbjerg N, et al. Placental magnetic resonance imaging T2* measurements in normal pregnancies and in those complicated by fetal growth restriction. Ultrasound Obstet Gynecol 2016 Jun;47(6):748-754.

(245) Sinding M, Peters DA, Frokjaer JB, Christiansen OB, Uldbjerg N, Sorensen A. Reduced placental oxygenation during subclinical uterine contractions as assessed by BOLD MRI. Placenta 2016 Mar;39:16-20.

(246) Pinar H, Sung C, Oyer C, Singer D. Reference values for singleton and twin placental weights. Fetal & Pediatric Pathology 1996;16(6):901-907.

(247) DeLong ER, DeLong DM, Clarke-Pearson DL. Comparing the areas under two or more correlated receiver operating characteristic curves: a nonparametric approach. Biometrics 1988 Sep;44(3):837-845.

(248) Sorensen A, Sinding M, Peters DA, Petersen A, Frokjaer JB, Christiansen OB, et al. Placental oxygen transport estimated by the hyperoxic placental BOLD MRI response. Physiol Rep 2015 Oct;3(10):10.14814/phy2.12582.

(249) Sinding M, Peters DA, Frokjaer JB, Christiansen OB, Petersen A, Uldbjerg N, et al. Prediction of low birth weight: Comparison of placental T2* estimated by MRI and uterine artery pulsatility index. Placenta 2017 Jan;49:48-54.

(250) Wright C, Morris DM, Baker PN, Crocker IP, Gowland PA, Parker GJ, et al. Magnetic resonance imaging relaxation time measurements of the placenta at 1.5 T. Placenta 2011 Dec;32(12):1010-1015.

(251) Gowland PA, Freeman A, Issa B, Boulby P, Duncan KR, Moore RJ, et al. In vivo relaxation time measurements in the human placenta using echo planar imaging at 0.5 T. Magn Reson Imaging 1998 Apr;16(3):241-247.

(252) Ong SS, Tyler DJ, Moore RJ, Gowland PA, Baker PN, Johnson IR, et al. Functional magnetic resonance imaging (magnetization transfer) and stereological analysis of human placentae in normal pregnancy and in pre-eclampsia and intrauterine growth restriction. Placenta 2004 May;25(5):408-412.

(253) Gowland P. Placental MRI. Semin Fetal Neonatal Med 2005 Oct;10(5):485-490.

(254) Derwig I, Barker GJ, Poon L, Zelaya F, Gowland P, Lythgoe DJ, et al. Association of placental T2 relaxation times and uterine artery Doppler ultrasound measures of placental blood flow. Placenta 2013 Jun;34(6):474-479.

(255) Burton GJ, Jauniaux E. Sonographic, stereological and Doppler flow velocimetric assessments of placental maturity. Br J Obstet Gynaecol 1995 Oct;102(10):818-825.

(256) Laga EM, Driscoll SG, Munro HN. Quantitative studies of human placenta. I. Morphometry. Biol Neonate 1973;23(3):231-259.

(257) Derwig IE, Akolekar R, Zelaya FO, Gowland PA, Barker GJ, Nicolaides KH. Association of placental volume measured by MRI and birth weight percentile. J Magn Reson Imaging 2011 Nov;34(5):1125-1130.

(258) Andescavage NN, du Plessis A, Limperopoulos C. Advanced MR imaging of the placenta: Exploring the in utero placenta-brain connection. Semin Perinatol 2015 Mar;39(2):113-123.

(259) Baker PN, Johnson IR, Gowland PA, Hykin J, Adams V, Mansfield P, et al. Measurement of fetal liver, brain and placental volumes with echo-planar magnetic resonance imaging. Br J Obstet Gynaecol 1995 Jan;102(1):35-39.

(260) Yao AC, Moinian M, Lind J. Distribution of blood between infant and placenta after birth. Lancet 1969 Oct 25;2(7626):871-873.

(261) Barcroft J. Researches on pre-natal life. 1946.

(262) Huen IK. Assessment of placental and fetal oxygenation in normal and abnormal pregnancy using magnetic resonance imaging. 2014.

(263) Wedegartner U, Kooijman H, Andreas T, Beindorff N, Hecher K, Adam G. T2 and T2* measurements of fetal brain oxygenation during hypoxia with MRI at 3T: correlation with fetal arterial blood oxygen saturation. Eur Radiol 2010 Jan;20(1):121-127.

(264) Li H, Gudmundsson S, Olofsson P. Uterine artery blood flow velocity waveforms during uterine contractions. Ultrasound Obstet Gynecol 2003 Dec;22(6):578-585.

(265) Oosterhof H, Dijkstra K, Aarnoudse JG. Uteroplacental Doppler velocimetry during Braxton Hicks' contractions. Gynecol Obstet Invest 1992;34(3):155-158.

(266) Bakker PC, van Geijn HP. Uterine activity: implications for the condition of the fetus. J Perinat Med 2008;36(1):30-37.

(267) Olofsson P, Thuring-Jonsson A, Marsal K. Uterine and umbilical circulation during the oxytocin challenge test. Ultrasound Obstet Gynecol 1996 Oct;8(4):247-251.

(268) Oosterhof H, Dijkstra K, Aarnoudse JG. Fetal Doppler velocimetry in the internal carotid and umbilical artery during Braxton Hicks' contractions. Early Hum Dev 1992 Aug;30(1):33-40.

(269) Bleker OP, Kloosterman GJ, Mieras DJ, Oosting J, Salle HJ. Intervillous space during uterine contractions in human subjects: an ultrasonic study. Am J Obstet Gynecol 1975 Dec 1;123(7):697-699.

(270) Boyd PA. Quantitative structure of the normal human placenta from 10 weeks of gestation to term. Early Hum Dev 1984 Jun;9(4):297-307.

ISSN (online): 2246-1302
ISBN (online): 978-87-7112-919-9

AALBORG UNIVERSITY PRESS